Mechanical & Aerospace Engineering Theses & Dissertations

Mechanical & Aerospace Engineering

Spring 2018

A Cost Effective Design for a Propeller Thrust/ Torque Balance

Nicholas Barrett Sadowski
Old Dominion University

Recommended Citation

A COST EFFECTIVE DESIGN FOR A PROPELLER THRUST/TORQUE BALANCE

by

Nicholas Barrett Sadowski
B.S. May 2013, Virginia Military Institute

A Thesis Submitted to the Faculty of
Old Dominion University in Partial Fulfillment of the
Requirements for the Degree of

MASTER OF SCIENCE

MECHANICAL ENGINEERING

OLD DOMINION UNIVERSITY
May 2018

Approved by:

_____
Drew Landman (Director)

_____
Sean Commo (Member)

_____
Colin Britcher(Member)

ABSTRACT

A COST EFFECTIVE DESIGN FOR A PROPELLER THRUST/TORQUE BALANCE

Nicholas Barrett Sadowski
Old Dominion University, 2018
Director: Dr. Drew Landman

Wind tunnel balances are used with aircraft models, propellers, and components to measure applied forces and moments. The design and manufacture of a balance is often for a specific test, test article and conditions. This paper discusses the theory, design, calibration, and testing of a new small propeller balance for use in a low-speed wind tunnel. The new balance is named the ODU15X15.

Theory discussed herein covers how the two measurement components, thrust and torque, affect the balance design. These loads generate strains which are in turn read by strain gages arranged in Wheatstone bridges. The design follows well known practices established at NASA Langley for single-piece balances.

Design considerations include constraints on geometry shape/size, thermal compensation, vibration inputs, balance sensitivity requirements, and safety. Analysis of the balance is performed using solid computer aided design models and iterative finite element analysis. Goals for this design were to create a cost effective balance, made using only conventional machining, made out of a single billet or section of tubing, and to create a balance capable of measuring loads more accurately then those commercially available for the relatively low loads predicted. The ODU15X15 is designed to read 15 lbs thrust and 15 in-lbs torque.

Calibration, including theory, set-up, design, and procedures, follows the principles of Design of Experiments. A LabView code is used to record voltage outputs from Wheatstone

bridges with known loads applied to the balance. Fixtures are used to apply the static thrust and torque loads. Calibration of the balance resulted in less than ±0.1% full-scale error at a ninety five percent confidence level. Confirmation points provided additional assurance of model adequacy.

Wind tunnel trials were performed with a Scorpion SII-4020-420kv motor, and a 3 blade 16 X 8 Master Airscrew propeller at conditions representative of previous testing with NASA GL-10 propeller candidates. While further testing is needed, results indicate that the balance performance was superior to the commercial load cell.

Acknowledgements

I would like to thank Dr. Landman my advisor for taking a chance with me on this endeavor. I had never met or had a class with him prior to starting this balance design which is a large gamble because he did not know my work ethic or my commitment level. A friend of mine, Tony Ramirez, recommended I talk to him about possible thesis topics so I emailed him to set up a meeting and the rest is history. Dr. Landman has done quite a bit for me from creating the topic on through to completion of my thesis, and I definitely could not have done it without you sir. Dr. Peter Parker of NASA thank you for all of the reference material, for taking time out of your busy schedule to meet with me to discuss the design of my balance, for all of the helpful inputs you provided along the way, and the experience working with you and seeing some of the NASA facilities. Sean Commo and the rest of the NASA balance group thank you for your support in the development of this balance. Lastly but definitely not least I would like to thank my parents who constantly pushed me to do my best, and to take the road less traveled.

NOMENCLATURE

A_m = Cross Sectional Area of Measuring Beam

A_S = Cross Sectional Area of Strap

b = Base of Beam

β = Strap Twist Constant

b_f = Base of Flex Beam

b_m = Base of Measurement Beam

C_P = Power Coefficient = $(2\pi Q)/(\rho N^2 D^5)$

C_T = Thrust Coefficient = $T/(\rho N^2 D^4)$

C_Q = Torque Coefficient = $Q/(\rho N^2 D^5)$

D = Propeller Diameter

E = Modulus of Elasticity

η = Efficiency = $J(C_T/C_P)$

F = Applied Force

G = Shear Modulus of Elasticity

GL = Gage Length

γ_{AF} = Non-Dimensional Shear Correction Factor

γ_y = Shearing Deflection due to Horizontal Translation

γ_z = Shearing Deflection due to Vertical Translation

h = Height of Beam

h_f = Height of Flex Beam

h_m = Height of Measurement Beam

h_s = Height of Strap

I = Inertia

I_f = Inertia of Flex Beam

I_m = Inertia of Measurement beam

I_s = Inertia of Strap

J = Advance Ratio = V/ND, Where V is Wind Tunnel Velocity

κ = Timoshenko Shear Coefficient

k_f = Spring Constant Flex Beam

k_m = Spring Constant Measurement Beam

k_{mT} = Spring Constant Measurement Beam Thrust

k_{mQ} = Spring Constant Measurement Beam Torque

K_{RT} = Total Spring Constant

K_y = Spring Constant Due to Translation in the y Direction

K_z = Spring Constant Due to Translation in the z Direction

K_{yz} = Spring Constant Due to Twisting of Beam About its Own Axis

l = Length of Beam

l_e = Length of Strap

l_s = Length of Strap

l_f = Length of Flex Beam

l_m = Length of Measurement Beam

L_{NF} = Load Proportion Flex Beam

L_{NM} = Load Proportion Measurement Beam

M = Moment

M_0 = Moment About Cantilevered End of Measuring Beam

N   = Motor Speed, Revolution per Second

n   = Number of Beams

n_f = Number of Flex Beams

N_y = Load Proportion Due to Translation in the y Direction

N_z = Load Proportion Due to Translation in the z Direction

N_{yz} = Load Proportion Due to Twisting of Beam About its Own Axis

Q   = Torque

r   = Distance From the Neutral Axis to The Center of the Torque Measurement Beam

ρ = Density

r_y = Distance From Origin to The Center of Beam Along y-Axis

r_z = Distance From Origin to The Center of Beam Along z-Axis

R_C, R_B = Reaction Forces

RM   = Rolling Moment

σ_{rg} = Total Rolling Moment Stress Under Strain Gage

σ_y = Stress Due to Translation in the y Direction

σ_z = Stress Due to Translation in the z Direction

σ_{yz} = Stress Due to Twisting of Beam About its Own Axis

SMG   = Maximum Stress in Measurement Beam Under Strain Gage

θ_1 = Slope at Cantilevered End of Measuring Beam

T   = Thrust

V   = Voltage

y   = Distance to the Neutral Axis of Beam

TABLE OF CONTENTS

LIST OF TABLES

LIST OF FIGURES

Figure   page

1   INTRODUTION

Wind tunnel balances are used with aircraft models, propellers, and components to measure applied forces and moments. The design and manufacture of a balance is often for a specific test article and conditions. For each specific application, the range of expected loads, and dynamic characteristics to be seen by the balance, must be known prior to the commencement of a design. This ensures that the balance is tuned to read certain load bands and that the highest quality of data is collected during the experiment as accuracy is typically proportional to full-scale load ranges. The National Aeronautics and Space Administration (NASA) Langley Research Center designs, manufactures, and tests internal balances, which are constructed from a single piece of metal (monolithic). Currently, Electro Discharge Machining (EDM) is used in the manufacturing of most internal balances. This is often a costly process that uses a rapid series of electrical current discharges between two electrodes to remove material from the piece being machined. The purpose of this thesis is to design and analyze a balance using a cost effective design. In doing so the creation of such a balance will aide smaller research organizations to design and build balances tailored closer to their needs, which could produce higher quality test results compared to commercial load cells not tuned to the design range. The design of this balance is modeled after some of the characteristic geometries of the NASA internal balances, but is manufactured using only conventional machining processes.

1.1   Background

Propeller performance is typically characterized by coefficients derived from two parameters: thrust and torque. The sensitivity and overall accuracy of the balances used to measure the loads produced by the propeller is critical to the outcome of the test. Therefore,

balances may be designed on a case by case basis to optimize sensitivity and minimize uncertainty for a specific load range. This paper will discuss the development and use of such a balance primarily in support of testing the "Greased Lighting 10" (GL-10) motor and propeller arrangement. The GL-10 is an unmanned aircraft prototype developed by NASA and is capable of vertical takeoff. Previous research studying the propeller performance characteristics on the GL-10 was performed at Old Dominion University (ODU) by Duvall and others (1). Duvall's test utilized a six-axis, Gamma-sensor multi-axis load cell by ATI Industrial Automation. This balance is capable of reading forces up to one hundred pounds and moments of 100 in-lbs. However, Duvall's testing only required two components, thrust loads between one and twelve pounds and torques between one and 15 in-lb. Although the testing revealed viable results, it is thought that with a balance designed specifically for the range of loads produced by the propeller, greater fidelity could be achieved. Design considerations for the balance include operating conditions, material analysis, geometric analysis, electrical requirements, and temperature compensation requirements.

The second goal of this work is to provide design guidance for cost effectively manufacturing a two-component balance. Currently balances require specialized tooling to machine very small geometries. NASA utilizes a process called Electro Discharge Machining (EDM) to remove small amounts of material using spark erosion. The finished cut size should not leave any geometry smaller than about thirty thousandths of an inch wide otherwise EDM runs the risk of damaging the piece (2). The EDM process will be discussed further in the following sections. This machining process is very slow and hence expensive and is not readily available to all research facilities. The creation of a design that utilizes conventional machining would expand opportunities to develop balances designed to be sensitive to predicted test loads

on a case by case basis. In addition, smaller research facilities could benefit from the reduced cost and conventional approach to machining. Access to these balances should allow these facilities to contribute higher quality test results.

This paper will discuss the design, test, and manufacture of a balance tuned to measure loads of 15 lbs. thrust, and 15 in-lbs. of torque; henceforth called the ODU15X15 balance. The ODU15X15 balance is made of aluminum bar (or tube) and aluminum plate. Manufacturing processes utilized in the creation of the prototype balance include but are not limited to conventional and Computer Numerical Control (CNC) milling, drilling, and tapping.

1.2   Problem Statement

This research focused on design of a low-cost propeller balance with full scale ranges of 15 lb thrust and 15 in-lb torque and sensitivity of at least 1 mV/V. The design is limited to the use of conventional machining processes, the use of common and easily obtainable materials, the use of square tubing as the basic body geometry, and overall low cost of manufacture and assembly. Conventional machining is limited to drilling, milling, and tapping. Milling is done through the use of CNC for this prototype, but manual methods would suffice. It is hoped that the design documentation is not limited to the constraints of the ODU15X15 balance, but generally applicable.

1.3   Literature Search

1.3.1 Balance Designs

There are three general types of internal strain gage balances: moment, force, and direct read. Each of which is designed with specific advantages. All three types of balances are made to mount to a test stand using a non-metric sting mounting and have separate loading sections.

Moment balances are used to read one force and five moments; two pitching moments, two yaw moments, one rolling moment, and one axial force. These forces are read through gages mounted to cantilevered beams. An advantage to this balance type is that it can be made through a single piece of material which makes it highly accurate. Disadvantages are that the balance requires large clearances inside the models due to the deflection required to generate strains. These deflections also make second order interaction terms more important, increasing calibration difficulty. Figure 1 shows typical Calspan (a commercial manufacturer of balances) internal moment balances (3).

Figure 1: Calspan Internal Moment Balances

Force balances are used to read five forces and one moment; two normal forces, two side forces, one axial force, and one rolling moment. Force balances are also utilized in the testing of aircraft models. These multi-piece balances use a rod and shell arrangement to measure forces applied to the fuselage. Figure 2 shows the typical arrangement of the components.
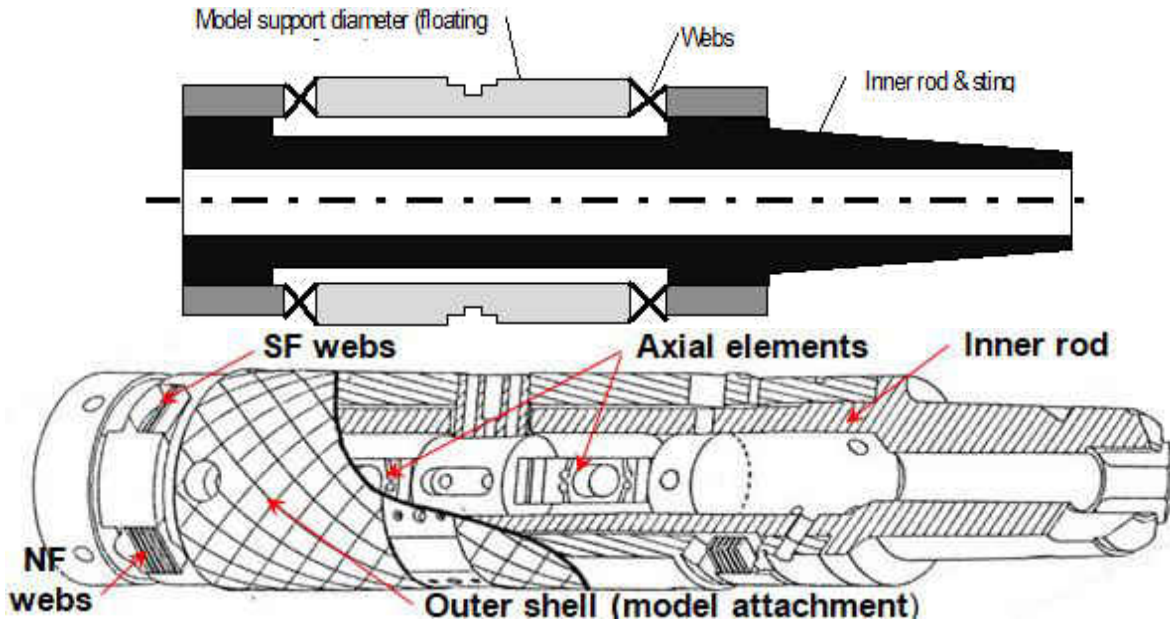
Figure 2: Force Balances

Gages are attached to the webs, and measure the tensile and compressive strains. The webs transmit the load from the shell to the rod. Advantages to using force balances are that they are very stiff, under certain conditions can have higher load capacities then moment balances, and second order interaction terms are less important. Disadvantages of the force balances are that they are expensive to manufacture, they are typically less accurate when installed in the model (due to load path and induced stress problems), and the minimum diameter is 1" (4). Two commercially produced force balances are the Task and Calspan (Triumph); both of which come in various sizes.

Direct-read balances are used to read all six degrees of freedom (i.e. one rolling moment, one pitching moment, one yaw moment, one normal force, one side force, and one axial force). A disadvantage to direct read balances is the temperature compensation difficulty is increased.

1.3.2 NASA Langley Balance Designs

The designs of the thrust section and torque cage in the ODU15X15 balance are based on existing internal balance designs developed by NASA Langley. Figure 3, taken from (2), shows two typical NASA internal moment balances.
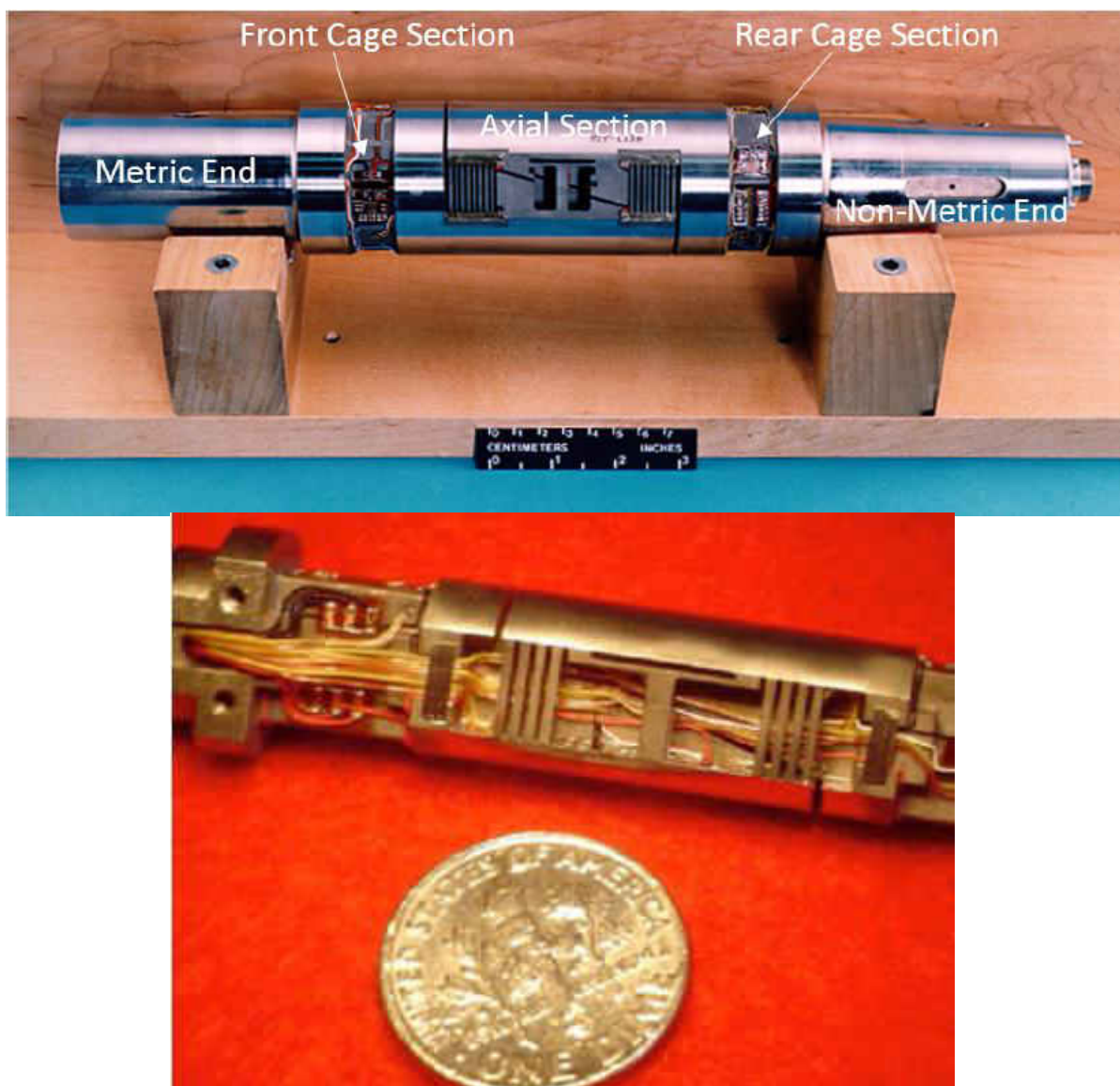
Figure 3: NASA Internal Strain Gage Moment Balances

All NASA Langley balances follow nomenclature for the geometry as shown in Figure 4 and Figure 5.
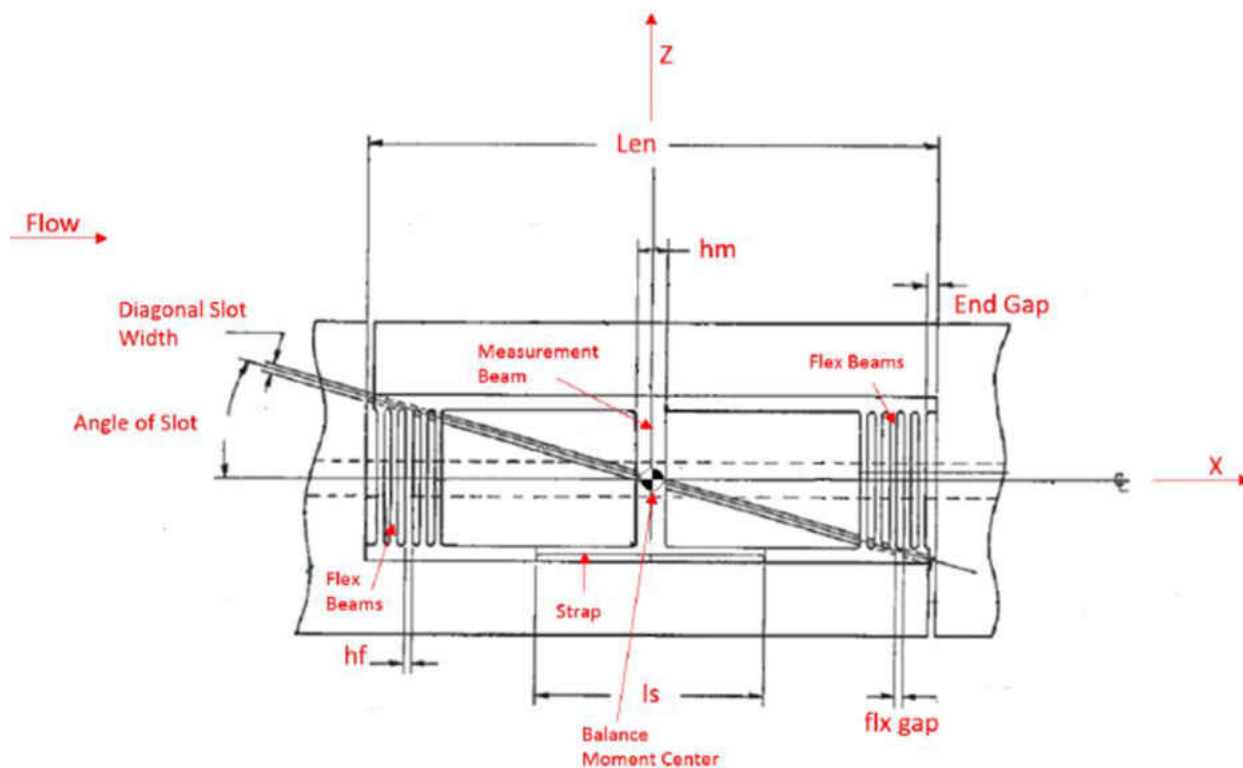
Figure 4: Thrust Section Nomenclature
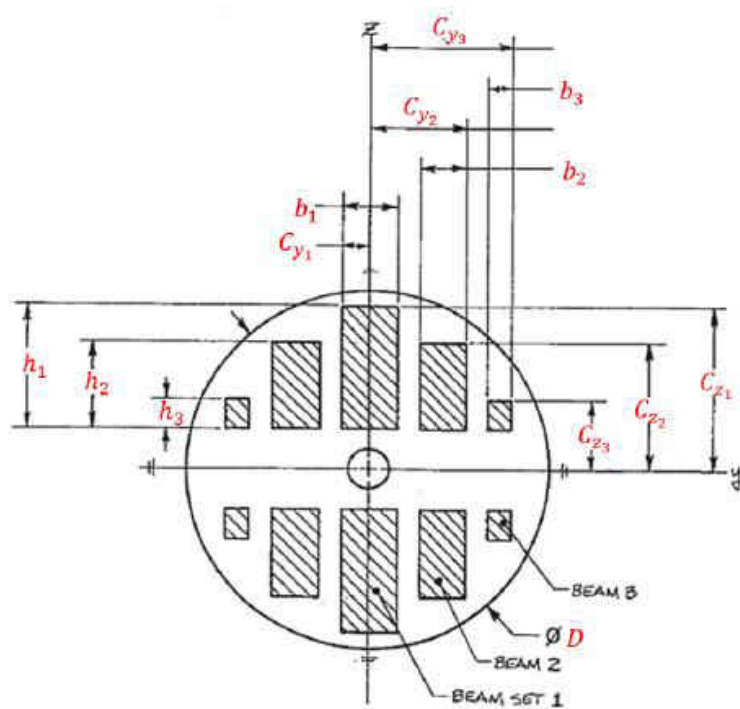
Figure 5: Torque Cage Nomenclature

These figures are adapted from reference 2. The thrust section is the most detailed section of the NASA balance containing the measurement beam, flex beams, the strap, and end gaps. These features are used to measure the thrust force applied to the balance, stiffen the geometry while allowing for deflection in the thrust direction, create a single mode of bending for the measurement beam, and create a moment between the top and bottom of the balance, respectively. The single mode of bending is preferred to the double mode or "S" shape bending. This is because the stress at the center of the S-beam is effectively zero causing the stress gradient to increase making strain harder to measure. The single mode of bending also creates the pure bending moment across the measurement beam required to measure the thrust force. These geometries can range in size, varying with load ranges, but are typically very small. The torque section contains mostly measurement beams. In the case of Figure 5 there are three different beam sets. In the NASA balances, this section can be designed to measure rolling moment, pitching moment, yawing moment, side forces, and normal forces. An analysis of the structure is completed to determine the optimal locations for strain gaging to measure forces and moments of interest.

In Figure 3, note the size differences between the two balances. Both balances are made from a single piece of solid bar stock and through the process of conventional machining and EDM, material is removed to create the very small and complex geometries required to read forces. EDM uses a rapid pulsation of electric current between two electrodes to remove material, the "tooling" electrode and the "work piece" electrode which are separated by a dielectric fluid. Material is removed from both electrodes in the form of tiny craters between nanometers and hundreds of micrometers wide. This is ideal for precision balance manufacture. It is important to note however, that the electrodes do not touch during the machining operations

as this could cause unwanted geometries, such as larger divots. Many NASA balances are made of a single piece of material in order to avoid hysteretic effects associated with mechanical fasteners. To make the measurement beam compliant, a blind cut must be made to remove material between the measurement beam and the center of the raw bar stock. This could not be achieved through conventional or CNC milling in a three-axis process (plunge cut in Z direction and side cuts in X and Y directions) as shown in Figure 6.
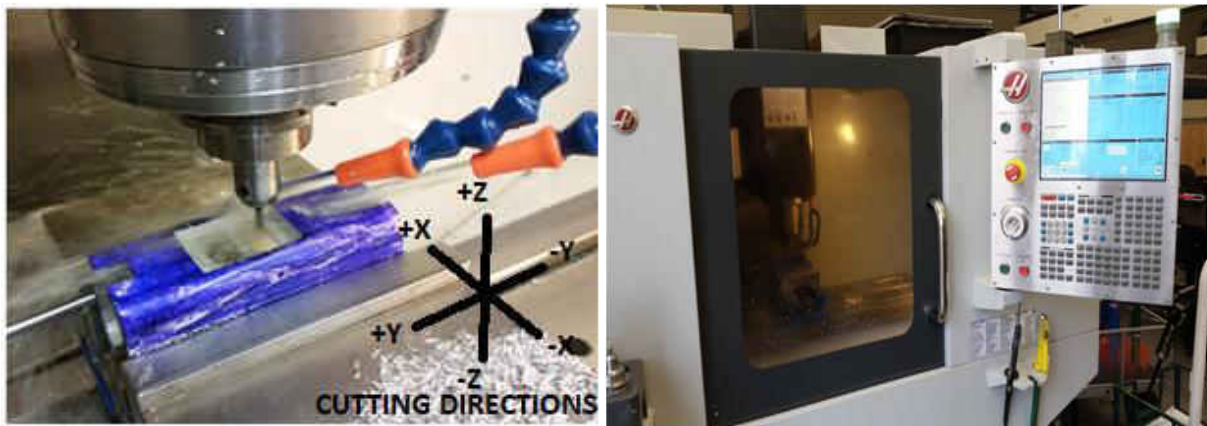
Figure 6: ODU15X15 Balance Being Cut on CNC Machine

NASA Langley balances are made to match as closely as possible the maximum expected loads of a test with the full scale loads of the balance (5). This ensures the greatest resolution achievable by the instrument.

Balances were not always made from a single piece of material. Before the advent of EDM most balances contained fastened joints. These joints caused problems within the balances zero shift and hysteresis, and occurred as a result of joint movement when the balance was loaded (6), as shown in Figure 7. Zero shift is a difference in unloaded outputs. Hysteresis arises from path dependency in load application.
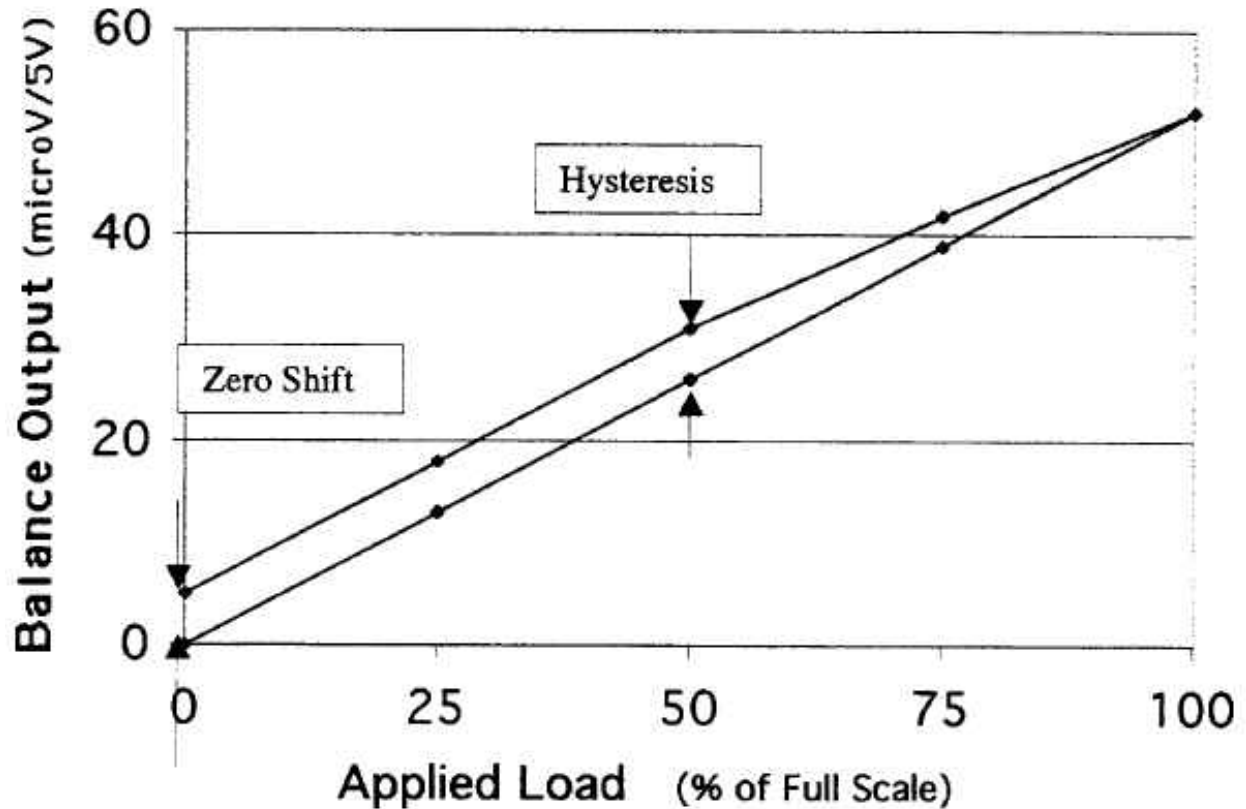
Figure 7: Example Output vs. Applied Load of Balance with Hysteresis and Zero Shift

1.4   ODU Propeller Test Stand and Wind Tunnel Description

The test stand used by Duvall and developed by the ODU 2016 "Greased Lightning-10" senior design group (1) served to define the basic space available for the new balance design. The stand's strut is a hollow streamlined high-strength steel tube with an interface plate. This shape is used to minimize aerodynamic interference. Since the stand is hollow it allows the motor system's compressed air supply tubing, balance signal cable, and motor electrical supply cables to be run through the stand to the motor. The stand also provides mounting points for the streamlined nacelle. Figure 8 shows the set-up used by Duvall during his testing.
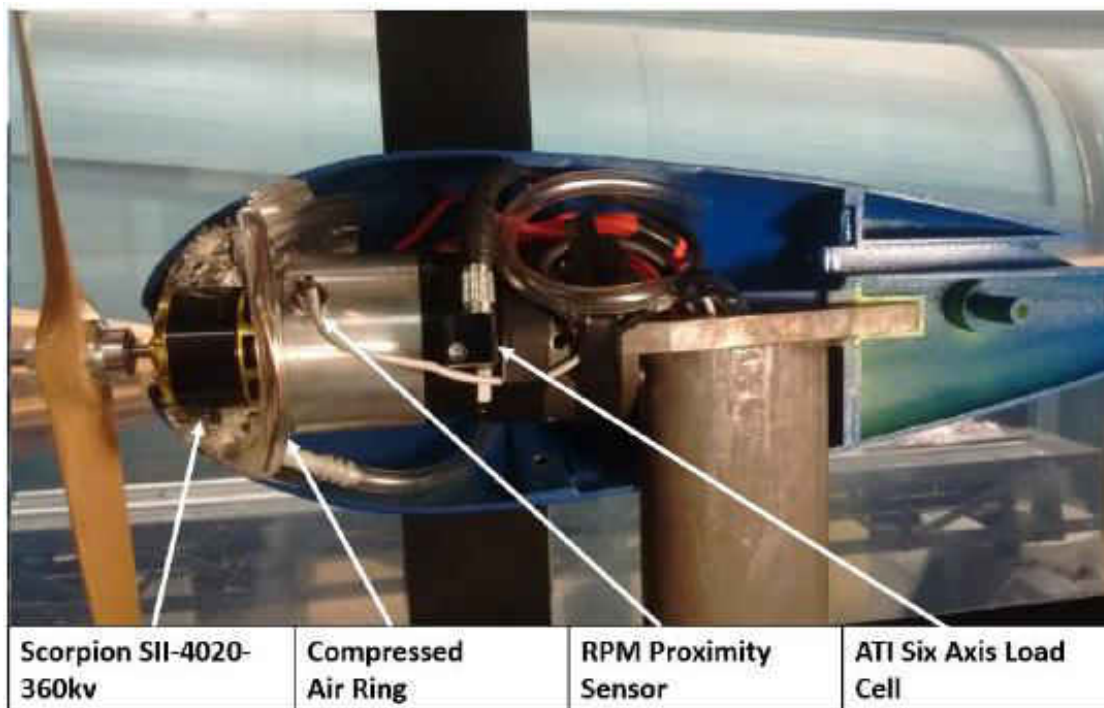
Figure 8: ODU GL10 Propeller Test Stand Set-up
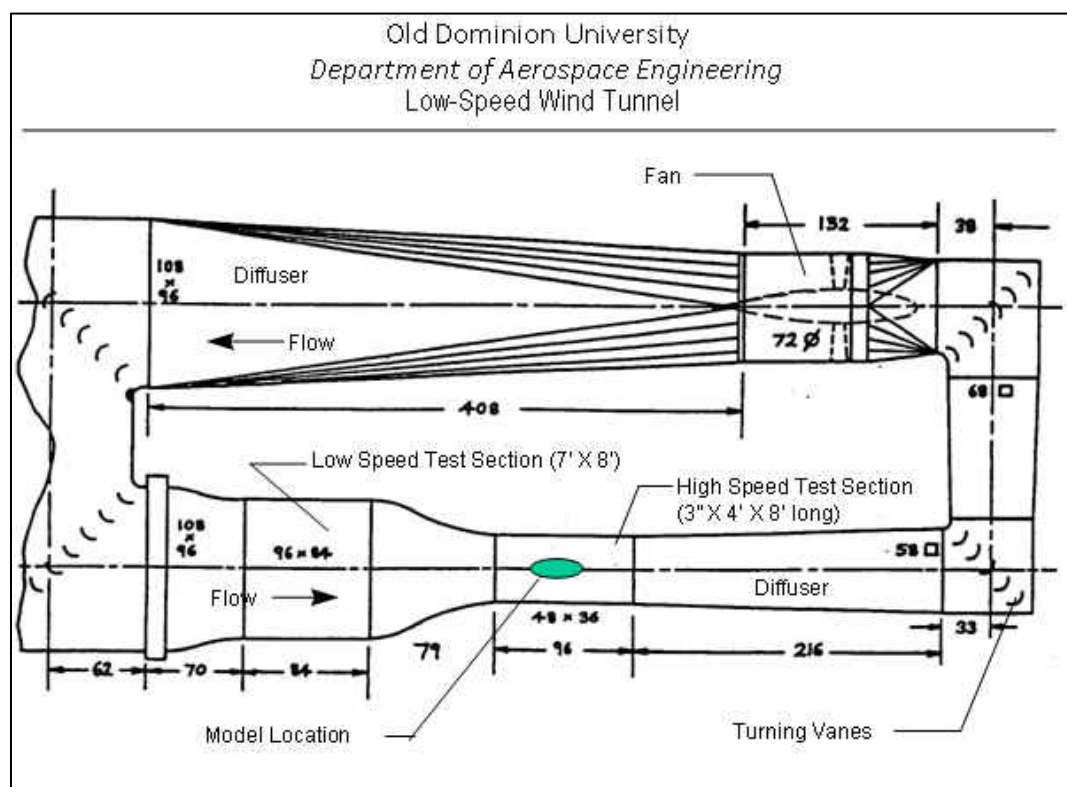
Figure 9: ODU Wind Tunnel Diagram (Dimension in Inches/Feet)

       The wind tunnel used at ODU for the GL 10 propeller performance and acoustic testing is of a closed return design. Figure 9 shows the location of the propeller test stand (model location) in the high speed test section. At this location in the wind tunnel, freestream velocities are available up to 50 meters per second. Wind tunnel fan speed can be set precisely using a variable frequency drive which is commanded by a LabVIEW program to provide closed-loop control of tunnel velocity or dynamic pressure.

2   BALANCE DESIGN THEORY (NASA Langley)

2.1   Governing Equations

The following closed-form equations were developed by NASA over the years in the balance design group. A recent NASA LaRC force measurement group summary document serves to provide all required analytical relations to perform a complete stress analysis on a balance with separate axial section and cages reference 2. This document was used to understand pure axial forces acting on the thrust section, pure rolling moments acting on the torque cage, and was used for basic sizing purposes. Combined loadings are of interest in the design of the ODU 15X15 balance and will be addressed during the FEA.

This section starts by studying the effect of a pure axial force acting on the thrust section of the balance. While the NASA balances are designed to have an axial force acting in the drag direction, the free body diagrams and governing equations are identical for the thrust balance design herein; the only difference being the force applied is in the opposite direction. In order to determine the stress in the beams, the deflection of the structure under an applied load must be determined. Figure 10 shows the free body diagrams for the strap and measurement beam of the thrust section under a pure axial load. The two members are shown in an exaggerated deformed state.
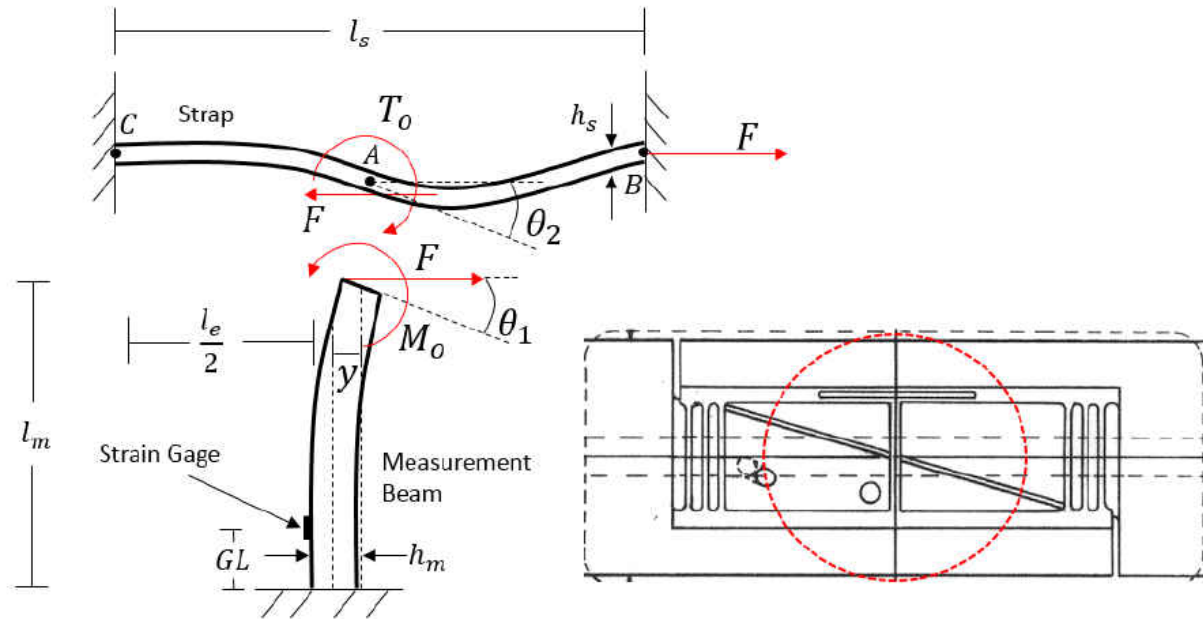
Figure 10: Thrust Section Free Body Diagram.

In order to determine the total deflection of the measurement beam, the analysis will determine the total deflection of point A which has components of deflection from both the measurement beam and the strap.

The measurement beam as shown in the picture above can be modeled as a cantilevered beam. Two factors allow for this choice: [1] the existence of the strap which provides compliance, and [2] the rigidity of the balance body. Making the measurement beam thinner than the body of the balance decreases the stiffness of the measurement beam and allows it to deform before the body. The rigidity of the body creates a "fixed" constraint. The strap allows the axial force to be transferred to the other side of the measurement beam, and allows the end of the measurement beam to remain perpendicular to the neutral axis of the beam, thus eliminating a second fixed constraint and keeping the beam from double bending. This will be discussed further in section 3.3. Due to its thickness, the measurement beam closely follows the

Timoshenko bending beam theory. The Timoshenko theory ($k = 5/6$) allows for the calculation of the shear component of the deflection which is given below.

$$y_{shear} = \frac{Fl_m}{\kappa A_m G} = \frac{(6Fl_m)}{5A_m G} \qquad (1)$$

Where A_m is the cross sectional area of the measurement beam, and l_m is the length of the measurement beam. The bending component of deflection is given by the standard equation for a bending cantilevered beam as follows written in terms of balance nomenclature.

$$y_{bending} = \frac{Fl_m^3}{3EI_m} = \frac{M_0 l_m^2}{2EI_m} \qquad (2)$$

The two strap components of deflection come from the rotation of the strap and the axial force applied to it. Below is the free body diagram of the strap; the bottom diagram shows the strap split at point A.
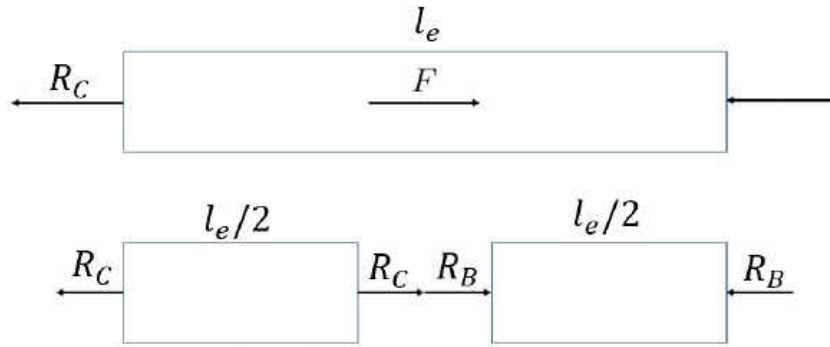
The displacement of point A due to the axial force from one end relative to the other end of the strap is zero because both ends of the straps are fixed. This means that F is equal to $2R_C$ which is equal to $2R_B$. This reveals the axial component of the strap deflection.

$$y_{axial} = \frac{Fl_e}{4A_s E} \qquad (3)$$

Where A_s is the cross sectional area of the strap. The final component of the total deflection is the rotational component of the strap caused by the thickness of the strap.

$$y_{thickness} = \frac{h_s}{2}\theta_1 = \frac{h_s}{2}\left(\frac{Fl_m^2}{2E\,I_m} - \frac{M_0 l_m}{E\,I_m}\right) = \frac{h_s}{4}\frac{Fl_m^2}{E\,I_m}(1 - 2\beta) \qquad (4)$$

Where θ_1 is the slope of the measurement beam at point A and h_s is the thickness of the strap. The total deflection is then given as the sum of all these components.

$$y = y_{bending} + y_{shear} + y_{axial} + y_{thickness} \qquad (5)$$

Now that the deflection has been determined, the spring constant for the measurement beam can be determined by dividing the applied force by the displacement. Giving

$$k_m = \frac{F}{y} = \frac{3E\,I_m}{l_m^3}\,\alpha \qquad (6)$$

where

$$\alpha = \left(1 + \frac{3h_s}{4l_m} - \frac{3\beta}{2}\left(1 + \frac{h_s}{l_m}\right) + \frac{3E}{10G}\left(\frac{h_m}{l_m}\right)^2 + \frac{l_s h_s^2 I_m}{16 l_m^3 I_s}\right)^{-1} \qquad (7)$$

The flex beam spring constant is given as.

$$k_f = \frac{n_f b_f h_f^3 E \gamma_{AF}}{l_f^3} = \frac{12E\,I_f \gamma_{AF}}{l_f^3} \qquad (8)$$

where

$$\gamma_{AF} = \left(\left(\frac{h_f}{l_f}\right)^2 2.4(1+\mu) + 1\right)^{-1} \quad (9)$$

The load proportion ratios are then given as.

$$L_{NM} = \frac{k_m}{k_m + k_f} \quad (10)$$

$$L_{NF} = \frac{k_f}{k_m + k_f} \quad (11)$$

Proportion ratios between the measurement and flex beams are recommended to be between 60:40 and 50:50, and are based on historical data. The load is distributed such that 60 % is placed on the measurement beam and 40 % is on the flex beams.

Using the load proportions for the measurement and flex beams the maximum stress can be determined. Maximum stress in the thrust section measurement beam due to the applied axial force is given by:

$$SM = \frac{F\,L_{NM}l_m(1-\beta)\left(\frac{h_m}{2}\right)}{\frac{b_m h_m^3}{12}} = \frac{6F\,L_{NM}l_m(1-\beta)}{b_m h_m^2} \quad (12)$$

Now accounting for the gage length (GL):

$$SMG = \frac{6F\,L_{NM}(l_m(1-\beta)-GL)}{b_m h_m^2} \quad (13)$$

where

$$\beta = \frac{48\left(\left(\frac{h_m}{l_e}\right)^2+\frac{h_m}{l_e}+\frac{1}{3}\right)-\frac{h_s l_e I_m}{l_m^2\,I_s}}{96\left(\left(\frac{h_m}{l_e}\right)^2+\frac{h_m}{l_e}+\frac{1}{3}\right)+2\left(\frac{l_e\,I_m}{l_m\,I_s}\right)} \quad (14)$$

Now to determine stress in the torque section due to the applied torque a similar procedure is followed. The following analysis will cover the design of a balance with multiple, rectangular cross section, measurement beams under a pure torque load. Figure 11 shows the effect for the torque load on the torque section measurement beams (2).
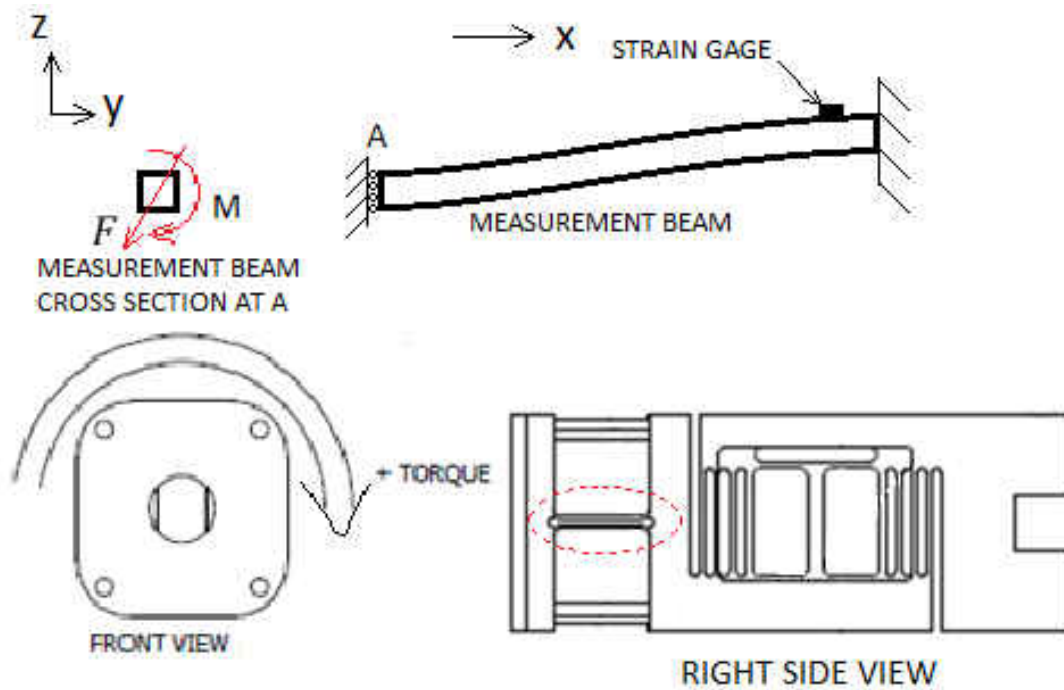
Figure 11: Balance with Torque Applied

First the spring constants for the beams are determined. In this case there will be three spring constants due to the translation in the y direction, translation in the z direction, and rotation of the beam around its own axis in bending (7).

The spring constant due to y translation of the beam group is as follows:

$$K_{y_i} = \frac{n_i h_i b_i^3 \gamma_y r_z^2 E}{l_i^3} \qquad (15)$$

Where n_i is the number of beams in a particular i^{th} cage set, l_i is the length of the measurement beam in the ith cage set, and r_z is the distance from the center of the balance to the center of the ith

beam member along the z axis. In the case of Figure 5 for beam set one n_i would be 2 and for Figure 11 n_i would be 4.

The spring constant due to z translation of the beam group is as follows:

$$K_{z_i} = \frac{n_i b_i h_i^3 \gamma_z r_y^2 E}{l_i^3} \qquad (16)$$

The spring constant due to twisting of the beam group about its own axis is as follows:

$$K_{yz_i} = \left(\frac{n_i E}{12}\right) \left(\frac{b_i h_i}{l_i}\right)^3 (\gamma_z + \gamma_y) \qquad (17)$$

These spring constants again can be combined to create a total spring constant for the torque cage, and with that load proportion ratios can be calculated.

$$K_{R_T} = \sum_i^n \left(K_{y_i} + K_{z_i} + K_{yz_i}\right) \qquad (18)$$

$$N_{y_i} = \frac{K_{y_i}}{K_{R_T}} \qquad (19)$$

$$N_{z_i} = \frac{K_{z_i}}{K_{R_T}} \qquad (20)$$

$$N_{yz_i} = \frac{K_{yz_i}}{K_{R_T}} \qquad (21)$$

Now the stresses can be determined for the beam group.

$$\sigma_{y_i} = \frac{3RMl_iN_{y_i}}{n_ih_ib_i^2r_z} \qquad (22)$$

$$\sigma_{z_i} = \frac{3RMl_iN_{z_i}}{n_ib_ih_i^2r_y} \qquad (23)$$

$$\sigma_{yz_i} = \frac{18RMl_iN_{yz_i}\left(\left|\gamma_{z_i}-\gamma_{y_i}\right|\right)}{n_i(b_ih_i)^2\left(\gamma_{z_i}+\gamma_{y_i}\right)} \qquad (24)$$

where

$$\gamma_{z_i} = \left(\left(\frac{h_i}{l_i}\right)^2 (2.4)(1+\mu)+1\right)^{-1} \qquad (25)$$

$$\gamma_{y_i} = \left(\left(\frac{b_i}{l_i}\right)^2 (2.4)(1+\mu)+1\right)^{-1} \qquad (26)$$

Accounting for the gage length the maximum stress under the strain gage for torque measurement beams is given as follows.

$$\sigma_{r_g} = \left(\sigma_{y_i} + \sigma_{yz_i}\right)\left(GL_yGL_x\right) + \sigma_{z_i}GL_x \qquad (27)$$

3 DESIGN

3.1 Operating Conditions

In order to begin the design process for a balance, the operating conditions of the test must be determined. This includes the loads that will be applied to the balance, the weights of the components, the number of blades on the propeller, and the speed of the motor and propeller. Ensuring that the design load of the balance is close to the actual load produced by the propeller is essential to achieve accurate results. By maximizing measurement resolution, the actual expected maximum load should be near the full scale limit of the balance. The expected maximum load for this testing is 15 lbs. thrust and 15 in-lbs. of torque. The motor used in the testing of this propeller is a Scorpion SII-4020-420kv and will operate at a maximum of 10,000 revolutions per minute. It will primarily drive two/three blade propellers but should accommodate any number of blades. The balance will also be designed to accommodate different motors if desired.

3.2 Material

A number of considerations go into the determination of the material used to making a balance. The mechanical, thermal, and electrical properties of the material help narrow the list. This paper will mostly discuss the mechanical and thermal characteristics of the material as the manufacturing of this balance is through conventional machining and will not require a material that is capable of conducting electricity.

The material strength, modulus, and ductility are directly tied to the ability of the balance to read load through strain. In order to design a balance with the ability to read small loads such as the 15 lbs. thrust and 15 in-lbs. torque anticipated for the GL-10 propeller the material must be

flexible enough that when the load is applied strains build in the structure. However, if the material is not stiff enough the strain gages can become overstressed and delaminate from the surface of the balance. Conversely, if the material is too stiff then the strain gages attached to the structure will have no differential to read since the resistance of the gage will not change significantly. Stress and strain in the elastic region are related through Hooke's Law.

$$\epsilon = \frac{\sigma}{E} \qquad (28)$$

Since the strain is inversely proportional to the modulus of elasticity, materials with high modulus produce less strain for a given stress. When considering extremely small geometric features it may be more advantageous to change to a material with a lower modulus in order to increase the size of the geometries thereby decreasing manufacturing difficulty.

The thermal characteristics play a large role through the addition of error during the use of the balance. During wind tunnel testing, the motor generates heat that can cause the balance to expand causing thermal stain. This growth can then be detected by the strain gages as the balance is heated. In order to avoid this issue a material with a low thermal coefficient of expansion should be considered. However, this effect can also be dealt with during calibration, which will be discussed further later. In the case of a balance with multiple test sections reading the same attribute, the transfer of heat to the balance can cause one test section to expand faster than another. This can also lead to an inaccurate reading if the Wheatstone bridge is set-up between two different test sections. By using a material with a high thermal conductivity the material reaches a thermal equilibrium faster than materials with low thermal conductivity; thus allowing uniformity among the test sections. However, due to geometry constraints requiring large gaps in the conduction path of heat in the balance, the best option may be to keep the entire bridge on one test section if possible.

Electrical thermal compensation is also to be considered in the determination of the material. Some strain gages come with passive thermal compensation that accounts for a specific material's coefficient of thermal expansion. If the wrong gage is used for the material selected than the gage will not properly compensate. Additional passive thermal compensation can be invoked and is discussed further in section 3.5.

While the material cost is much less significant than manufacturing costs for the balance, it is important to note the various factors that can reduce it. While the imagination is limitless in the Computer Aided Design (CAD) of a balance, manufacturers might not have the same vision. Many require a minimum purchase, particularly for the more exotic high strength steels. It is important when starting a design to investigate possible manufacturers. Taking into consideration the specifications they use to make the material, whether the material they provide is stock and can be ordered in small quantities, and the available cross sections of tubing and bar that they provide. Pay considerable attention to the inner and outer radii. These radii do affect the stiffness of the balance and should not be ignored. The more exotic or custom the order, typically the more the part will cost.

6061-T6511 Aluminum was chosen as the material to be used for the ODU15X15 balance. This is because the loads seen by the balance are low, alloy 6061 is common and inexpensive, and 6061's material properties are well suited for this design. NASA typically uses high strength steel for balances; however since the ODU15X15 has such small loads applied to it steel would not be practical. The geometries of the cage and thrust sections would have to be cut much smaller than they would for aluminum to achieve the proper gage output. This would cause issues with both manufacturing of the balance, and mounting of strain gages. CNC machining would likely break the thin beams, and if it didn't, there would likely not be enough physical

room to affix the strain gages. 6061 has a low yield strength compared to steel and other aluminum alloys (i.e. 7075-T6), and is easily welded.

3.3   Geometry

A balance's geometry is dictated by the load path. The geometry must be designed to isolate specific loads. Errors can be introduced into the strain gage reading if the balance deflects out of plane. For internal strain gage balances suitable for aircraft wind tunnel testing, NASA Langley recommends a separate axial section to reduce interaction (2). Other forces and moments should be measured in cage sections that can combine loads. While this balance is for propeller testing, the idea of isolating the torque and thrust measurement sections was very attractive as it should lead to little interaction. Figure 12 shows the separated torque and thrust sections on an iteration of the balance design.
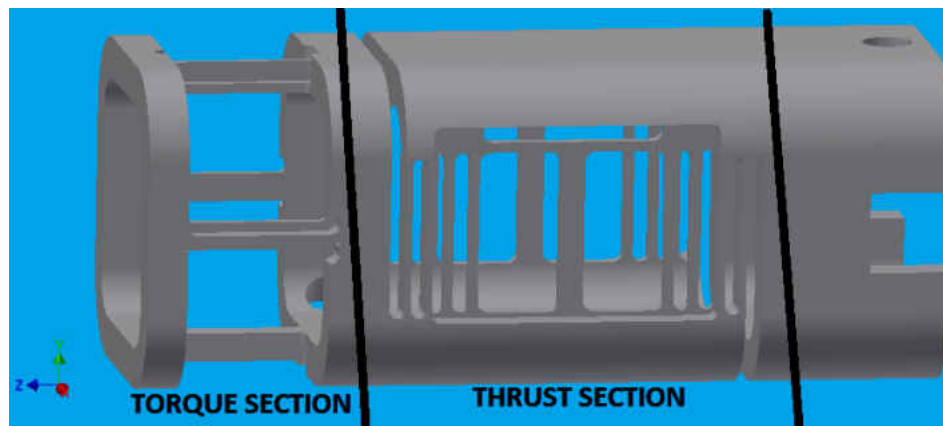
Figure 12: Section Identification on Complete Balance

This section will break down the two different sections of the balance and identify key geometric pieces. For geometric nomenclature see Figures 4 and 5.

3.3.1 Thrust Section

In the case of designing a thrust section, where thrust is measured in the Z direction, the balance must be stiff enough in the Y and X directions so it does not deflect under load. If the

balance does move in the X and Y directions no significant displacements should be seen across the measurement beam as this would complicate the calibration of the balance and development of calibration load schedules. Figure 13 shows the Z component of displacement with only the end gaps of the balance's thrust section with a 15 lb force pushing from left to right. The right side has a fixed constraint on the end. Note that the results below are of a previous version of the design, they are exaggerated, actual loading would not cause the structure to foul, and are only being used to illustrate the effects of the end gaps.
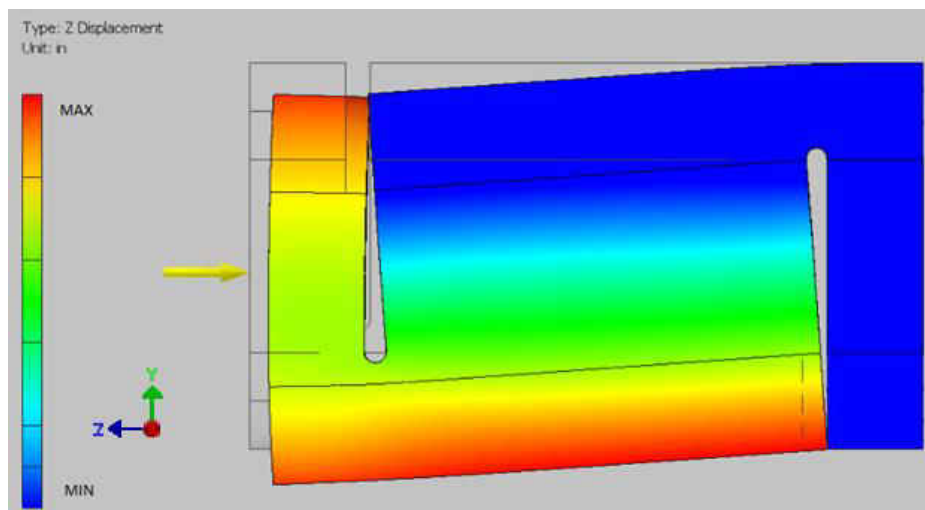
Figure 13: Z Displacement of Thrust Section End Gaps

The end gaps provide the load path required to read thrust by creating a moment between the top, and bottom portions of the balance between the gaps. The upper portion of the balance in blue has no displacement in Z while the lower portion of the balance in red has the maximum displacement. Note that the gaps also cause the entire thrust section to angle in the y-direction. This is acceptable because the far right portion and far left portion of the balance, referring to Figure 13 above, remain perpendicular to the Z axis and uniformly displace as shown by the slight variation vertically in color on either end. Figure 14 below, also for illustration only, shows the X and Y components of displacement for the same geometry and load constraints.
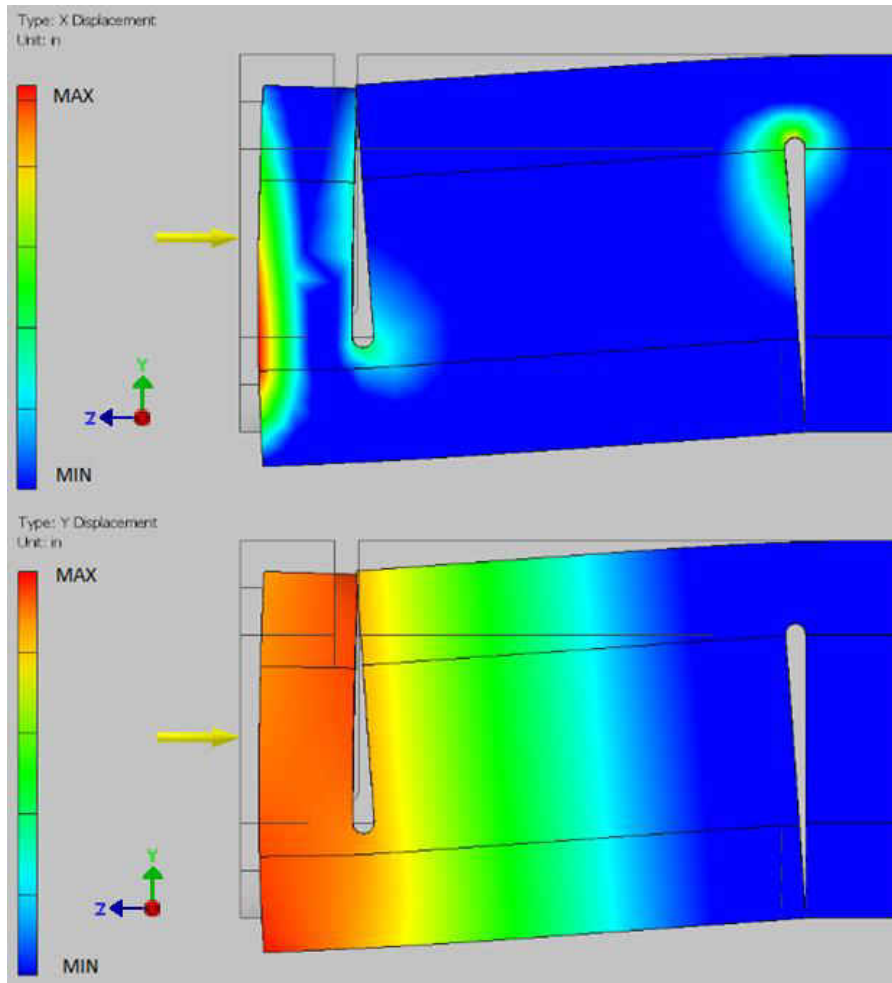
Figure 14: X and Y Displacements of Thrust Section Vertical Cuts

Both the X and Y displacement figures show uniform vertical profiles in the thrust section. This ensures that the structure is not deflecting in other directions absorbing the load. Although the structure does deflect downwards, the profile of displacement in the Y direction is uniform from the top to the bottom, meaning that when the measurement beam is added the Y displacement will not contribute to a false reading by the strain gage. Also the displacements predicted in the X and Y directions are negligible compared to the Z direction which will be shown later. The next important characteristic of the thrust section is the strap attached to the top of the measurement beam. As shown in Figure 15, the strap allows the end of the measurement beam to be perpendicular with its neutral axis.
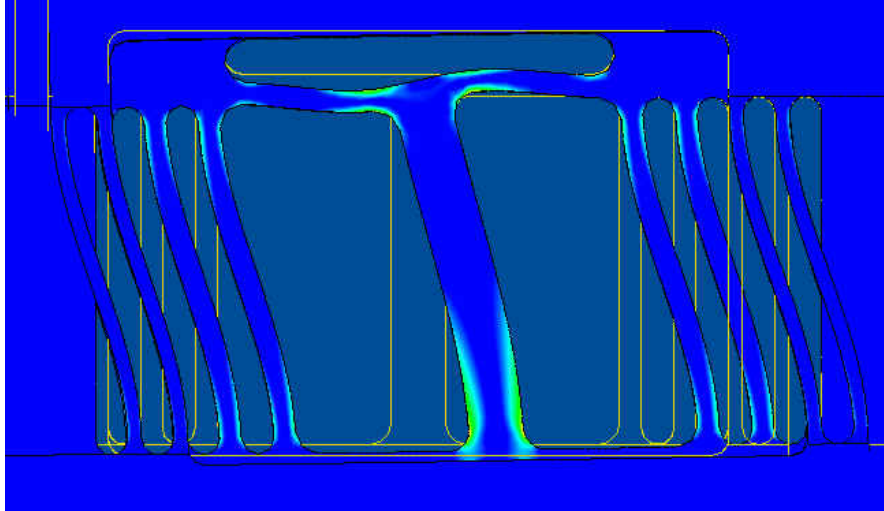
Figure 15: Strap Deformation Under Load

Having this condition on the end of the beam causes the beam to bend only at the side opposite the strap, which makes it easier to predict the stresses/strains at the bottom of the measurement beam (2). If a slot was not present, the measurement beam would go into double bending as shown in the flex beams. The flex beams allow the balance to deform in the Z direction while at the same time stiffen the balance in other directions to prevent other forces or moments such as torque to be transmitted to the measurement beam of the thrust section. Flex beams can vary in size in a single balance as shown in the design of the ODU15X15 balance or be they can all be the same size on the same balance. This will be discussed further in the dynamic analysis section. When determining the thickness of the measurement beam the width of the strain gage needs to be considered. Thinning the beam can be done in order to raise the strain in the beam, however if the beam becomes too thin there will not be sufficient room for the strain gage. It is preferred to have the entire mesh width of the gage on the beam. Gages and gage placement will be discussed further later.

3.3.2 Torque Section

The torque section has fewer geometric characteristics then the thrust section. It consists of only a measurement beam and a stiffener that runs along the center of the measurement beam. The stiffener can be made in two different ways.
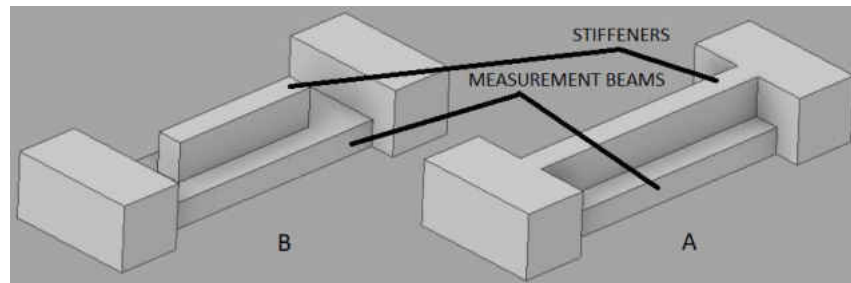
Figure 16: Torque Section Measurement Beam Stiffener Configuration

The stiffener can run the length of the measurement beam as shown in Figure 16(A), as in the case of the ODU15X15 balance, or the two ends of the stiffener can be removed so that the stiffener only exists in the measurement beam's length center as shown in Figure 16(B). Careful consideration needs to be taken into account when using the latter case as it is prone to the generation of stress concentrations at the stiffener's end. The stress concentrations could cause stress gradients in the area of measurement on the measurement beam and cause false readings (5). The torque cage of the ODU15X15 balance utilizes a simple four beam geometry to measure the rolling moment. The beams are centered on the faces of the balance, as opposed to the corners, to reduce the amount of force required to generate stress in the measurement beams. By moving the beams closer to the center, the distance (moment arm length d; a and b in Figure 17) between the beams and the tube neutral axis is decreased; stiffening the moment arm and increasing the force applied to the measurement beam thereby increasing the stress.

$$\boldsymbol{F} = \frac{\boldsymbol{M_1}}{\boldsymbol{r}} \qquad (29)$$

Where M_1 is the moment affected by the change in distance r.
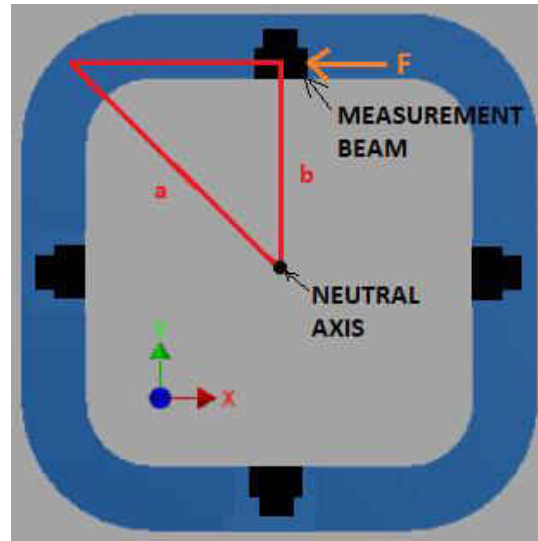
Figure 17: Effect of Distance Between Neutral Axis and Measurement Beam

An alternative way to increase stress in the torque measurement beams is to increase their length. Doing this increases the bending stress of the measurement beam by increasing the moment applied.

$$\sigma_{bend} = \frac{M_2 y}{I} = \frac{F\,d\,y}{I} \qquad (30)$$

Where M_2 is the moment affected by the change in distance d.
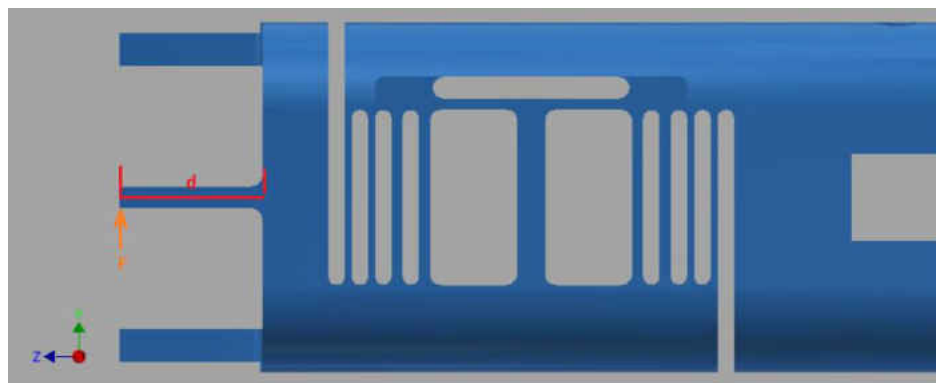
Figure 18: Effect of Measurement Beam Length

Increasing the length of the torque cage measurement beams can cause issues with the dynamic stiffness of the balance; especially if a large load is to be placed on the end of the balance during any phase of testing.

NASA Langley has a number of different cross sections used in the cage section in order to read multiple moments and forces. The most commonly used cross section is shown in Figure 19 (2). All require the use of EDM in manufacturing.
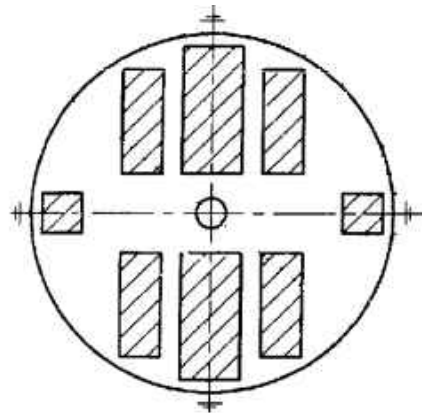
Figure 19: NASA's Most Commonly Used Cage Cross Section Design

3.3.3 Mounting Interfaces

The test stand interface on the ODU15X15 balance is similar to the testing mounts used by Duvall (refer to Figure 8). So in the case of the design of the ODU15X15 balance, the addition of the fastened joints is a necessity for interfacing to existing hardware. The ODU15X15 balance mount to the test stand is based on the existing stand geometry, and is shaped partially by the decision to use a hollow body design. The ODU15X15 balance has a relief in the end that allows the balance to fit over top of the test stand. Two fasteners pass through the top of the balance, into two holes in the stand, and thread into the bottom mount support as shown in Figure 20. It is important to note that the lower portion of the stand is not attached to the bottom mount support or fastener in any way thus eliminating any binding concerns.

Figure 20: ODU15X15 Balance Stand Attachment

These fasteners keep the balance from coming off of the stand while the relief keeps the balance from rotating. The mount of the motor to the ODU15X15 balance is modeled after the existing motor mounts used in Duvall's experiment shown in Figure 21.
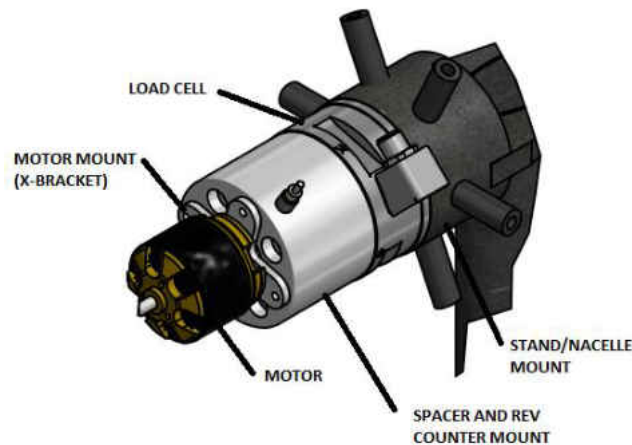
Figure 21: Duvall Experimental Set-up

However, in lieu of multiple spacers and adapters one adapter is used to both bridge the gap between the nacelle and motor, and mount the motor to the balance. In Duvall's setup the X-bracket is mounted to the back side of the motor and then the bracket is mounted. This motor mounting strategy will be incorporated into the adapter eliminating the X-bracket. The adapter also contains a spigot which minimizes the rotation of the adapter to the balance and houses the RPM sensor.

Figure 22: ODU 15X15 Test Adaptor

While this adapter could have been incorporated into the balance as a single piece, having the separate adapter allows for the installation of different motors. The mounting geometry of the ODU15X15 balance differs from that of the most common NASA balances in multiple ways. NASA balance mounting strategies try to avoid fasteners, a single piece of material is used to make the entire balance, and the bodies of the balances are round and solid. While not ideal, the multiple pieces of the ODU15X15 aid with mounting the motor to the balance along with securing the balance on the stand. The typical NASA wind tunnel balance uses a specially designed sting interface as shown in Figure 3 section 1.2. The tapered non-metric sting end mounts the balance to the test stand while the cylindrical metric side mounts the fuselage model to the balance. Conversely, NASA's FF family of balances utilizes metric and non-metric fastener interface, similar to the ODU 15X15 balance as shown by the FF09 in Figure 23.
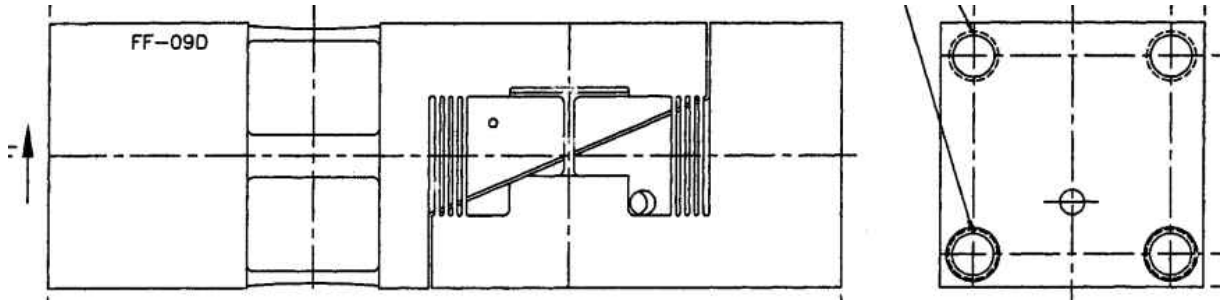
Figure 23: NASA FF09 Balance

Similarities between the two balances include a 4-beam cage, square body, and fastener jointed interfaces. This balance is made of a single piece of bar stock, but has not been hollowed into a tube. A couple distinct differences include the lack of stiffeners on the torque measurement beams and a measurement beam that does span the complete width of the thrust cage. Another large difference between the FF09 and the typical NASA internal balance is that the balance moment center is not located at the center of the thrust section measurement beam.

3.4 Electrical/Sensitivity Requirements

In order to achieve the resolution required to read loads, the balance must be designed to produce a band of stresses ideal for strain gages. NASA LaRC design practices target an output of 1 mV/V for each strain-gage bridge (2). In rearranging Equation 31, stress can be calculated and used in an iterative process to determine the ideal geometry for the balance.

$$output \left(\frac{\mu V}{V}\right) = \sigma \left(\frac{GF}{E}\right) * 10^6 \qquad (31)$$

Rearranged

$$\sigma = \frac{\left(output\left(\frac{\mu V}{V}\right)*\frac{E}{GF}\right)}{10^6} \qquad (32)$$

where GF is the gage factor = 2.2, E = $9.993*10^6$ psi is the modulus of elasticity of the balance material, sigma is the stress, and V is voltage. The 1 mV/V output equates to 4.542 ksi. In order

to complete a design it is infeasible to have every test section output the ideal value so a range of acceptable stresses must be determined. For the purpose of this experiment a range of 4 - 6.8 ksi (or 0.8806 - 1.5 mV) was chosen. Gages are placed as close to the bottom of the measurement beam as possible avoiding the fillets. Figure 24 shows the gage locations on the ODU15X15 balance and identifies the associated Wheatstone bridges.
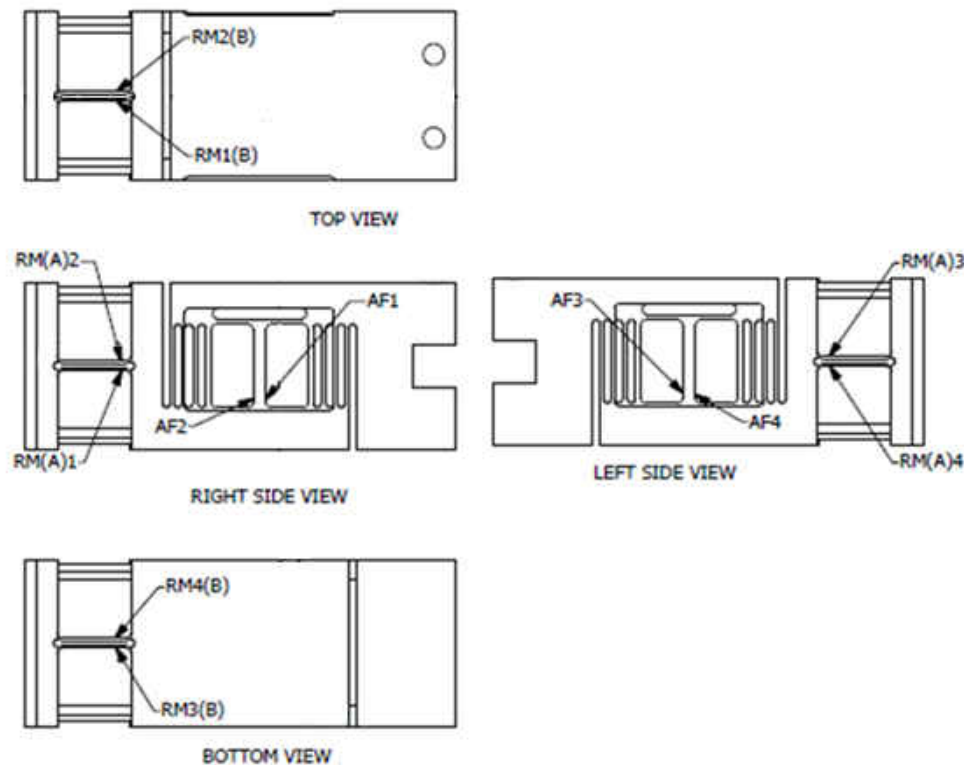
Figure 24: Strain Gage Locations on ODU15X15

Gages used on the ODU15X15 balance are SK-13-050AH-350 made by Micro Measurements. These gages were selected to place small gage active grids in areas of high stress levels, and avoid steep stress gradients, as well as match thermal expansion coefficients for aluminum. The higher the stress under the gage the better the resolution of the system (8). High strain levels and creep can cause issues with gage adherence to the balance surface. Prior to installation of gages the resistance of each gage should be checked and gages with similar resistances should be used

together. Information regarding the application of the gages to the balance such as bonding

agent, clamp pressure, etc. is contained in Appendix A. As shown in Figure 24, two bridges,

RM(A) and RM(B), are used to measure the torque component produced by the propeller and

one bridge (AF) is used to measure thrust.
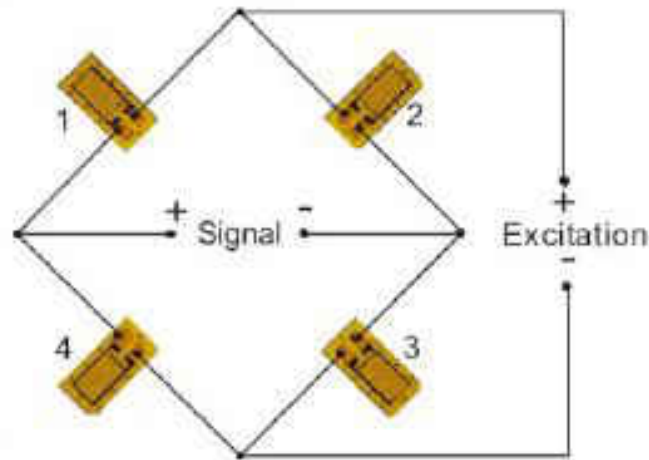
Figure 25: Wheatstone Bridge

 A full Wheatstone bridge is used in order to maximize the output of the bridge, average out gage

misalignments, and average out thermal effects (8). In order to maximize output, two gages (1

and 3) of the bridge are placed in tension while the other two gages (2 and 4) are placed in

compression. For a full Wheatstone bridge, voltage output can be represented in terms of the

gage resistances as shown in Equation 33 (9).

$$\frac{V_{out}}{V_{in}} = \left(\frac{R_4}{R_4+R_1} - \frac{R_3}{R_2+R_3}\right) \qquad (33)$$

Having two torque bridges is not absolutely necessary to capture the torque data. This

was done in the case of the ODU15X15 as a redundancy since there were two extra cage beams.

However, combining both sets of bridges provides a robust signal.

Careful placement of gages on torque cage beams can reduce the effects of side and

normal forces. Equation 34 gives the stress output for the bridge, and can be used to determine

the effect of forces on a particular bridge by inserting positive values for gages in tension, and negative values for gages in compression.

$$Output = \frac{(1+3)-(2+4)}{4} \qquad (34)$$

Evaluating this equation on bridge RMA with a normal force applied downward on the balance it can be shown that the placement of the gages produces zero output under this load. This means that the bridge would not register a voltage output based on an applied normal force, and the weight of components mounted to the end of the balance would not excite the bridges.

$$Output = \frac{((-1)+(1))-((1)+(-1))}{4} = 0$$

In cases where multiple attributes are required to be measured this can be especially useful to eliminate interactions.

Alternate methods for mounting the gages include affixing the bridges all on one beam or on consecutive beams. The small size of the torque measurement beams does not allow for the installation of all four gages of a Wheatstone bridge on one beam. However, if it were possible this would reduce thermal effects on the bridge, and while a second gage could be installed further down the beam, it would not have the same excitation as the first gage. This is because the maximum stress of a beam is seen at the fixed end and linearly decreases toward the free end of the beam. Due to the asymmetry caused by the end gaps, mounting bridges on consecutive beams is not ideal either. This is because the upper portion of the balance is not fixed as the lower portion is, allowing for higher stresses to occur on the lower beam. By situating the bridge halves across from each other, the horizontal pairs RM(A) see very similar stresses/excitations while the vertical pairs RM(B) see a slight difference in stresses/excitations. Voltage data is measured and recorded using a National Instruments (NI) Data Acquisition Board (DAQ) and

LabView software. LabView code can be found in Appendix C. Calibration hardware and testing set-ups are discussed in section 4.1and wiring diagrams can be found in AppendixB.

3.5   Temperature Compensation

Temperature compensation can be achieved passively (through the addition of a resistor in the Wheatstone bridge) and actively (through calibration). Pre-stresses associated with the installation of strain gages create an offset of the output of the strain gage. This initial non-zero offset becomes the baseline for the rest of calibration/testing. When the balance is heated, thermal strain is sensed by the strain gages, which is caused by a number of factors. To passively combat these effects, a temperature sensitive wire/resistor is added to one leg of the Wheatstone bridge that will increase in resistance as the temperature rises.
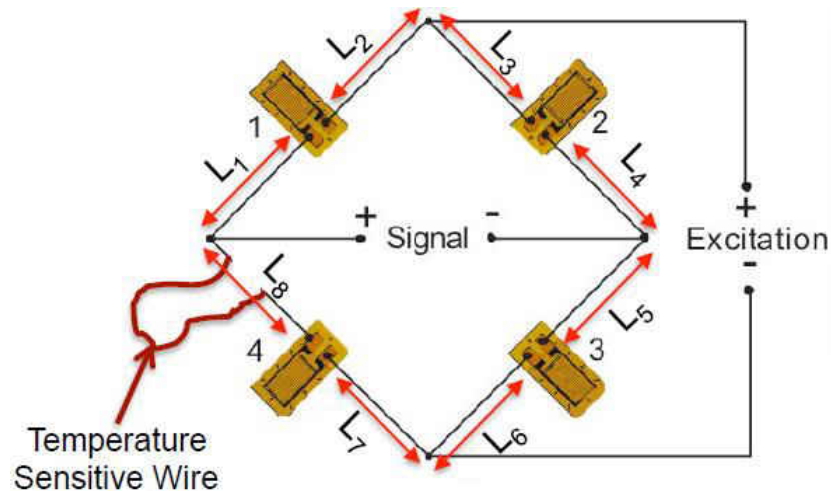
Figure 26: Wheatstone Bridge with Temperature Compensation

The size of the wire/resistor is determined by heating and cooling the balance, and iteratively changing the resistor size until the change in output voltage due to temperature only is between 3-5microV/V over an 80-180 $^\circ$F temperature range (8). A typical temperature compensation run is shown in Figure 27.
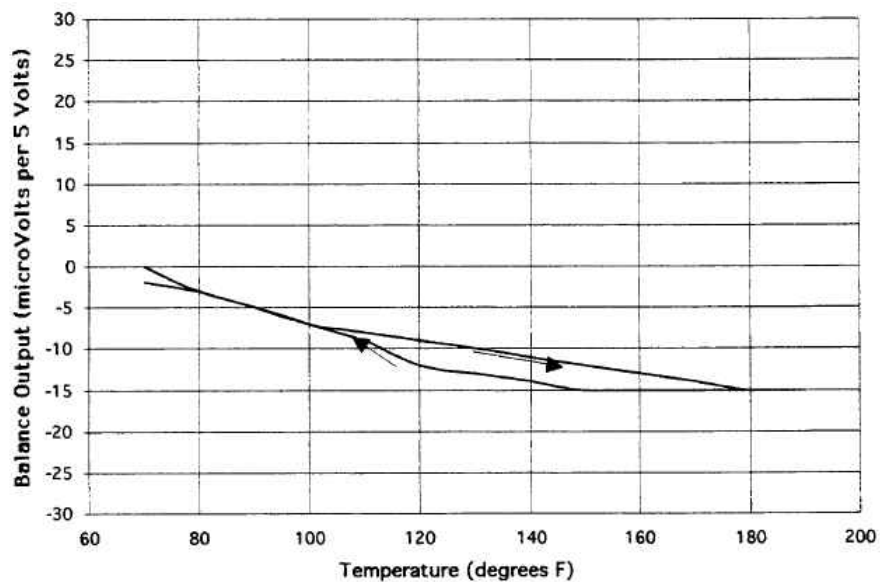
Figure 27: Example of Balance Temperature Compensation Run

3.6   Calibration Fixture

Pictured below are the calibration stands, and adapters.

Figure 28: Calibration Fixtures

Figure 29: Calibration Adapter

The calibration stands shown in Figure 28 were made using steel bar stock. The stand on the left is used to hold the balance in place, while the stand on the right is used in the application of the thrust load. A brief FEA was performed on both stands to ensure the structures minimally deflected under full load. The calibration adapter shown in Figure 29 is used to apply both the thrust and torque loads to the balance. The adapter (the square aluminum piece) is affixed to the front of the balance, and holds the torque arm (the long rectangular tube) in place. The torque arm was also analyzed through FEA. This analysis was done in order to minimize weight, while maintaining the stiffness of the beam. It was determined that a steel structural tube would provide the best stiffness to weight ratio compared to a solid piece of steel. The drawings used to make the test stand and adaptor can be found in AppendixD.

To apply known torques, dowel pins were used to precisely locate the arm to the metric end of the balance. The hardened steel dowel pins were chosen for their extremely tight

tolerance. The length of the adaptor arm was dictated by the strength of the material and the torque that was to be applied to the end of the balance. It is recommended to make the arm as long as possible to reduce the size of the weight that is to be added to the end of the arm. A 15 in long arm centered on the balance allowed a 2 lb weight in order to apply the full scale 15 in-lbs of torque.
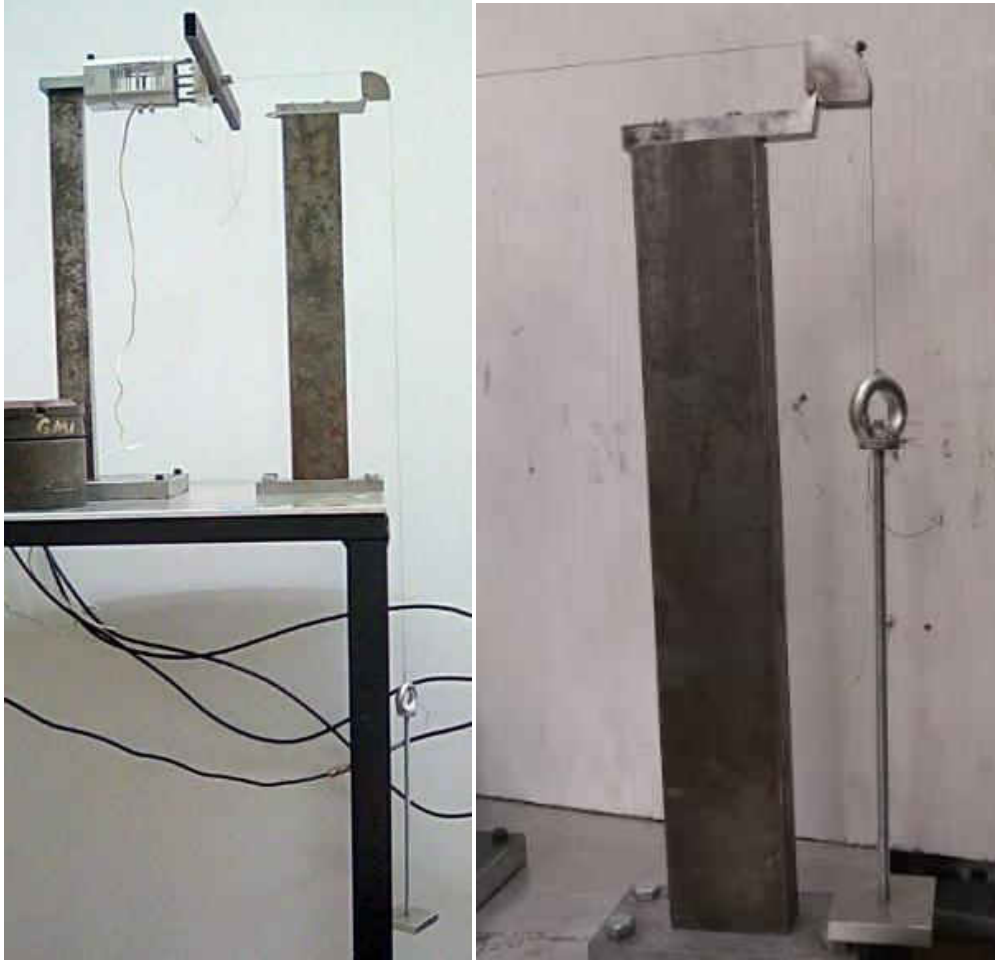
Figure 30: Calibration Set-up

A frictionless knife edge pivot was used with fishing line to apply the thrust load. The pivot has a set screw clamp that accommodates the stretch in the line under load. To ensure the pivot's weight has no affect on the readings it is necessary to ensure that the vertical face is perpendicular to the floor.

Figure 31: Pivot Orientation

The line is fastened to a load platen where the weights may be applied. On the opposite end at the adapter, the fishing line is fed through a drilled socket head cap screw and tied to a washer. The washer is held in place by the hex pattern of the socket head cap screw as shown in Figure 29. The tare weight is removed from the calibration using an iterative process discussed later.

The calibration stand is designed for minimum deflection so it is overly stiff for the forces applied. Alignment of the stand is critical to ensure that the thrust force is applied perpendicular to the balance.

3.7   Stress Analysis

Both a static and dynamic stress analysis were performed to ensure that the balance is sensitive to the force/moment ranges required, and that the propeller passing frequency

frequencies fall above or below the fundamental frequency of the balance. Autodesk Inventor (version 2016) software for finite element analysis was used for this study.

In both analyses, the material, constraints, contacts between components, and mesh are identical. Loads are only applied in the static case. The material properties for the aluminum used to make the balance are entered into the analysis. Figure 32 shows the material properties used for the 6061-T6511 aluminum.
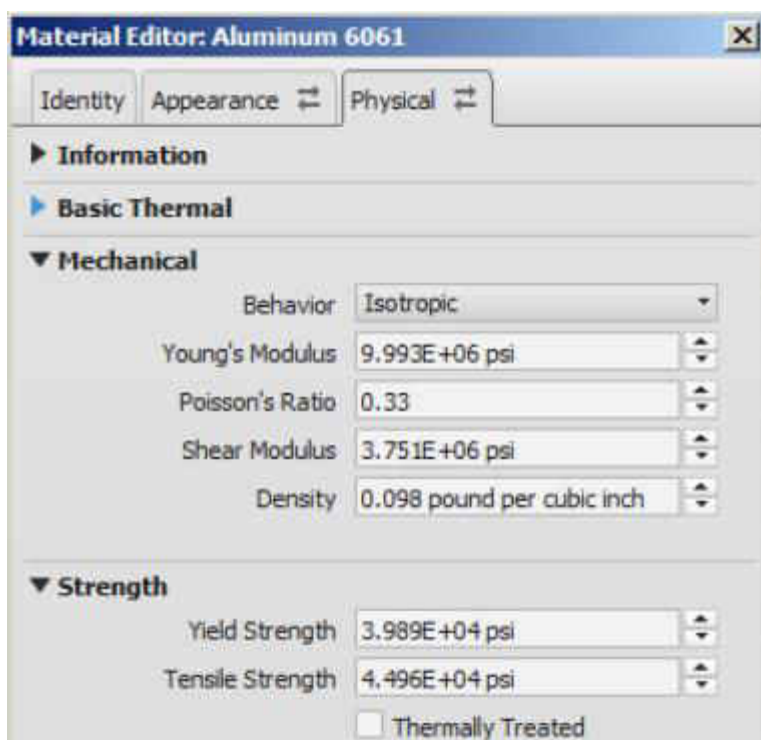
Figure 32: Material Properties of 6061-T6511 Aluminum

Boundary conditions (constraints and loads) are then applied to the balance and are shown in Figure 33. A fixed constraint is applied to the three balance surfaces that come into contact with the calibration/test stands. The mount supports are not included in this selection. A 15 in-lb torque applied clockwise around the z axis is placed on an imaginary cylinder with a diameter of 25mm fixed inside the endplate on the balance. The motor operates in the counter clockwise direction so the balance sees a moment of equal magnitude in the opposite direction. This outside

diameter of the cylinder represents the bolt circle diameter of the motor. A 15 lb force going from right to left, split between four bolt hole centers in this imaginary cylinder, are applied to the endplate face. A 1 lb force going straight down is placed on the edge of an imaginary rectangle that goes straight through the center of the balance to simulate the weight of all of the components attached to the end of the balance (i.e. motor, propeller, and fasteners). Inventor's gravity function was also activated.
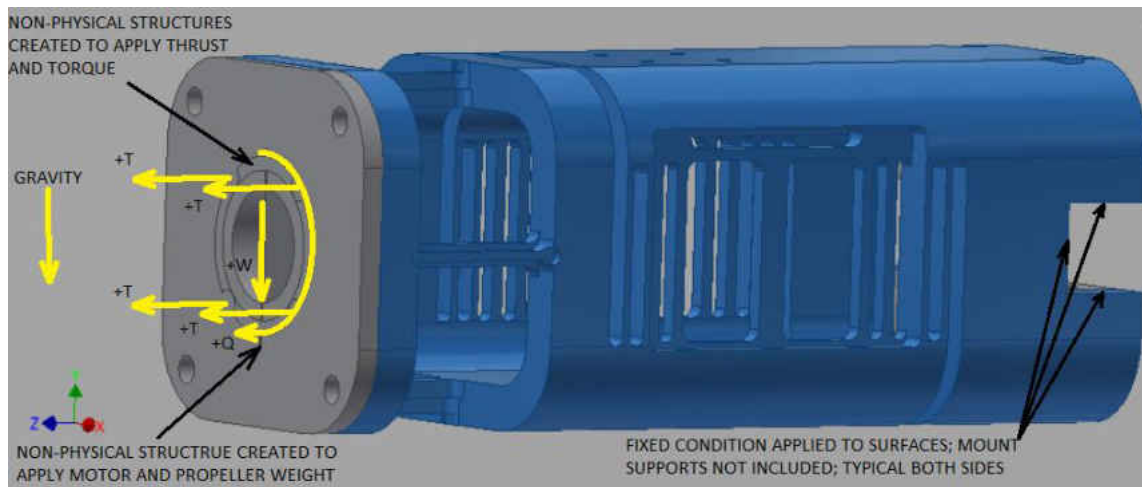
Figure 33: Stress Analysis Boundary Conditions

Once the boundary conditions are determined contacts between components are created. All surface contacts in this simulation are set to "bonded". This means that they are an ideal joint, and that the parts are not allowed to move in any way in relation to each other. Next a mesh is generated using Inventor's auto mesh feature. The mesh is then manipulated by adding local mesh controls to surfaces and edges. On the ODU15X15 a local mesh control is placed to change the size to 0.01 inches on all the measurement beam surfaces where strain gages are to be attached along with conjoining radii, as shown in Figure 34.
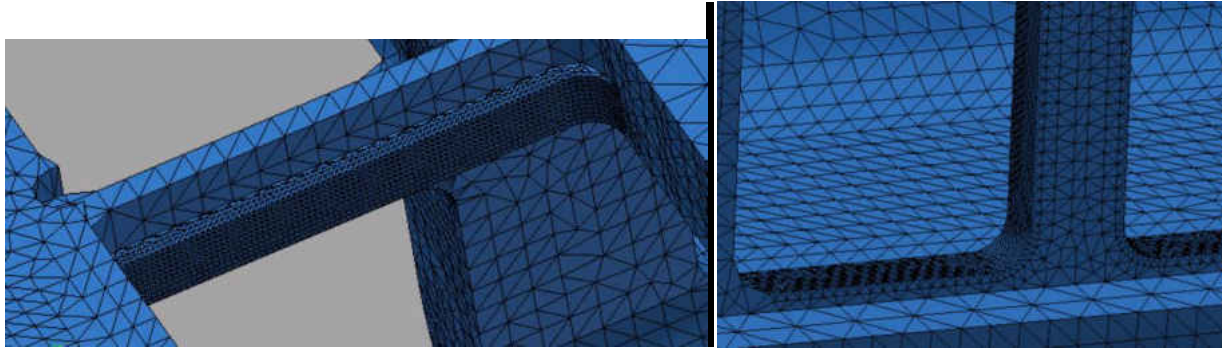
Figure 34: Typical Mesh on Measurement Beams

Most other critical/high motion surfaces (such as the thrust cage flex beams) have a local mesh

control of 0.05 inches (Figure 35) while the non-critical surfaces of the balance are left with the

original auto generated mesh size.
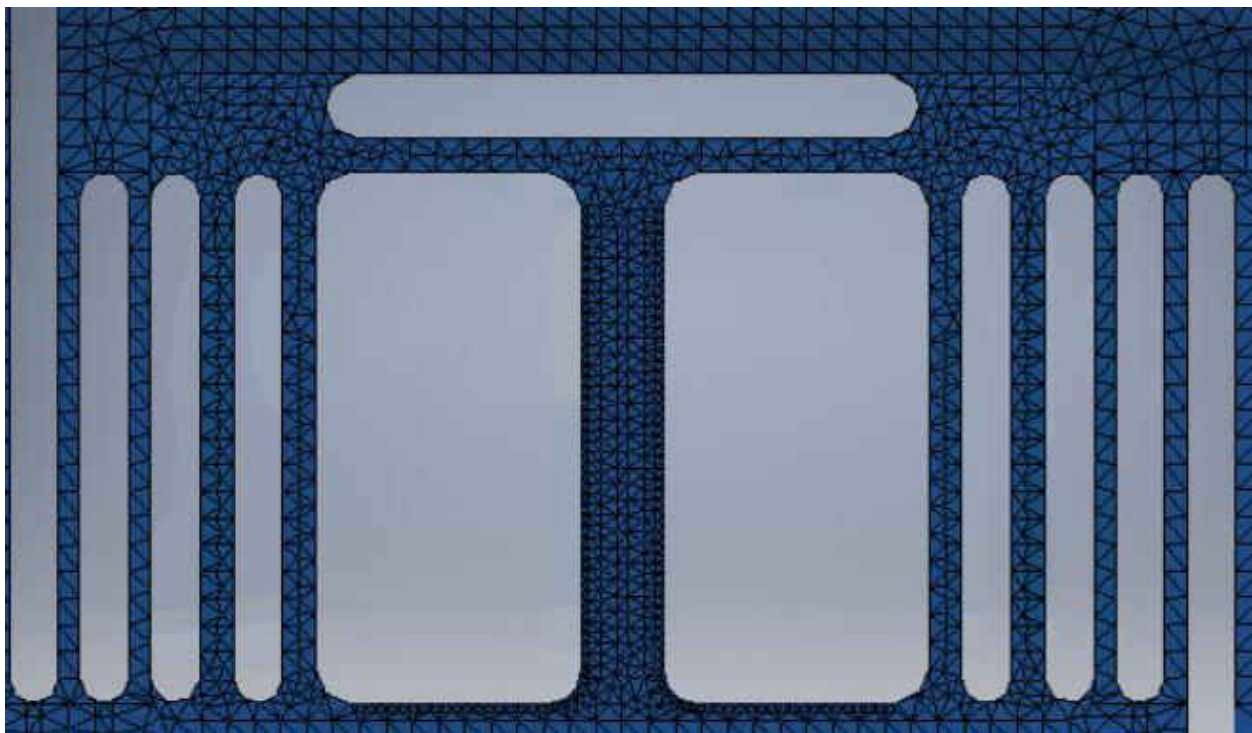
Figure 35: Thrust Section Mesh

In non-critical areas mesh size is not as important due to the lack of stress

gradients/concentrations. Note in Figure 36 below that the top and bottom right portions of the

balance are left with the original auto-generated mesh. Larger sections of the balance could be

covered in the auto-generated mesh. However since Inventor requires an entire continuous surface, or edge be picked to change the mesh size of an area; larger portions of the balance are covered in the 0.05 inch mesh control. Therefore any continuous plane not broken up by an edge will have the same mesh size over the entire section.
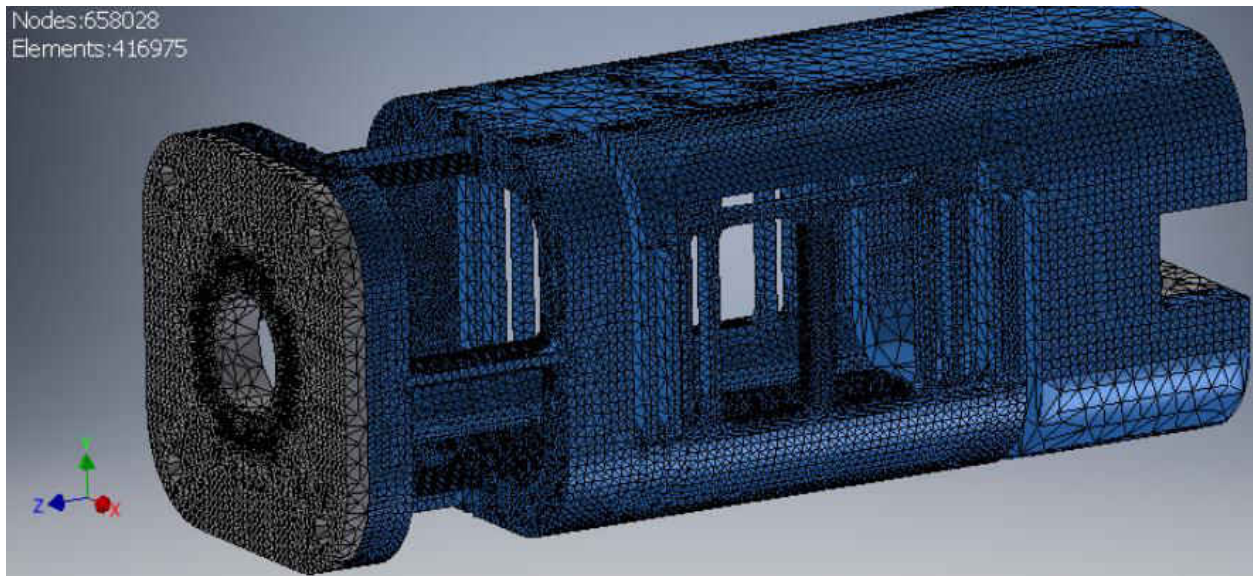
Figure 36: Full Balance Mesh

Due to the creation of the imaginary geometry to apply loads on the balance in specific locations, the auto-mesh feature generates a dense area of smaller elements on the surface of the end cap. The program assumes there is a high interest area at this point. However the imaginary structure and end cap are bonded to eliminate movement so no gradients will occur. A local mesh control is unable to change this effect. Once the mesh is generated the analysis can begin.

3.7.1 Static (Motor OFF) case

All of the static stresses calculated in the simulation fell within the 4 - 6.8 ksi range chosen (see section3.4). Figure 37 shows the acceptable results for the stress analysis.
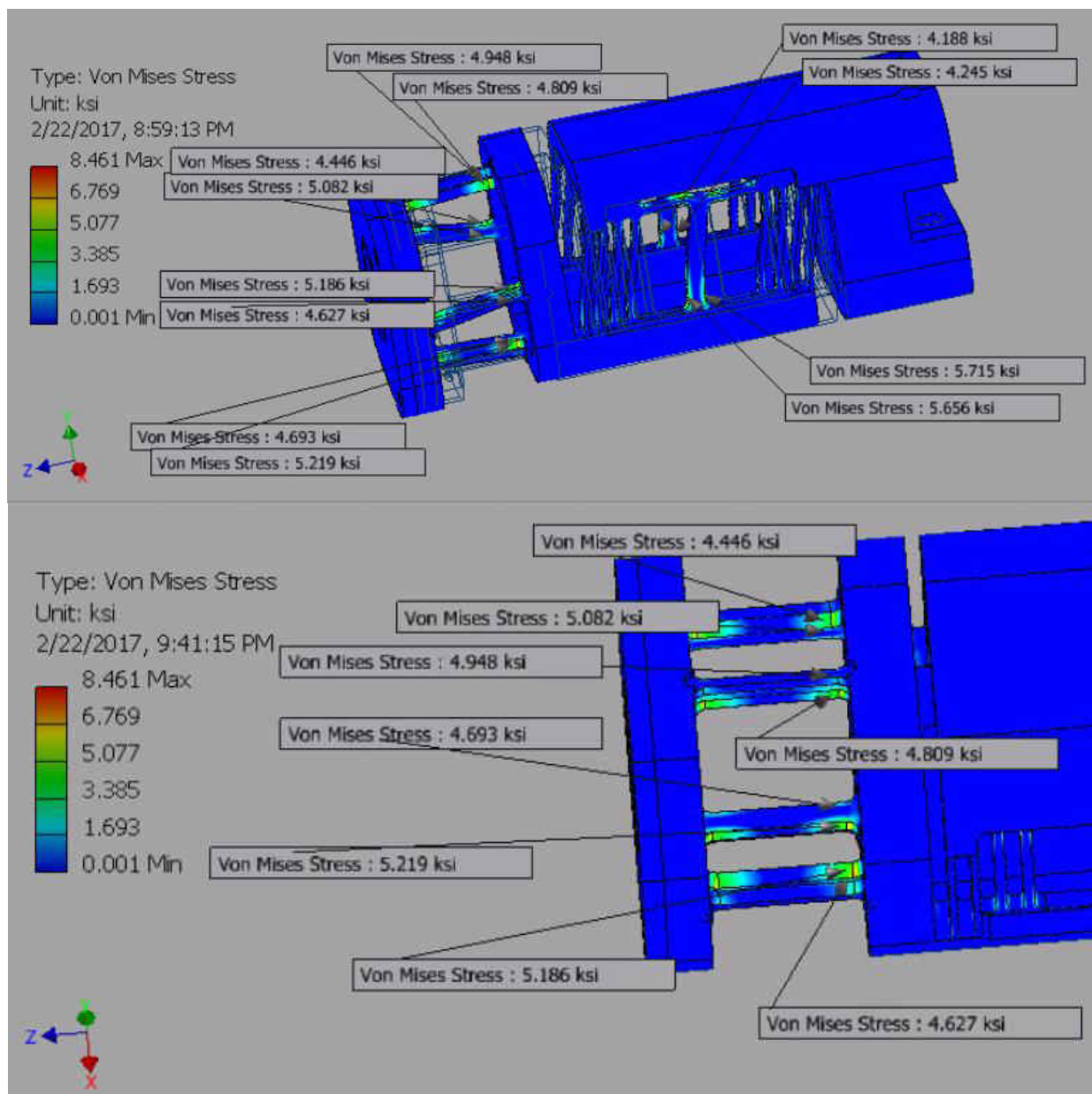
Figure 37: Stress Analysis (ksi)

Von Mises stresses resolve multi-directional stresses into an equivalent uniaxial stress at any particular location (10). Figure 38 shows the direction and surface where each stress component acts. Equation 35 defines the Von Mises stress.

$$\sigma_{eq} = \sqrt{\frac{1}{2}\left((\sigma_{11} - \sigma_{22})^2 + (\sigma_{22} - \sigma_{33})^2 + (\sigma_{33} - \sigma_{11})^2 + 6(\sigma_{12}^2 + \sigma_{23}^2 + \sigma_{31}^2)\right)} \qquad (35)$$
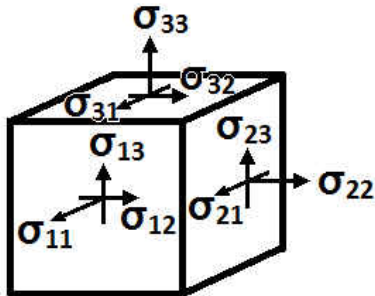
Figure 38: Von Mises Stresses

Figure 39 shows the typical placement of the FEA data probes on the thrust section. These probes allow the user to determine various attributes at particular points on the model
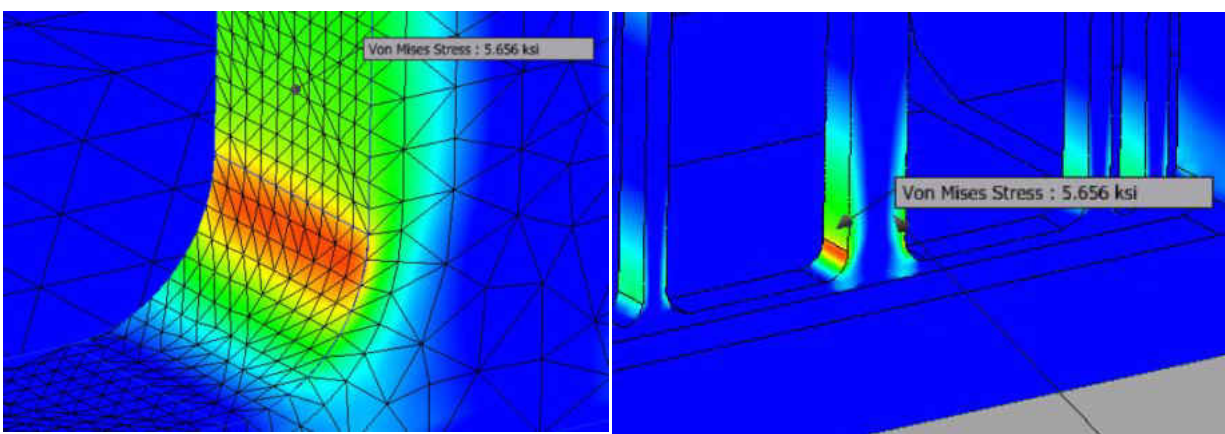
Figure 39: Thrust Section Typical Probe Placement

Figure 40 shows the typical placement of the probes on the torque section.
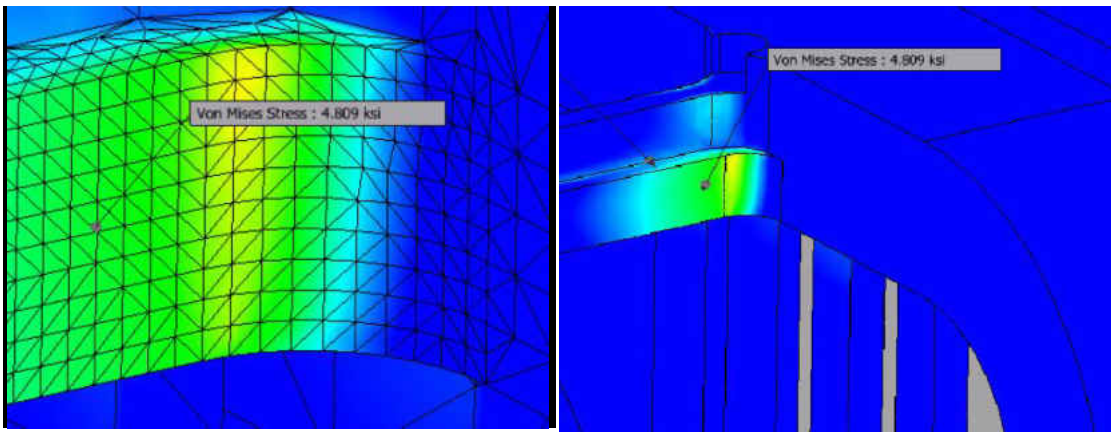
Figure 40: Torque Section Typical Probe Placement

Probes are placed approximately 0.04 inches from the fillets and centered on the measurement beam on both the thrust and torque sections (i.e. mesh grid spacing 0.01 inches). This position corresponds to the active grid center of the strain gage that is to be used with the inactive soldering tabs butted up against the edge of the fillet, as shown in Figure 41.
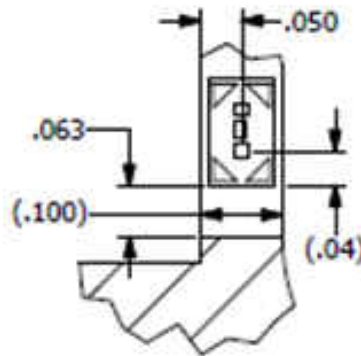
Figure 41: Typical Gage Placement on Thrust Section Measurement Beam

The radius of the thrust section fillets is 1/16 inch. The positions of the probes were determined by the geometry of the strain gage as well as the locations of the highest stress on the simulation. Torque, or the rolling moment, as it is called in the design of NASA internal balances, is hard to predict (5). It can also be measured in a number of different locations along the balance to include flex beams in the thrust section.

The displacements of the balance under load follow the conventions set forth by section 3.3 with slight variations. These asymmetric variations in displacement are considered negligible, and are most likely the result of the application of both thrust and torque (as opposed to the single load applied in the previous section), and the asymmetry in the geometry caused by the end gaps. The deflections presented in Figures 42-45 are due to full-scale torque and thrust applied simultaneously.
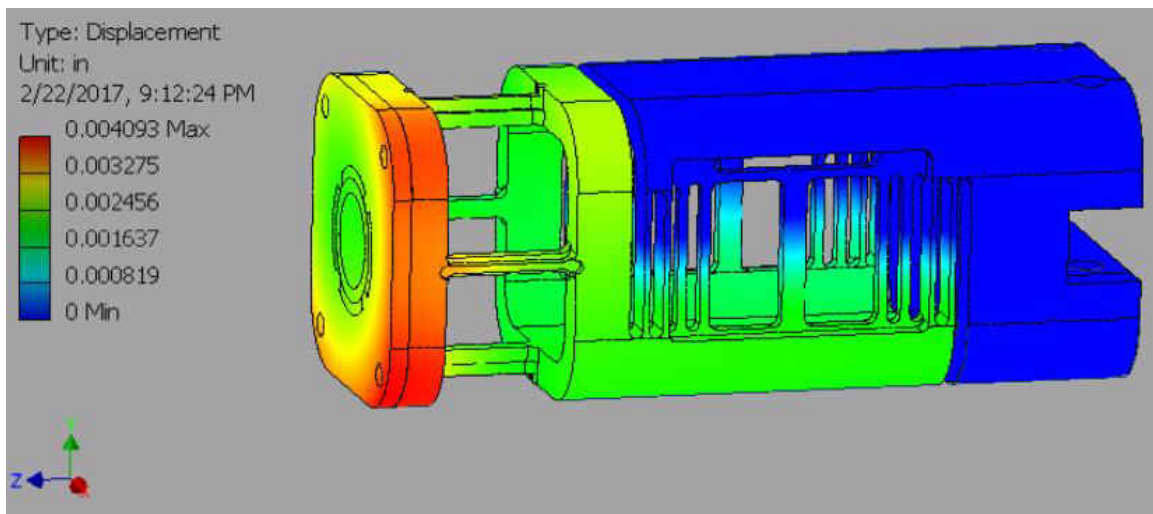
Figure 42: Resultant Displacement
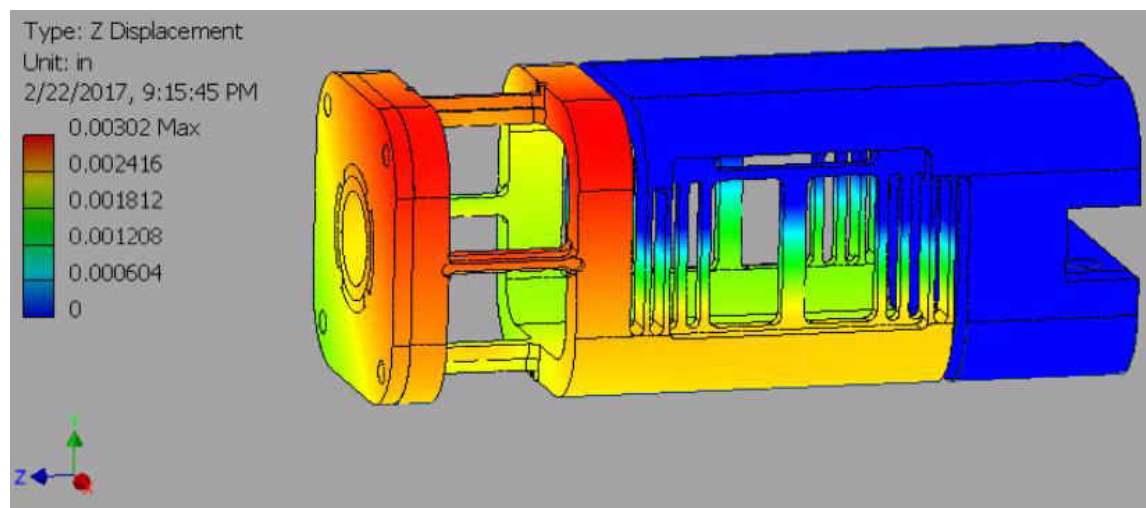
Figure 43: Z-Displacement
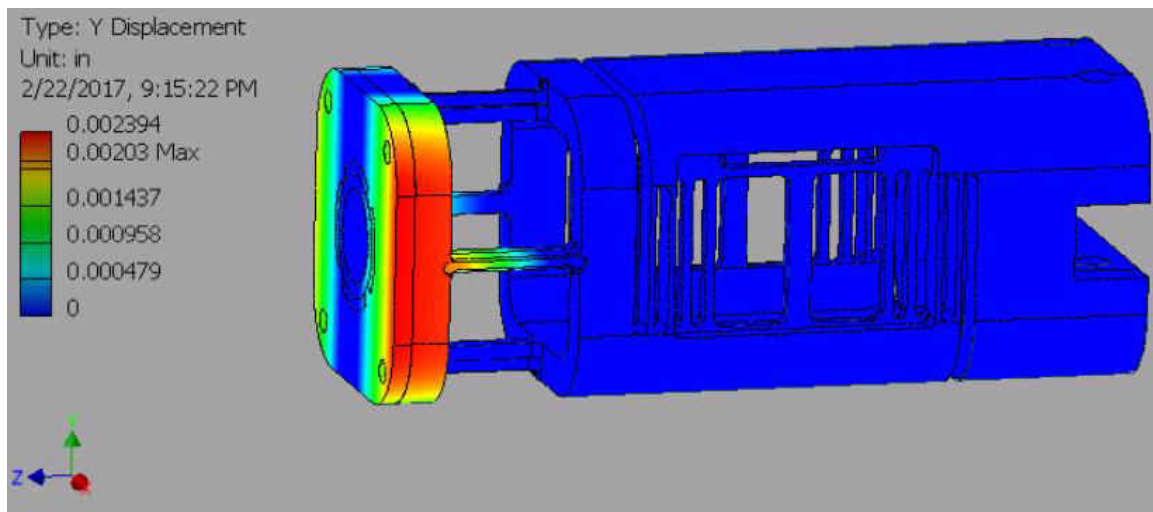
Figure 44: Y-Displacement
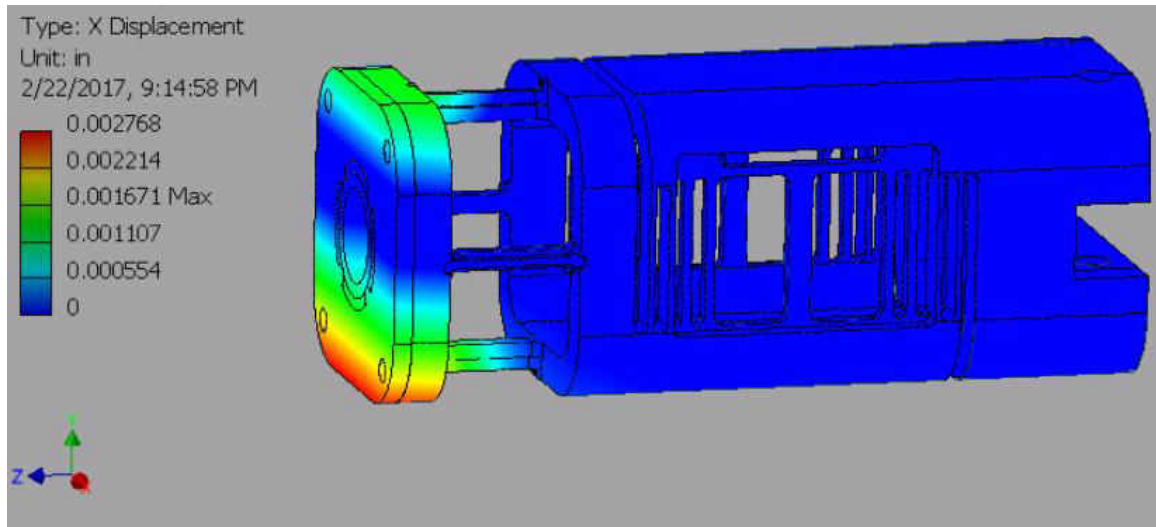
Figure 45: X- Displacement

Note that there is no displacement of the thrust section in the X or Y components, and that the torque measurement beams are almost solid in color in the Z component. This means that all of the strain gages placed on these measurement beams should read the force they are designed to read. A characteristic not shown above in section 3.3 is a similar displacement gradient in the torque section as the thrust section. This is shown in Figure 43, Figure 44, and Figure 45 above where the maximum displacement is on the left end of the torque measurement beam and no displacement on the right side creating a moment across the torque measurement beam.

The maximum displacement in the Z-component is 0.00302 inches. As before the maximum displacement is on the bottom of the balance and is almost uniform. There is less than 0.001 inches difference between the two thrust measurement beams. This is not considered to be an issue as the stresses meet the sensitivity requirements of the strain gages, the difference is very small, and the balance will be calibrated.

The load proportion ratio, addressed in section 2.1, was calculated for both the right and left sides of the balance under full load, as shown in Figure 46. Local probes were used to

determine stress values for all eight flex beams and the measurement beam. Probes were placed at the highest stress points on each of the beams.
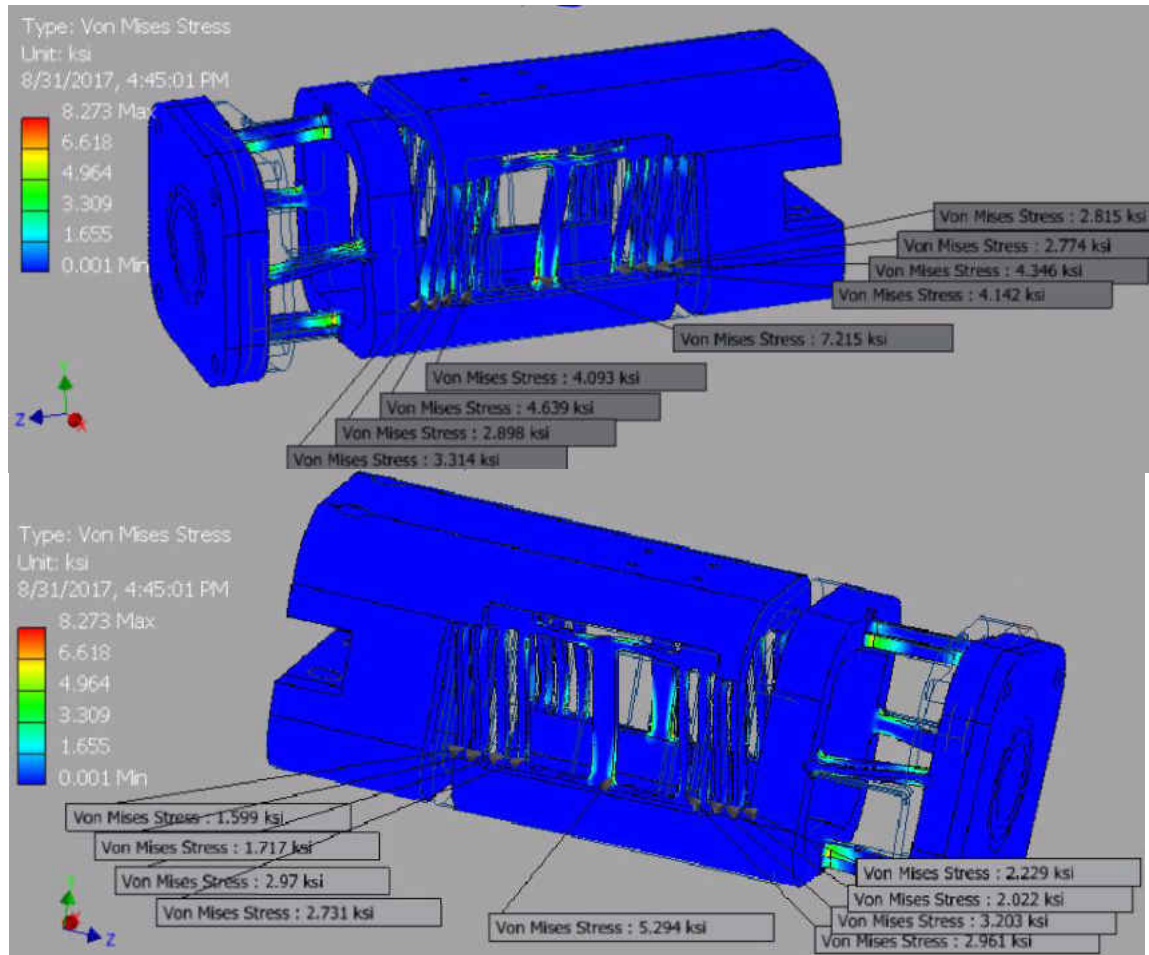
Figure 46: Stresses Used for Load Proportion Ratio

The equation below is used to calculate the ratio.

$$L_{NM} = \frac{\sigma_m}{\sigma_m + average(\sigma_f)} \qquad (36)$$

$$L_{NF} = \frac{average(\sigma_f)}{\sigma_m + average(\sigma_f)} \qquad (37)$$

The FEA analysis predicts that the load proportion ratio to be 0.665:0.335 for the right side, and 0.685:0.315 for the left side. The load proportion ratios were also analytically calculated using

Equations 10 and 11. L_{NM} = 0.5439, and L_{NF} = 0.4560. Due to the two different size flex beams on the balance, two spring constants were required to be calculated in the analytical method. These two spring constants were then added together to create an overall flex beam spring constant. The safety factor of the balance under load is shown below.
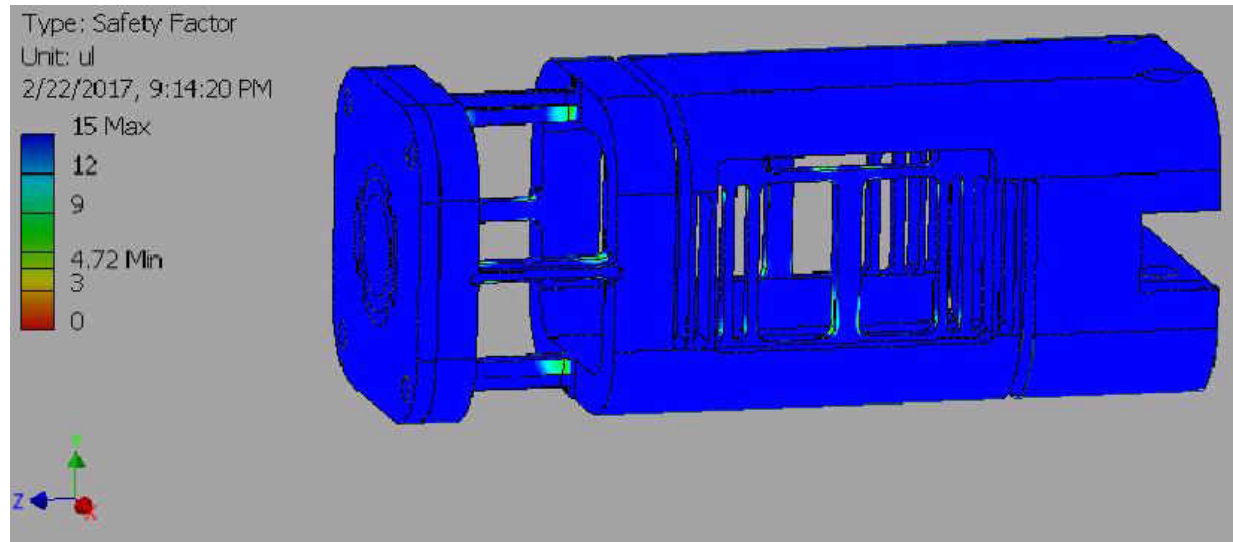
Figure 47: Safety Factor (4.72)

An analysis of the ODU15X15 balance using equations 13 and 27, presented in section 2.1, yield stresses under the strain gages of 5.41 ksi for the thrust measurement beams and 4.785 ksi for the torque measurement beams. Since the torque measurement beams do not have rectangular cross sections the equations in section 2.1 have to be modified to incorporate the proper area moments of inertia. The analytical and FEA analyses can be compared to calibration data where applied thrust is 14 lb and applied torque is 15 in-lb, such as run 1. The run 1 raw voltage data for thrust and torque are multiplied by 1000 to convert to mV, and then divided by the sense to get output in mV/V; giving Thrust = 0.9532 Torque1 = 1.017 Torque2 = 1.057. Applying Equation 34 to the FEA for each bridge the following stress outputs are obtained: Thrust = 4.933 ksi Torque = 4.835 ksi Torque = 4.917 ksi. These values show that the FEA stresses, analytical stresses, and actual balance outputs correspond well (1 mV/V = 4.542 ksi). Note that 15 lbs thrust is applied in

the FEA, while 14 lbs thrust is applied in the calibration. For detailed calibration information see section 4.

3.7.2   Dynamic (Motor ON) case

A frequency analysis was performed to find the balance's natural frequency. A one lb mass cylinder is constrained to the end of the balance to simulate the motor and propeller component's mass, and position of the center of gravity. Using the speed of the motor, a passing frequency output can be calculated for a given number of blades on a propeller. This value is used in the frequency analysis and the design of the balance in order to avoid (above or below) exciting the natural resonance in the balance (11). As an example consider a rotational speed of 10,000 RPM and a two blade propeller. The frequency to be avoided is 333 Hz.

$$\frac{10,000\frac{Rev}{min}}{60\frac{sec}{min}} * 2\ blades = 333\ Hz \qquad (38)$$

Figure 48 shows the final modal analysis of the ODU15X15 balance, which has a fundamental of 107 Hz. A full modal analysis will also predict higher frequencies and should be evaluated.
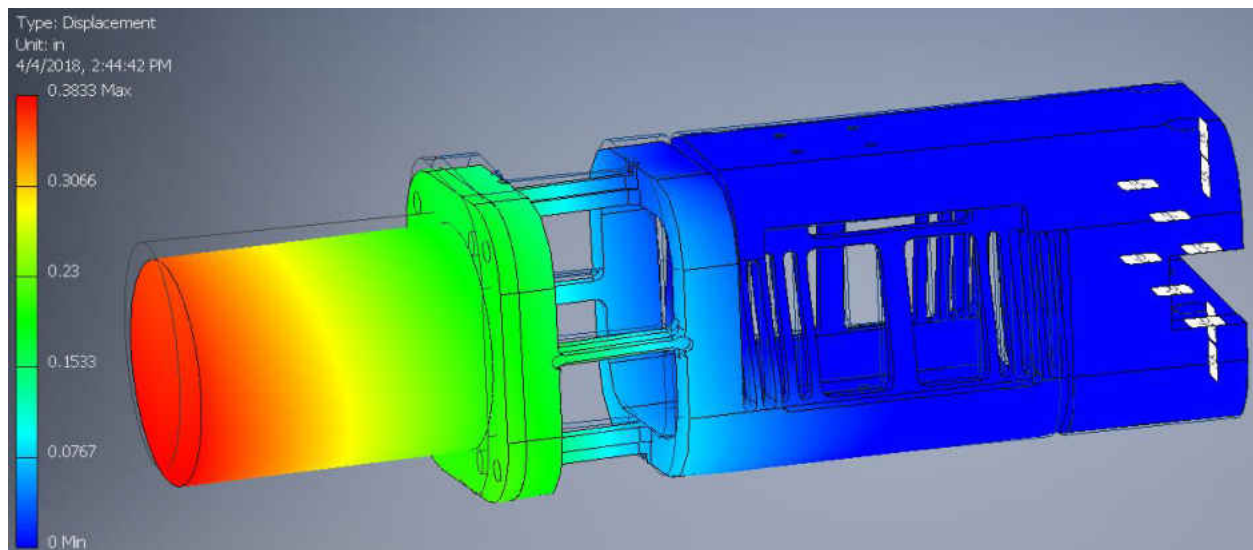
Figure 48: Frequency Analysis

While this analysis is done through computer simulation, a physical test could also be performed. In RUAG's propeller balance development, unsteady frequency testing was employed. The balance and test article were excited to a set frequency while load measurements were completed (11). Frequencies chosen were based on propeller blade count and RPM. Use of the ODU15x15 will require careful consideration of the dynamic loads on a case by case basis. It is important to use balanced propellers to avoid excitation.

4   CALIBRATION

4.1 Calibration Set-up

The calibration of a balance requires a number of different components. This includes a power supply, junction box, weight platens, the previously described test stands and arms, and a voltage data acquisition system. See sections 3.4 and 3.6 for the design discussion of these components. The rig allows for known static forces to be applied to the balance, while the stand and data acquisition equipment provide a rigid support to keep the balance from moving and record the voltage outputs of the balance, respectively. The final calibration set-up is pictured below.
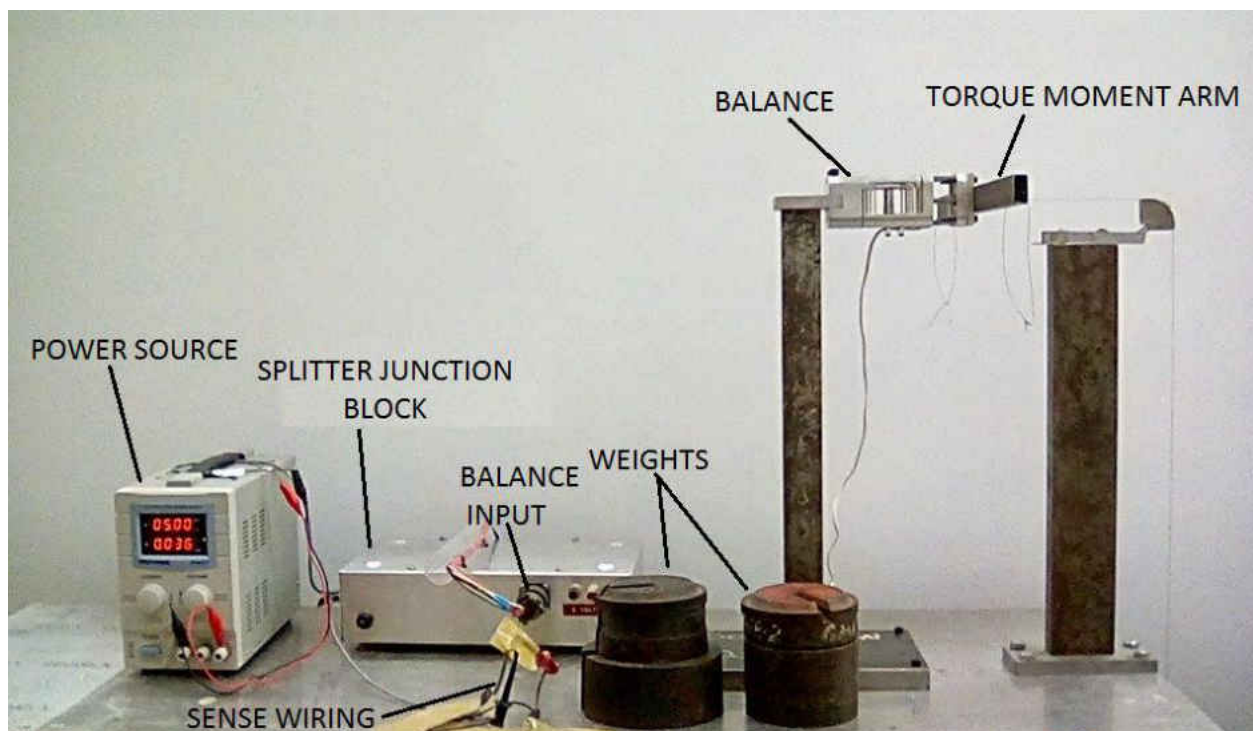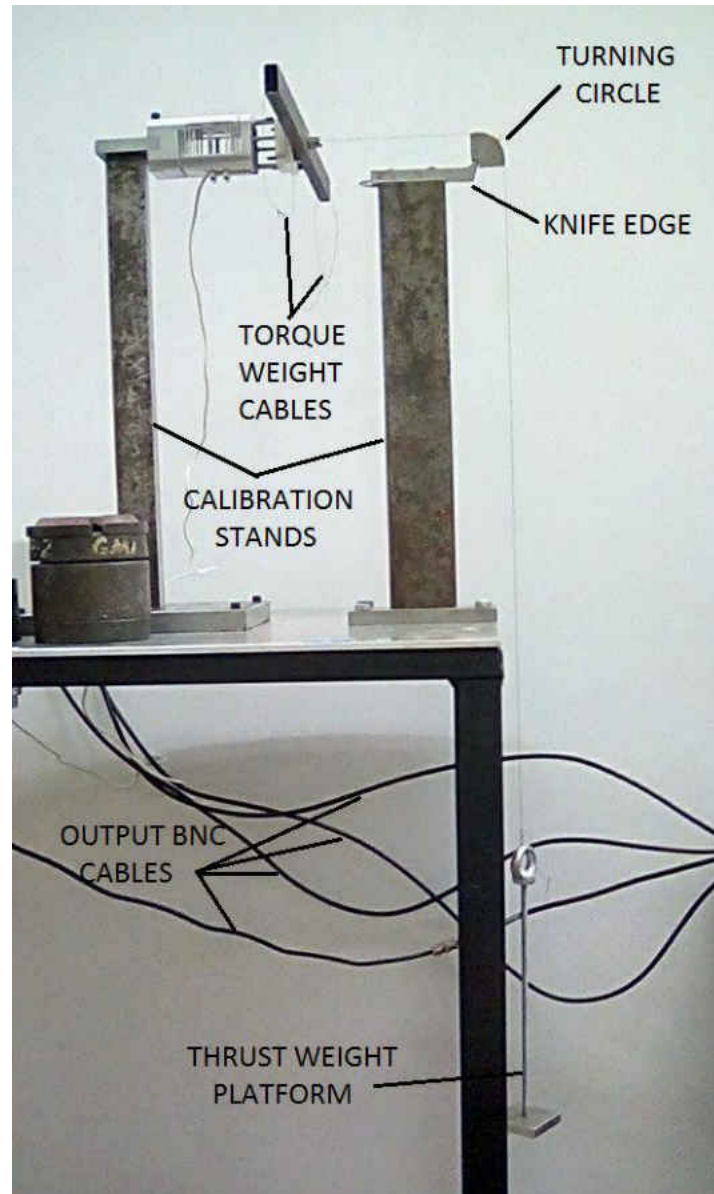
Figure 49: Calibration Set-up

A junction box is used in order to direct all of the current flows, and to create a robust connection between each of the components. As shown in the photo above the power is supplied to the balance bridges from the left side of the junction box. The voltage source and sense lines connect to the bottom of the junction box. BNC connectors are used on the back side of the box to provide the output signals for each of the Wheatstone. BNC cables with low pass filters, which filter out anything above 40 Hz, are then used to connect the splitter junction box to the DAQ

(exits right), which then connects to the computer. Sense lines are used to monitor the actual voltage supplied to the balance. Using sense to measure the voltage at the bridge supply, it is determined that the power supply is to be set to 5.14 volts in order to achieve the required 5 volt input at the bridges. The wire length from the balance to the splitter junction box if 6ft. Current supplied to the balance is determined by the power supply module and was recorded to be 0.042 amps at the time of calibration.
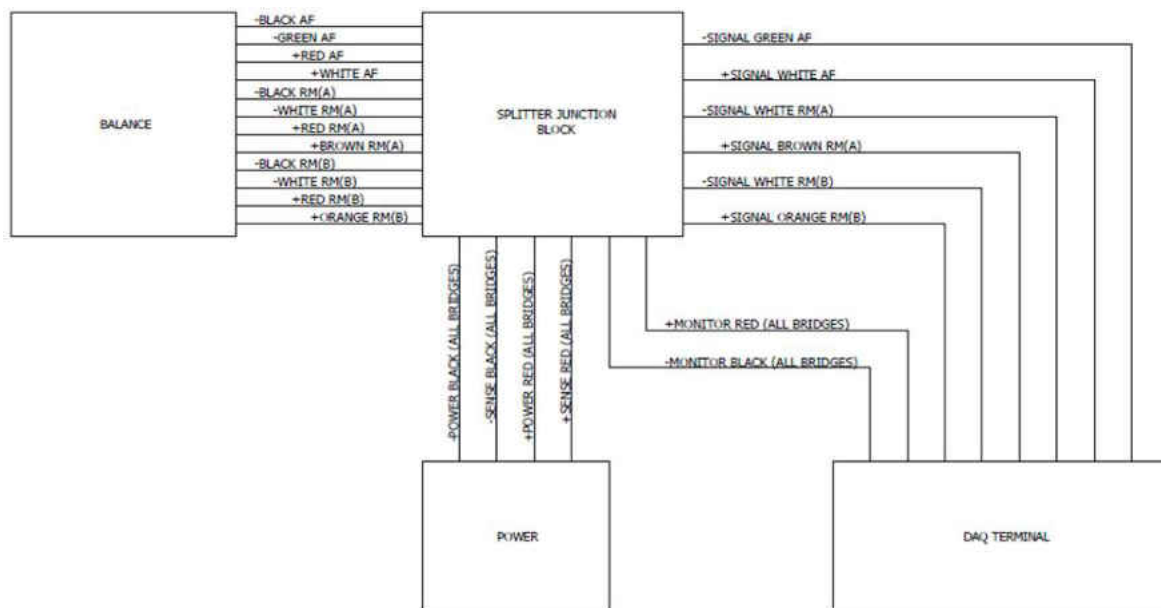
Figure 50: Calibration Wiring Diagram

The complete calibration wiring diagram is provided in Appendix B.

The calibration stands are installed on a level rigid metal table. The table is a tube steel frame with a piece of 0.25 inch thick aluminum plate covering the top. The assemblies are aligned to each other with spirit levels and by taking measurements from the bases using calipers.

With the stands installed and the wiring in place, the balance can be installed onto the calibration stand. The attachment point for the balance is identical to the attachment point used to mount the balance during testing. The adapter is then assembled. Two tapered dowel pins locate

the torque moment arm onto the adapter plate. A socket head cap screw with a hole running through it is then installed on the center of the adapter plate to apply the thrust loads and hold the torque moment arm in place. Fishing line long enough to hang off the table, as shown in Figure 49, is tied to a washer and then the other end is fed through the hole in the socket head cap screw. The washer stops the line from passing completely through the fastener, as shown in Figure 29. The adapter is then installed onto the balance, and fishing line is looped through the holes on either end of the torque moment arm, tied off, and hung for the duration of calibration. The knife edge pivot is then installed to the top of the opposite calibration stand. The line passes over the turning circle and hangs. The bolt on the turning circle is used to hold the turning circle in place while no load is applied. Only the vertex of the knife edge pivot comes into contact with the knife edge. A weight platform is then hung from this fishing line where it will remain for the duration of the calibration process. To verify the perpendicularity of the thrust line to the balance in the horizontal plane a square is placed along the torque moment arm. If adjustments are needed the holes in the knife edge are large enough to slightly modify its position. In the vertical plane a level and a pair of calipers are used. The level is set along the top of the balance and the calipers are used to measure between the level and the fishing line near the balance and then again near the knife edge. The knife edge was then shimmed until the two measurements matched. The torque arm did not require adjustments, because the arm is fitted with dowel holes to locate it precisely to the adapter plate, the bottom of the weight mounting holes are flush with the center of the beam, and the holes are 7.5 inches from the center of the balance.

4.2 Calibration Procedure

A calibration must be completed in order to relate the voltage output to the force being applied. This is done by applying known loads and recording the voltage output of the bridges. With this information, an empirical math model can be created to relate applied loads to electrical signals. The best calibrations are achieved when the balance experiences the same environmental conditions during calibration as it will see during testing (6).

The calibration load schedule for the ODU15X15 balance was completed using the principles of Design of Experiments (12). A sequential experiment featuring a 2^k factorial design and subsequent augmentation to a Central Composite Design (CCD) was proposed.
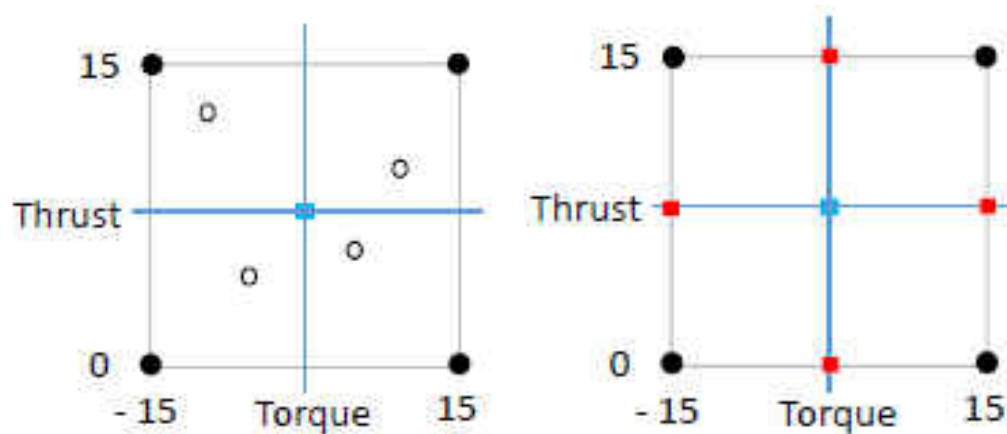
Figure 51: Factorial and CCD Calibration Designs

The left square with the solid black and center blue data points represents the required data points to produce a first order plus two factor interaction model. This is the classic factorial design. The open circles in the interior of the square are confirmation points. These points are used to compare measurements to empirical model predictions. The right square shows the additional points required in red to produce a quadratic model. Using the factorial design, the center points allow a test for quadratic curvature. That test result will decide whether a full quadratic model would better represent the data. Available weights for the calibration dictated

that the thrust limits be dropped to 14 lbs. The final design load schedule featuring the factorial

design in block one and the extra points required for the CCD in block 2 is given in Table 1.

Center points are included in both blocks. The run schedule is fully randomized.

Block	Run	Type	Thrust (lb)	Torque (in-lb)
Block 1	1	Factorial	14	15
Block 1	2	Factorial	0	15
Block 1	3	Factorial	0	-15
Block 1	4	Confirmation	12	7.5
Block 1	5	Confirmation	2	7.5
Block 1	6	Center	7	0
Block 1	7	Confirmation	4	-7.5
Block 1	8	Confirmation	5	7.5
Block 1	9	Confirmation	12	-7.5
Block 1	10	Center	7	0
Block 1	11	Factorial	14	-15
Block 1	12	Center	7	0
Block 1	13	Factorial	0	15
Block 1	14	Factorial	0	-15
Block 1	15	Factorial	14	-15
Block 1	16	Factorial	14	15
Block 2	17	Axial	14	0
Block 2	18	Axial	0	0
Block 2	19	Axial	7	15
Block 2	20	Axial	7	-15
Block 2	21	Axial	0	0
Block 2	22	Axial	7	15
Block 2	23	Axial	14	0
Block 2	24	Center	7	0
Block 2	25	Center	7	0
Block 2	26	Axial	7	-15

Table 1: Calibration Run Schedule

Prior to starting the calibration experiment, the balance must be powered for a few hours to

ensure that all electrical components have reached a steady state temperature. Once the warm-up

is complete, weights were added and removed to the load platens in accordance with the run

schedule shown in the table one. Each run of the schedule consists of an initial zero applied load

recording (tare), a loaded recording per the schedule, and a final tare recording. The recordings take 20 measurements approximately 1 second apart. This data is then filed raw and averaged by the LabView code. See Appendix C for the full LabView code. See Appendix E for the averaged raw results from calibration.

4.3 Calibration Results

Calibration of the balance reveals that the balance performs with error commensurate with typical NASA LaRC wind tunnel balances. During initial calibration runs, the voltage supply to the balance allowed for large ranges of input voltages. This problem was remedied by switching to a more robust supply. No other issues were seen during the calibration of the balance. With this data, a 2nd order regression model was generated using ordinary least squares fitting to accurately predict the thrust and torque loads. The models output a response in millivolts per volt of excitation using inputs of lb and in-lb for the thrust and torque respectively. The regression models (shown in Table 2) are then input into the Labview code for use during testing. Loads are solved for iteratively in the LabView code using the methods shown in reference 13.

	Thrust (mv/V)	Torque (mv/V)
Intercept	-4.1630E-06	-5.3645E-05
Thrust (lb)	6.8202E-02	6.5685E-04
Torque (in-lb)	-1.4048E-04	1.3799E-01
Torque x Torque (in-lb) (in-lb)	-5.9117E-06	-4.7799E-06
Torque x Thrust (in-lb) (lb)	4.2239E-07	-1.2544E-05
Torque x Torque (in-lb) (in-lb)	7.3980E-06	-2.8944E-06

Table 2: Calibration Regression Models

The regression models were used to predict responses at the design point locations and at four interior confirmation points. Traditionally the standard deviation of the residuals is used to help

assess model adequacy and provide a metric for accuracy. In recent years, NASA LaRC has also added confirmation point residuals. Two standard deviations provide an approximate 95 % confidence interval half width. This value is often used to quantify accuracy and expressed as a percent of full scale reading. Results for the ODU15X15 are reported in Table 3.

	Thrust	Torque
Standard Deviation of All Residuals	0.052%	0.032%
95% Confidence Interval (all residuals)	±0.104%	±0.065%
Standard Deviation of Model Residuals	0.044%	0.033%
95% Confidence Interval (model residuals)	±0.089%	±0.067%

Table 3: Accuracy Metrics for Thrust and Torque (% of Full Scale Reading)

5   WIND TUNNEL TRIAL EXPERIMENT

Wind tunnel testing the ODU15X15 was performed to evaluate improvements in measured propeller performance characteristics in comparison to Duvall's experiment. Initial testing of the ODU15X15 balance shows improvement, but further testing is needed to completely characterize the ODU15X15 balance performance.

5.1   Equipment

The electrical setup for balance testing is exactly the same as calibration except for the addition of the motor, current meter, revolution counter, throttle control, and power supplies for the additional items. See the wiring diagram below for details and refer to Appendix B.
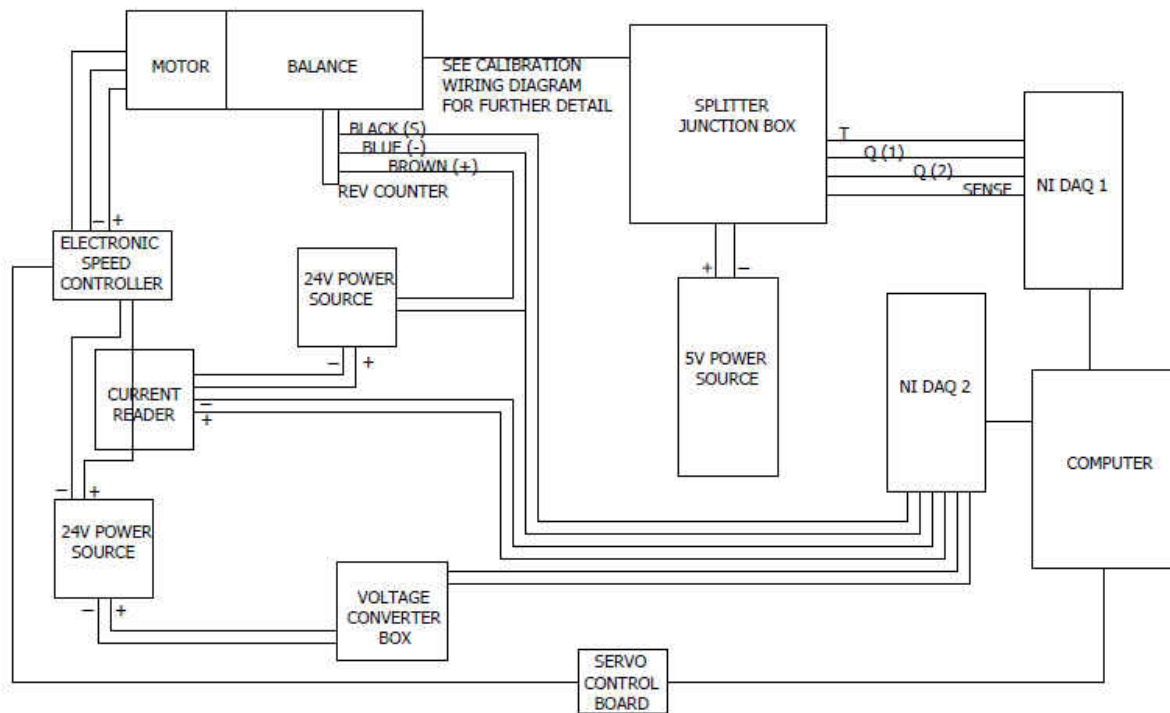
Figure 52: Wind Tunnel Trial Experiment Wire Diagram

A Sorensen (DCS55-55E) power supply set to 24V is used to power the motor. The positive motor wire is passed through a CR Magnetics (CR5211-100) DC current transducer, and then connected to the Castle electronic speed controller (Phoenix Edge 50) along with the negative lead. From there it is connected to the Scorpion (SII-4020-420kv) motor. The power supply voltage is monitored by the NI DAQ (BNC-2110). Power supply voltage is reduced by a factor of 3.5 in the converter box. This reduction is done because the DAQ cannot read voltages higher than ten volts. Once the reduced voltage reaches the DAQ the test LabView program converts the voltage back. The electronic speed control input is connected to a Pololu (twelve-channel Mini Maestro) servo control board which then connects to the computer via a USB port. The Automation Direct (PD1-AN-3A) revolution counter is powered by the same Eventek (KPS3010D) power source, set to 24V, used to power the current transducer. A separate wire is used to bridge the counter to the DAQ system.

The test stand streamlined strut used during this testing is not the same test stand used by Duvall but rather is a few inches shorter and places the propeller nearer to the wind tunnel floor. The stand has the same streamlined strut cross section to minimize aerodynamic effects. Testing was completed without the nacelle installed. Below is a picture of the final test set-up without the propeller.
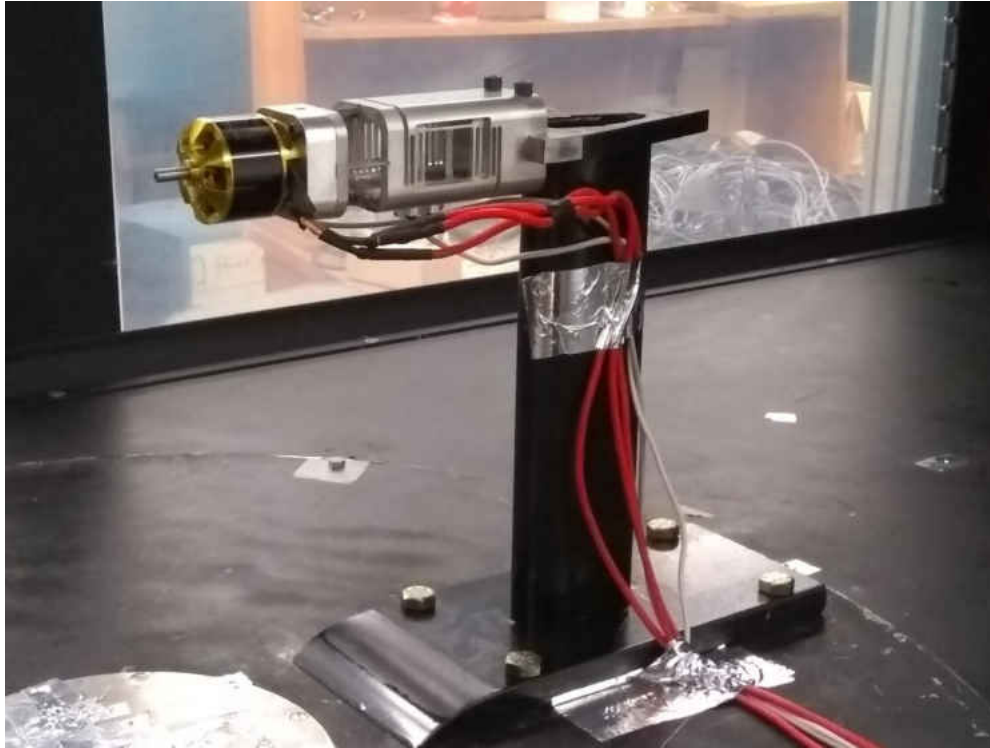
Figure 53: Final Test Set-up

The two torque bridge outputs are combined in the LabView code to produce one output for

torque. Torque, thrust, propeller revolutions per minute (RPM), tunnel dynamic pressure,

barometric pressure, and test section temperature are measured throughout the duration of

testing. A wind tunnel description can be found in section 1.4. The full LabView code for testing

is shown in Appendix C.

5.2   Use of Calibration

The regression models of section 4 were incorporated in the LabView data acquisition

code. The LabView code converts the voltage data received from each of the bridges to loads

using the iterative process described in reference 13. Prior to testing, all equipment is mounted.

A tare is taken before each run. This removes any zero shift that may have developed between

calibration and testing, and ensures the balance is reading as close to zero as possible.

5.3   Wind Tunnel Test Procedures

A Master Airscrew, 16 x 8, 3-blade propeller was used for trial tests. To start testing the LabView code was initiated, the motor was brought to a low RPM, and the wind tunnel was brought to a low speed. In order to sweep through advance ratios, the wind tunnel velocity was slowly/incrementally swept through a speed range until the propeller no longer produced thrust. Tunnel velocity was the only varied attribute during testing, and Table 4 shows the nominal points at which data was taken during testing. The reader is directed to reference 1 for background on propeller testing.

Wind Tunnel Test Velocities (m/s)
4
6.4
11.6
13.8
16
18.3
20
21.8

Table 4: Approximate Wind Tunnel Test Velocities

Propeller speed was fixed at 4800 RPM during all data collection periods. The points were chosen by experimentally finding the zero-thrust point as the final data point and starting at the lowest possible tunnel speed. At each point the tunnel was brought to speed first, then the motor was brought to speed. Once the system reached a steady state (normally a couple of seconds) data was collected, and then the propeller speed was dropped back down until the tunnel reached the next speed. The test run schedule was executed three times.

In order to combat any thermal effects due to heat produced by the motor during testing, between runs the motor was brought down to a low RPM and occasionally turned off. It is important to note that the propeller velocity affects the tunnel velocity although it does not affect the tunnel velocity measurement accuracy. After the motor is brought to speed the tunnel

velocity may need to be readjusted to hit the correct point, especially at low tunnel velocities. Averaged raw data testing results can be found in Appendix E.

5.4   Results

Raw test results show that the ODU15X15 balance performed with high precision, consistent with expectations, and yielded similar propeller characteristics as those developed by Duvall's testing. It is most important to look at the replicated values for a precision assessment as the absolute values are not corrected for tunnel wall effects nor was the streamlined nacelle present during testing as it would need to be modified from its current design. Figures 55, 56, and 57 show a high degree of repeatability of Power Coefficient (C_P), Thrust Coefficient (C_T), Torque Coefficient (C_Q), and Efficiency (η) for the three test runs.
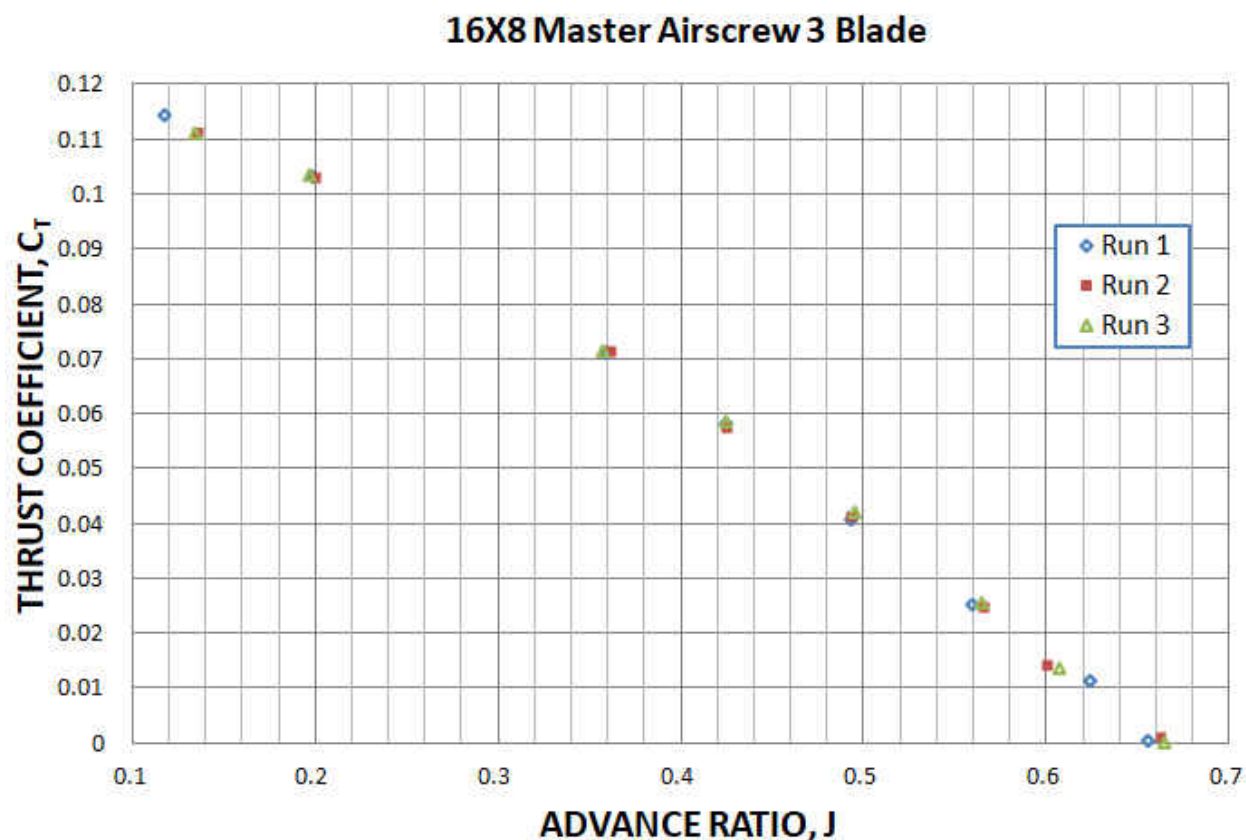
Figure 54: Thrust Coefficient Versus Advance Ratio
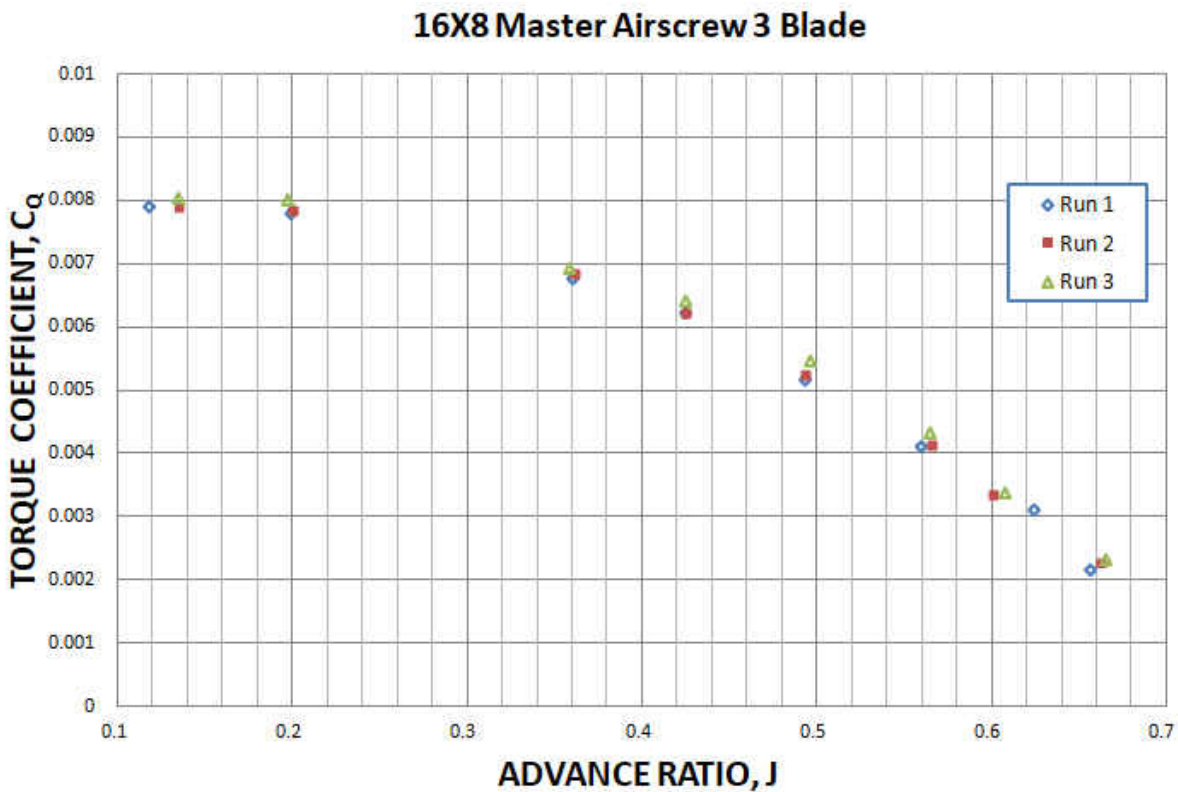
Figure 55: Torque Coefficient Versus Advance Ratio
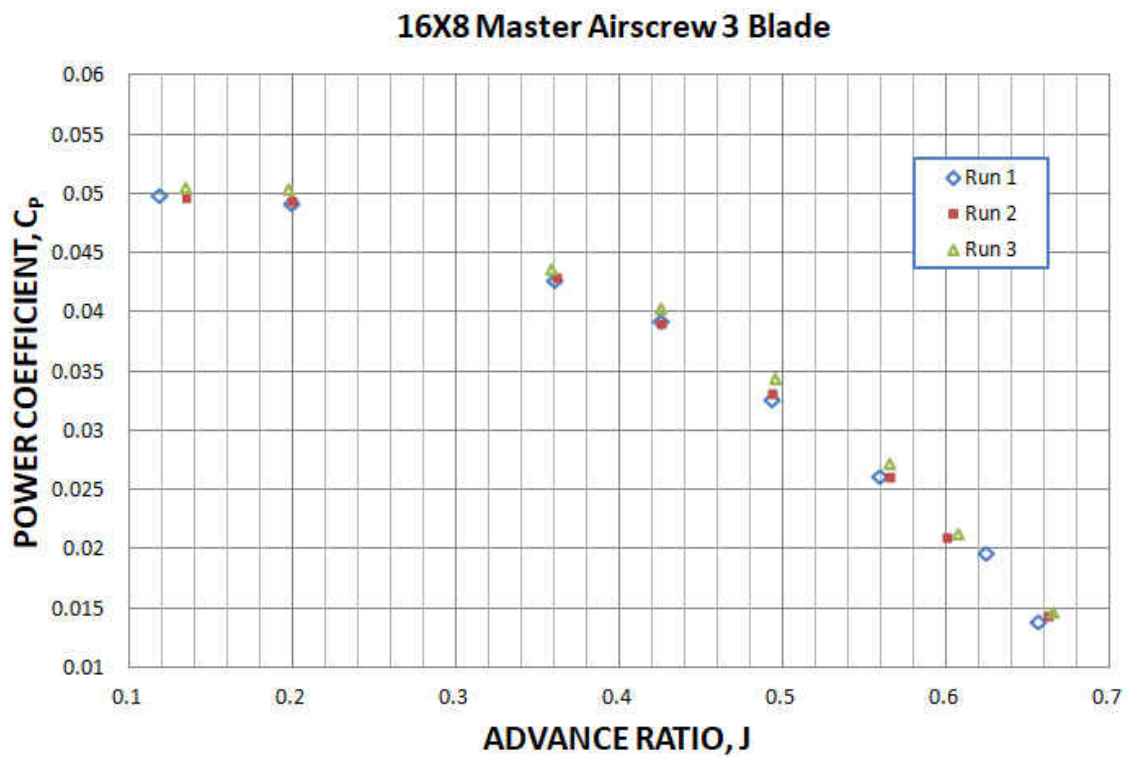
Figure 56: Power Coefficient Versus Advance Ratio
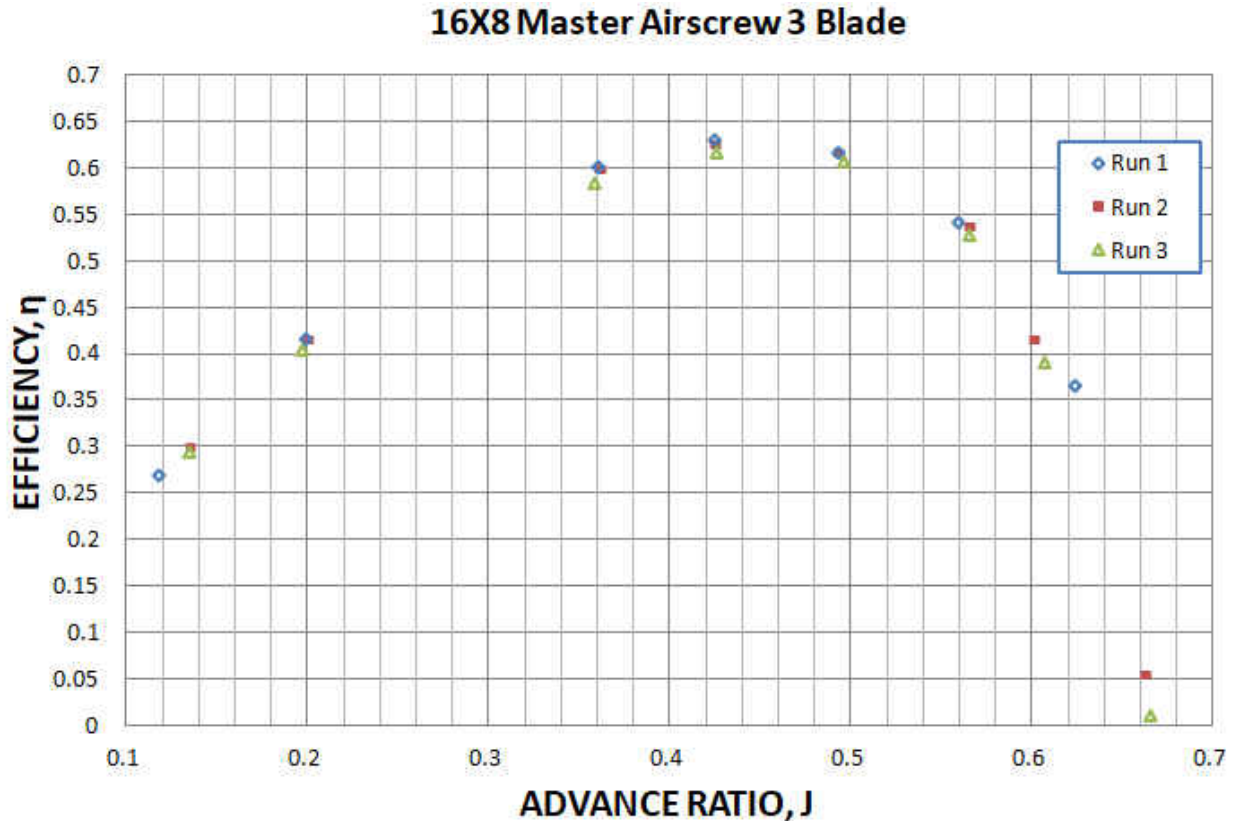
Figure 57: Efficiency Versus Advance Ratio

Where J is the Advance Ratio.

5.5   Uncertainty Assessment

An uncertainty assessment was performed to determine the balance's ability to predict propeller performance precisely. The graphs of Figure 58 show the performance curves for the propellers with 95% confidence bands. These bands were produced by first fitting a regression model to the three replicate trial runs using Design Expert software (14). The residual error is used to generate the confidence bands which are shown about the predicted mean values in the plots (12).
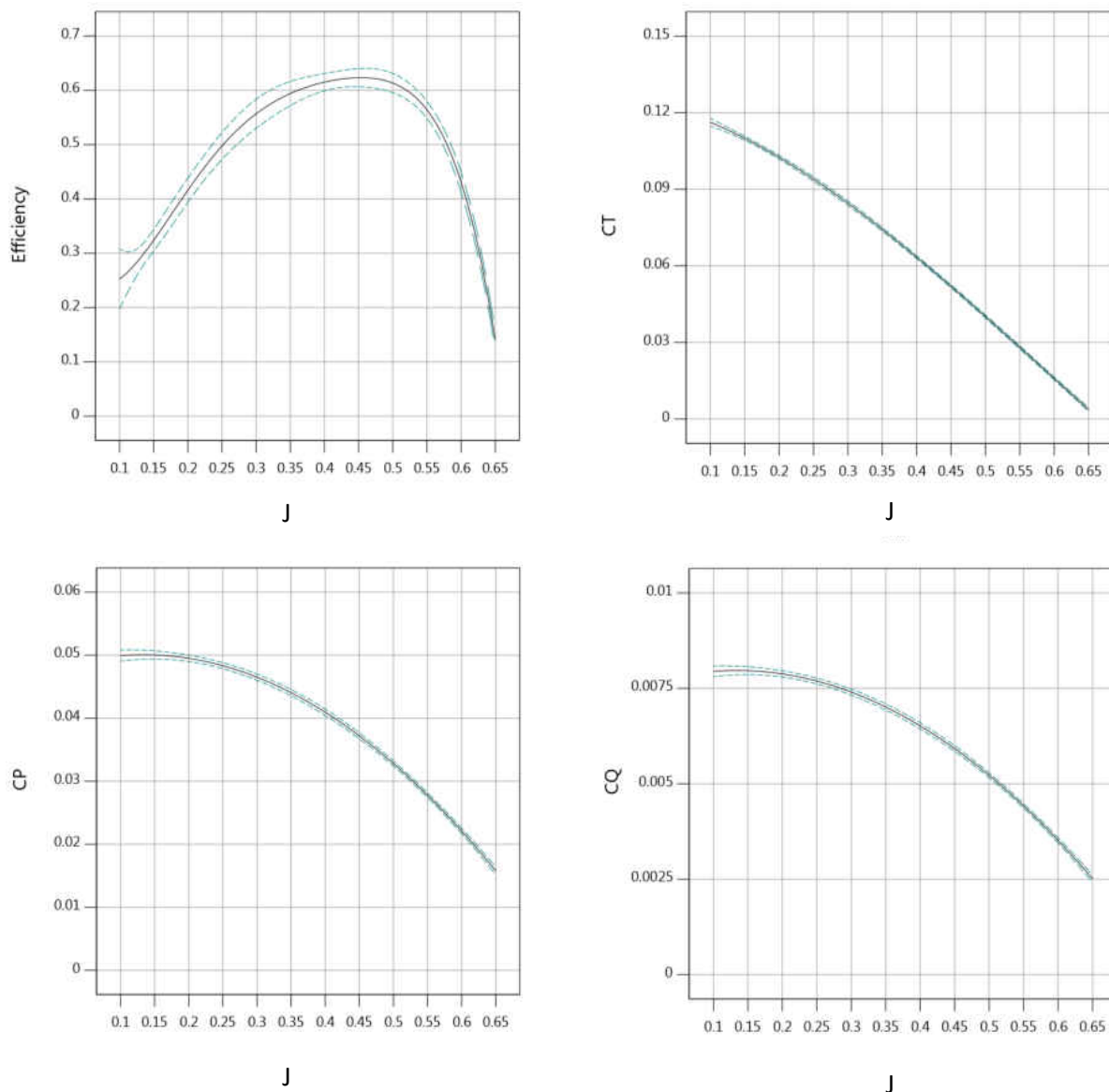
Figure 58: Performance Curves with 95% Confidence Interval Bands

The graphs can also be found in Appendix at enlarged scales. ANOVA analysis for the

regression models is provided in Table 5-Table 8. Metrics for goodness of fit and prediction

capabilities are provided by the R^2 family of statistics and shown in Table 9. R^2 describes the

percent variability in the response that is explained by the regression model. Adjusted and

predicted R^2 provide a metric for model over fitting and prediction capabilities respectively. All

are close in magnitude as desired and above 99%.

Source	Sum of Squares	df	Mean Square	F-value	p-value	
Model	0.0350	3	0.0117	14327.24	< 0.0001	significant
A-J	0.0086	1	0.0086	10559.32	< 0.0001	
A^2	6.760E-06	1	6.760E-06	8.31	0.0092	
A^3	8.710E-06	1	8.710E-06	10.71	0.0038	
Residual	0.0000	20	8.132E-07			
Cor Total	0.0350	23				

Table 5: C_T Regression Model

Source	Sum of Squares	df	Mean Square	F-value	p-value	
Model	0.0037	2	0.0019	3439.77	< 0.0001	significant
A-J	0.0022	1	0.0022	4131.87	< 0.0001	
A^2	0.0003	1	0.0003	524.80	< 0.0001	
Residual	0.0000	21	5.387E-07			
Cor Total	0.0037	23				

Table 6: C_P Regression Model

Source	Sum of Squares	df	Mean Square	F-value	p-value	
Model	0.0001	2	0.0000	3439.80	< 0.0001	significant
A-J	0.0001	1	0.0001	4131.90	< 0.0001	
A^2	7.161E-06	1	7.161E-06	524.80	< 0.0001	
Residual	2.865E-07	21	1.364E-08			
Cor Total	0.0001	23				

Table 7: C_Q Regression Model

Source	Sum of Squares	df	Mean Square	F-value	p-value	
Model	0.8622	5	0.1724	477.79	< 0.0001	significant
A-J	0.0103	1	0.0103	28.59	< 0.0001	
A^2	0.0137	1	0.0137	38.01	< 0.0001	
A^3	0.0590	1	0.0590	163.55	< 0.0001	
A^4	0.0075	1	0.0075	20.91	0.0002	
A^5	0.0034	1	0.0034	9.37	0.0067	
Residual	0.0065	18	0.0004			
Cor Total	0.8687	23				

Table 8: Efficiency Regression Model

	CT	CP	CQ	Efficiency
R^2	0.9995	0.9970	0.9970	0.9925
R^2 Adjusted	0.9995	0.9967	0.9967	0.9904
R^2 Predicted	0.9993	0.9961	0.9961	0.9868
Standard Deviation	0.0009	0.0007	0.0001	0.0190

Table 9: R^2 Model Fit Statistics

Numerical values for the 95% confidence intervals are provided for advance ratios of 0.2, 0.3, and 0.5 in Table 10. While no direct comparisons are possible yet due to the need to develop a streamlined test nacelle, initial results are encouraging. The confidence intervals show a high level of precision in comparison to the use of the commercially available multi-axis load cell of reference 1. Table 11 shows a comparison between typical values for two runs using the previous balance versus the ODU15X15.

J=0.2	Low	High
CT	0.1017	0.1033
CP	0.0490	0.0500
CQ	0.0078	0.0080
Efficiency	0.3939	0.4382

J=0.35	Low	High
CT	0.0735	0.0751
CP	0.0435	0.0446
CQ	0.0069	0.0071
Efficiency	0.5720	0.6163

J=0.5	Low	High
CT	0.0395	0.0408
CP	0.0324	0.0332
CQ	0.0052	0.0053
Efficiency	0.5957	0.6311

Table 10: 95% Confidence Intervals for Three Advance Ratios

Balance	Propeller Tested	CT	CP	CQ	Efficiency
ODU15X15	16x8, 3 Blade Master Airscrew	0.0009	0.0007	0.0001	0.0190
ATI (Old)	16 x 8, 2 Blade Aeronaut	0.0034	0.0018	0.0003	0.0844

Table 11: Comparison of One Standard Deviation Values for Old Versus New Balance

6   CONCLUSIONS AND FUTURE WORK

The ODU15X15 balance design has demonstrated that low-cost strain gage based transducers can be very accurate. The two-standard deviation values for the calibration model residuals were all under 0.1% full scale. These results compare very favorably to high precision machined balances in the NASA Langley balance library. The calibration models predicted all confirmation points within the prediction intervals after calibration. When operated during testing at 4800 RPM there were no signs of dynamic vibration issues, and the thrust and torque loads remained steady. It should be noted that the full range of the balance was not exercised, but by all accounts thus far there are no indications to show that it would not perform properly at its upper limits. Balancing propellers prior to testing and paying heed to the natural frequency should allow users to avoid any issues with vibration excitation.

Considerations for further research that could enhance the performance of future ODU balances, and testing include a finer tunnel velocity control, the removal of fastened joints in the design and mount strategy of the balance, and calibration rig precision and stiffness improvements.

Fastened joints have been known to cause issues with zero shifts and hysteresis in balances. The removal of the joint between the motor and the balance is difficult to justify due to the need for reusability of the balance with different motors. A new stand would need to be developed in order to integrate the balance and eliminate the fastened joint on the mounting end of the balance.

Using a single piece of material to make the adapter would ensure a more accurate positioning of the torque and thrust application points. However, holes would need to be cut into the arms and in other locations to reduce the weight. The calibration table stiffness should be

improved, and the calibration stand heights should be shortened to reduce the load applied to the table. A tool could be developed to verify perpendicularity of the thrust calibration line more easily. A manual measurement with a pair of calipers between flexible lines is difficult and introduces too much uncertainty.

During testing it was found that the tunnel velocity control currently used is coarsely incremented, and repeatability of tunnel speed for a particular data point is difficult. While no dynamic problems were seen during testing, attaching the torque measurement gages to the thrust section would reduce the length of the balance making it stiffer. However this has the potential to lower the precision of torque measurements. An increase in stiffness would increase the range of operating speeds when using propellers with numerous blades.

REFERENCES

1. **Duvall, Brian.** *Development and Implementation of a Propellor Test Capability For GL-10 "Greased Lightning" Propeller Design.* Norfolk : Old Dominion University, 2014.

2. **Phillips, Ben D.** *Force Balance Design Draft 72916.* Hampton : NASA Langely Research Center, 2016.

3. **Calspan.** Calspan Wind Tunnel Balance - Force Measurement Systems. *Moment Balance.* [Online] 2018. [Cited: January 8, 2018.] http://www.aerofms.com/moment_balance.

4. **Cahill, David and Richardson, Stan.** Internal Balance Training. Hampton : NASA Langley Research Center, 2008.

5. **Parker, Peter.** November 30, 2016.

6. **Rhew, Ray D.** *NASA LaRC Strain Gage Balance Design Concepts.* Hampton : NASA Langley Research Center.

7. **Moore, Robert F.** Effects of Torsion on Rectangular Fixed-Ended Beams. Hampton : NASA, 1967.

8. **Lynn, Chris.** Balance Design Overview and Lifecycle Discussion. Hampton : NASA Langley Research Center, 2014.

9. **Omega.** Practical Strain Gage Measurements. [Online] Agilent Technologies, 1999. [Cited: January 27, 2018.] https://www.omega.com/techref/pdf/StrainGage_Measurement.pdf.

10. **Norton, Robert L.** *Machine Design: An Intergrated Approach.* Upper Saddle River, NJ : Prentice Hall, 2011.

11. *Precise Measurement Technology Based on new Block-type and Rotating Shaft Balances.* **Zimmermann, Claus, Haberli, Werner and Monkewitz, Martin.** Chicago : American Institute of Aeronautics and Astronautics (AIAA), 2010.

12. **Montgomery, D C.** *Design and Analysis of Experiments.* NY : John Wiley and Sons Inc., 2011.

13. AIAA Standards Recommended Practice: Calibration and Use of Internal Strain-Gage Balances With Application to Wind Tunnel Testing. [Online] https://doi.org/10.2514/4.476464. AIAA R-091-2003.

14. Design Expert 10 Software. [Online] Stat Ease Inc. http://www.statease.com/.

APPENDIX

APPENDIX A. STRAIN GAGE SPECIFICATIONS
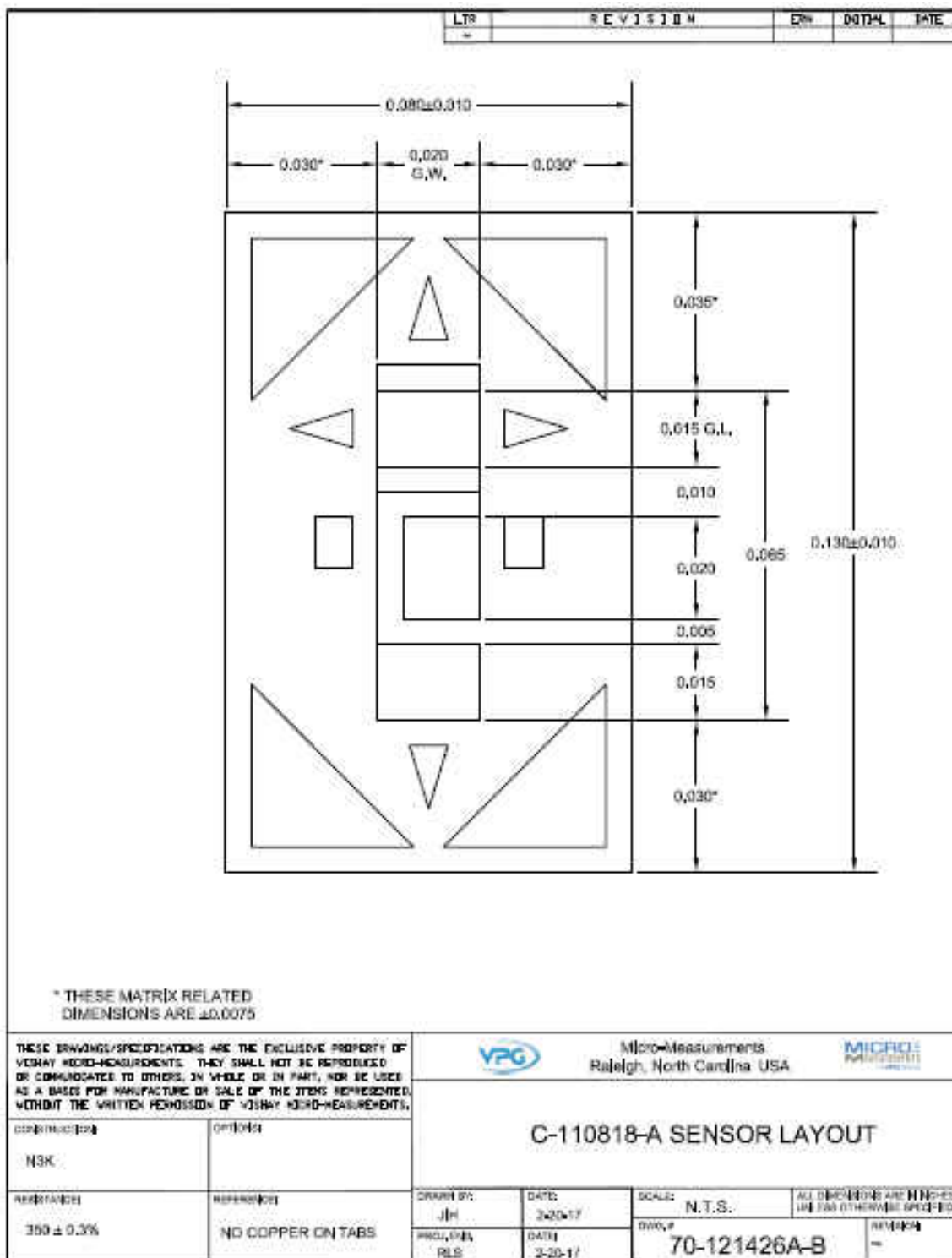
Strain-Gage Work Card

JOB NAME	ODU Balance	
CONTROL NO.	6310	DATE IN
JOB ORDER	4594	DATE STARTED 5/22/17
PROJ. ENG.	Drew Landman	DATE FINISHED 6/13/17
EXTENSION		TECHNICIAN Bloom

BRANCH _____ COMPETENCY _____

WORK REQ _Install AF + 2 roll bridges on balance as per drawing._

MAN-HOURS _____ APPROVED _____

STATION		AF	RA	RB				
GAGE TYPE		SK-13-050AH-350						
GAGE FACTOR		2.01 +/-1.0%						
LOT NUMBER		K47FF25						
BONDING AGENT		M-610						
CLAMPING PRESSURE		60 PSI						
CURE CYCLE		1hr@ 340°F						
POST CURE		2h@340°F						
SOLDER TYPE		361A						
RESISTANCE NO. 1	5	350.29	345.84	349.79				
RESISTANCE NO. 2	6	350.00 TC-A	350.09	349.86				
RESISTANCE NO. 3	7	349.96 TC-B	350.03	349.79				
RESISTANCE NO. 4	8	350.07	349.99 TC-B	349.73				
APP. STRAIN/BAL. WIRE								
INITIAL ELEC. ZERO @ 5 VDC		-.805	-.489	-.268				
FINAL ELEC. ZERO @ 5 VDC		-.972	-.533	-.410				
TEMP DRIFT BEFORE-AFTER T.C.		+.094 -.007	+.026 +.013	+.054 -.015				
FINAL RES. TO GROUND		>56Ω						
MOISTURE PROTECTION		M-coat A Gagekote 4e						

S.G. WIRE TYPE ___7/40___   CABLE _____   SLEEVING TYPE ~~nylon~~ Fiberglass

TEMP. SENSOR TYPE _____   CABLE LENGTH _____   SLEEVING TYPE _____

STRAIN GAGING PROCEDURE CODE

CLASS ___5___   TYPE _____

GAGES USED

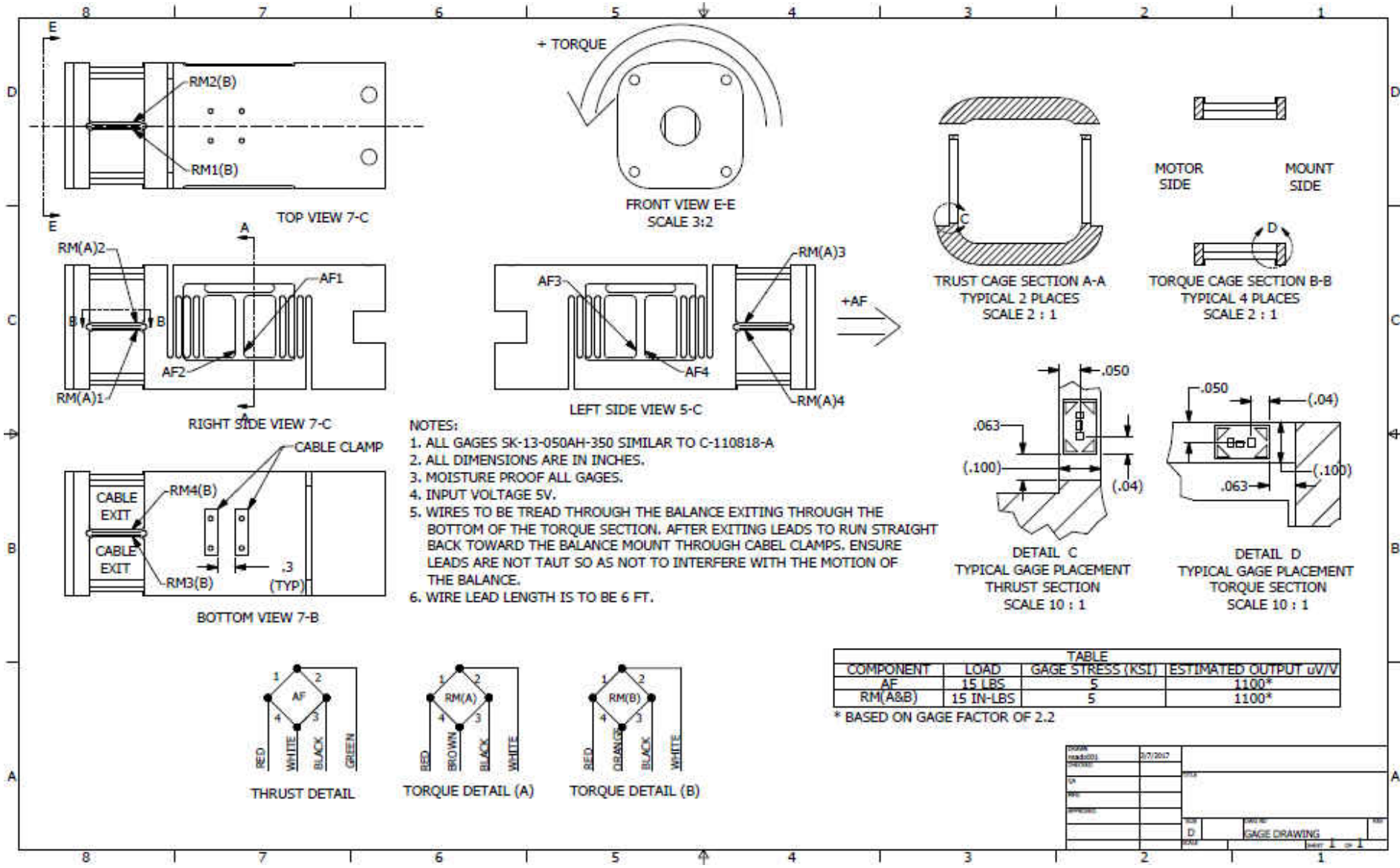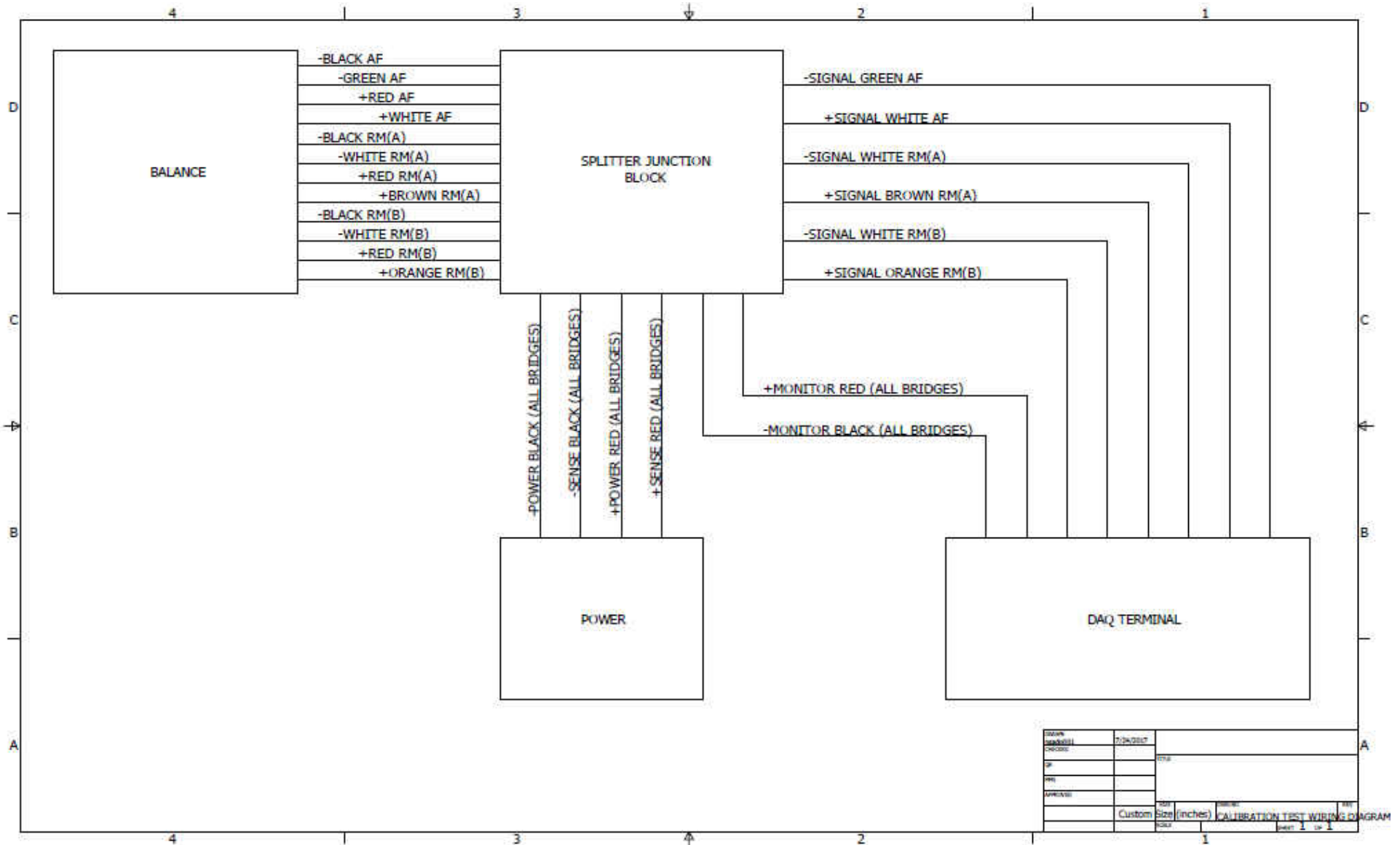| TYPE	SINGLES	T'S	ROSETTES
TOTALS			

REMARKS

* AF Gages were incorrectly numbered on drawing so signal leads were switched at chain terminals to correct for position AF when in tension.

APPENDIX B. WIRING DIAGRAMS

TOP VIEW 7-C

RM2(B)
RM1(B)

FRONT VIEW E-E
SCALE 3:2
+ TORQUE

TRUST CAGE SECTION A-A
TYPICAL 2 PLACES
SCALE 2 : 1

TORQUE CAGE SECTION B-B
TYPICAL 4 PLACES
SCALE 2 : 1

MOTOR SIDE   MOUNT SIDE

RIGHT SIDE VIEW 7-C
RM(A)2, AF1, AF2, RM(A)1

LEFT SIDE VIEW 5-C
AF3, RM(A)3, AF4, RM(A)4, +AF

BOTTOM VIEW 7-B
CABLE CLAMP, RM4(B), CABLE EXIT, CABLE EXIT, RM3(B), .3 (TYP)

NOTES:
1. ALL GAGES SK-13-050AH-350 SIMILAR TO C-110818-A
2. ALL DIMENSIONS ARE IN INCHES.
3. MOISTURE PROOF ALL GAGES.
4. INPUT VOLTAGE 5V.
5. WIRES TO BE TREAD THROUGH THE BALANCE EXITING THROUGH THE BOTTOM OF THE TORQUE SECTION. AFTER EXITING LEADS TO RUN STRAIGHT BACK TOWARD THE BALANCE MOUNT THROUGH CABEL CLAMPS. ENSURE LEADS ARE NOT TAUT SO AS NOT TO INTERFERE WITH THE MOTION OF THE BALANCE.
6. WIRE LEAD LENGTH IS TO BE 6 FT.

DETAIL C
TYPICAL GAGE PLACEMENT
THRUST SECTION
SCALE 10 : 1
.050, .063, (.100), (.04)

DETAIL D
TYPICAL GAGE PLACEMENT
TORQUE SECTION
SCALE 10 : 1
.050, (.04), .063, (.100)

THRUST DETAIL — AF — RED WHITE BLACK GREEN
TORQUE DETAIL (A) — RM(A) — RED BROWN BLACK WHITE
TORQUE DETAIL (B) — RM(B) — RED ORANGE BLACK WHITE

TABLE			
COMPONENT	LOAD	GAGE STRESS (KSI)	ESTIMATED OUTPUT uV/V
AF	15 LBS	5	1100*
RM(A&B)	15 IN-LBS	5	1100*

* BASED ON GAGE FACTOR OF 2.2

GAGE DRAWING

CALIBRATION TEST WIRING DIAGRAM

Connections shown in the diagram:

BALANCE to SPLITTER JUNCTION BLOCK:
- -BLACK AF
- -GREEN AF
- +RED AF
- +WHITE AF
- -BLACK RM(A)
- -WHITE RM(A)
- +RED RM(A)
- +BROWN RM(A)
- -BLACK RM(B)
- -WHITE RM(B)
- +RED RM(B)
- +ORANGE RM(B)

SPLITTER JUNCTION BLOCK to DAQ TERMINAL:
- -SIGNAL GREEN AF
- +SIGNAL WHITE AF
- -SIGNAL WHITE RM(A)
- +SIGNAL BROWN RM(A)
- -SIGNAL WHITE RM(B)
- +SIGNAL ORANGE RM(B)
- +MONITOR RED (ALL BRIDGES)
- -MONITOR BLACK (ALL BRIDGES)

SPLITTER JUNCTION BLOCK to POWER:
- -POWER BLACK (ALL BRIDGES)
- -SENSE BLACK (ALL BRIDGES)
- +POWER RED (ALL BRIDGES)
- +SENSE RED (ALL BRIDGES)

APPENDIX C. LABVIEW CODE

CALIBRATION LABVIEW
FRONT PANEL

Data Header   Time History

Num of samples
10

Reduced Data File 2
C:\Users\WindTunnel\Desktop\T-QBalSadowski\Data\test1red.txt

Raw Data File Path 2
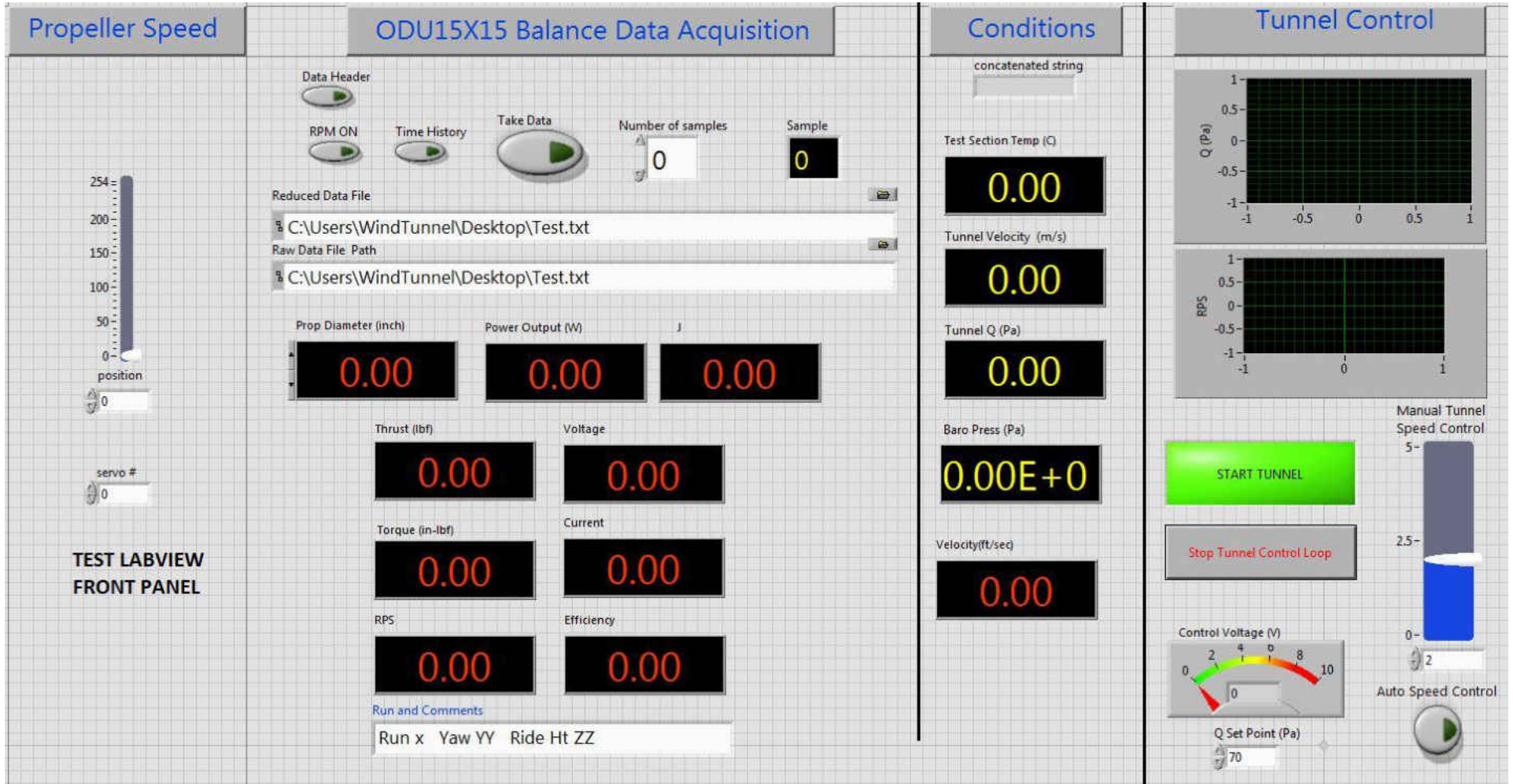C:\Users\WindTunnel\Desktop\T-QBalSadowski\Data\test1raw.txt

Thrust lbs
0

Thrust (volts)
0

Torque 1 (in-lbs)
0

Torque 1 (Volts)
0

Torque 2 (in-lbs)
0

Torque 2 (Volts)
0

Sense
0

Run and Comments
T-Q Bal Cal

CALIBRATION LABVIEW
BLOCK DIAGRAM

$$T=(((VT-0.02172218)/(0.02677095-0.02172218))*(15-0)+0);$$

$$Q=(((VQ-0.01809657)/(0.02818623-0.01809657))*(15+15)-15);$$

$$QQ=(((VQQ-0.01547232)/(0.02596432-0.01547232))*(15+15)-15);$$

LINEAR INTERPOLATION (USED TO VERIFY FORCES APPLIED POST CALIBRATION)

TRUE/FALSE SWITCH

Propeller Speed

ODU15X15 Balance Data Acquisition

Conditions

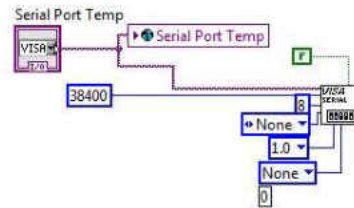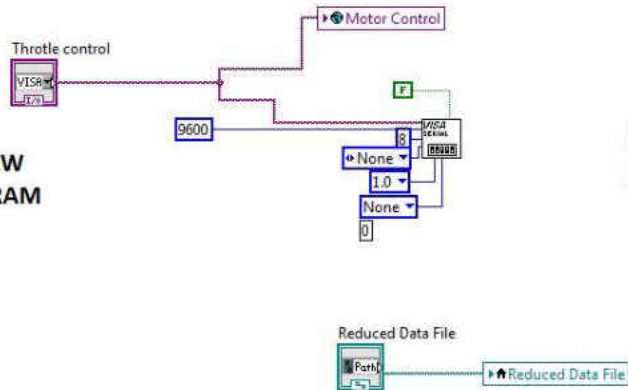**Tunnel Control**

Data Header

RPM ON   Time History   Take Data   Number of samples   Sample

position
0

servo #
0

TEST LABVIEW FRONT PANEL

Reduced Data File
C:\Users\WindTunnel\Desktop\Test.txt

Raw Data File Path
C:\Users\WindTunnel\Desktop\Test.txt

Prop Diameter (inch)   Power Output (W)   J
0.00   0.00   0.00

Thrust (lbf)   Voltage
0.00   0.00

Torque (in-lbf)   Current
0.00   0.00

RPS   Efficiency
0.00   0.00

Run and Comments
Run x   Yaw YY   Ride Ht ZZ

concatenated string

Test Section Temp (C)
0.00

Tunnel Velocity (m/s)
0.00

Tunnel Q (Pa)
0.00

Baro Press (Pa)
0.00E+0

Velocity(ft/sec)
0.00

START TUNNEL

Stop Tunnel Control Loop

Control Voltage (V)
0

Q Set Point (Pa)
70

Manual Tunnel Speed Control

Auto Speed Control

2

TEST LABVIEW
BLOCK DIAGRAM
2-1

TEST LABVIEW BLOCK DIAGRAM 3-1

$P=(Torque*0.1129844290241)*(RPS*2*Pi);$

Power Output (W)

PowerInput=V*C;

Velocity(ft/sec)

Velocity m/s
3.2808

Servo Control Code

Motor Control

timeout (10sec)
10000

Enable Termination Char

write servo # and position data to COM port

9600
8
None
None
0xAA
servo #
FF

Temperature and Barometric Pressure Readings

Serial Port Temp

TEST LABVIEW
BLOCK DIAGRAM
4-1

TEST LABVIEW
BLOCK DIAGRAM
5-1

Serial Port Barometer

VISA

▶ 🌐 Serial Port Barometer

TEST LABVIEW
BLOCK DIAGRAM
1-2

9600

8

None

1.0

None

0

VISA
SERIAL

True

🏠Reduced Data File▶

Write Data to File

Sample

1.23

i

0 [0..2]

True

22

N

Run and Comments

Data Header

abc

averaging

∧σµ

σ σ²

Fx (lbf) OFFLINE

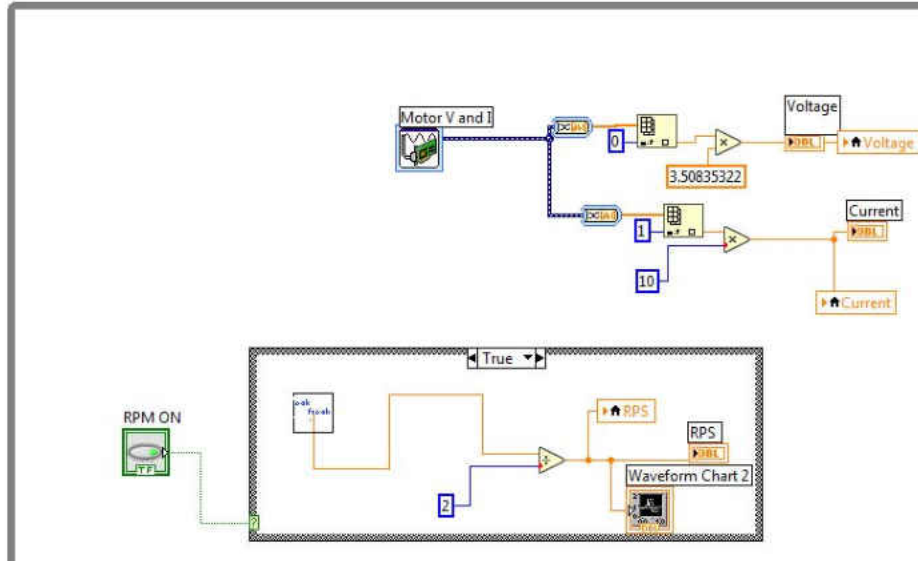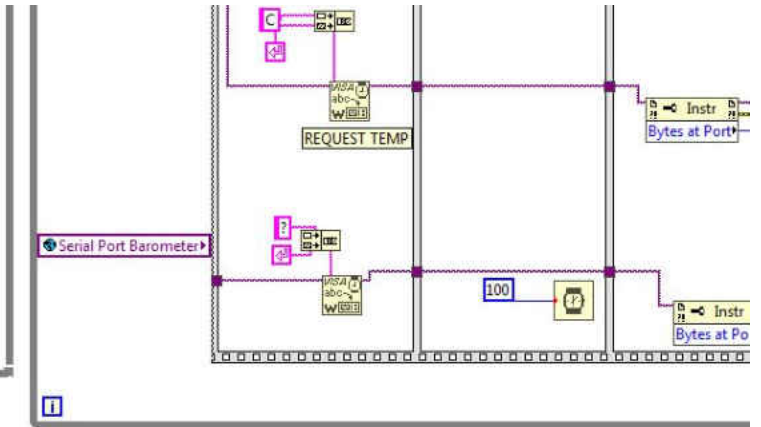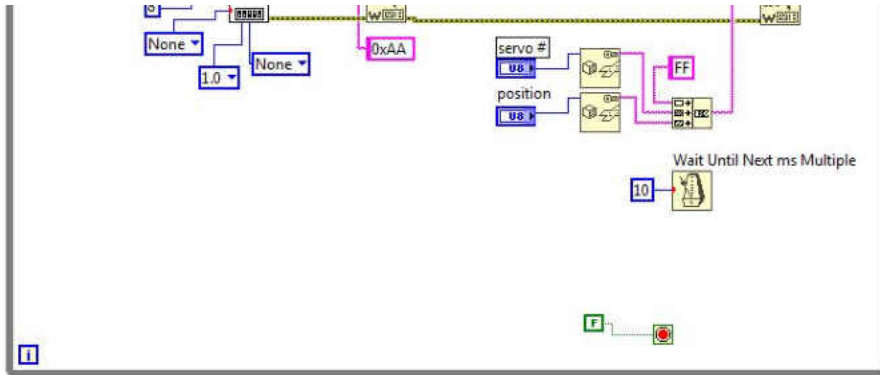Fy (lbf) OFFLINE

TEST LABVIEW
BLOCK DIAGRAM
2-2

TEST LABVIEW
BLOCK DIAGRAM
3-2

EXTRACT TEMP FROM STRING AND CONVERT TO NUMBER

C\s\s\n\r

\s

Temp

Test Section Temp (C)

Instr
Bytes at Port

Tunnel DP PSI 2

TEST LABVIEW
BLOCK DIAGRAM
4-2

M_Controller_B
EN.vi

Tunnel Mean Q

Auto/Manual Se
Current Q
Manual Control
Previous Voltage
Target Q
Output Voltage

DAQ Assistant

Control Voltage (V)

DBL
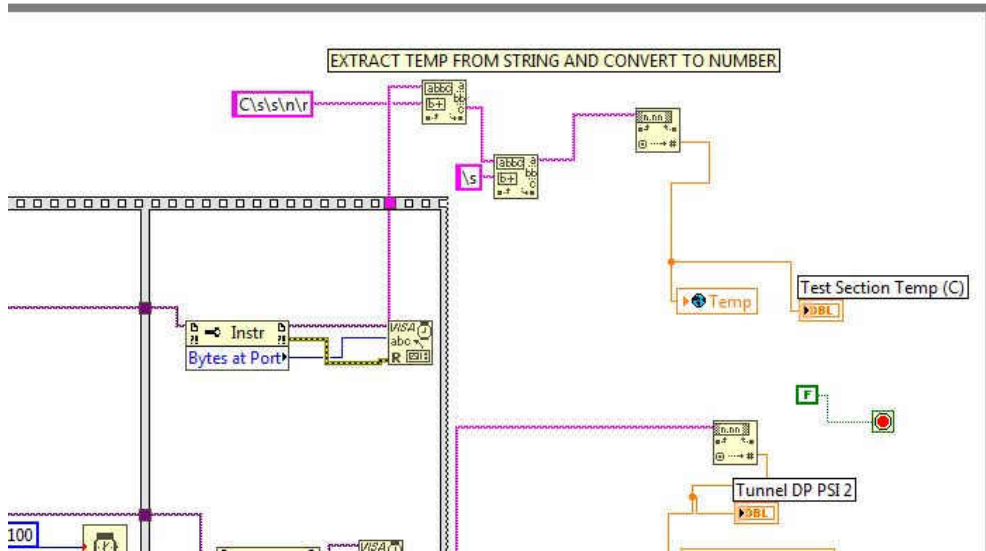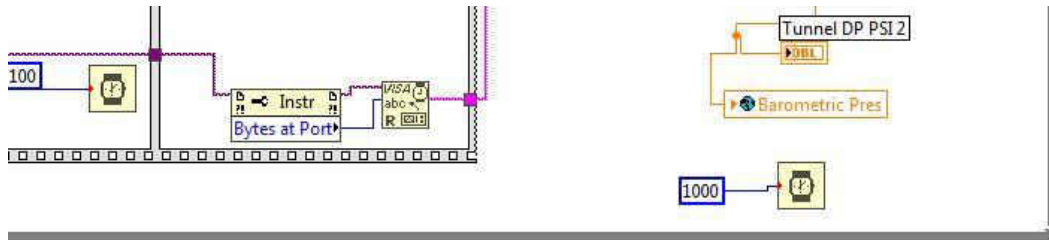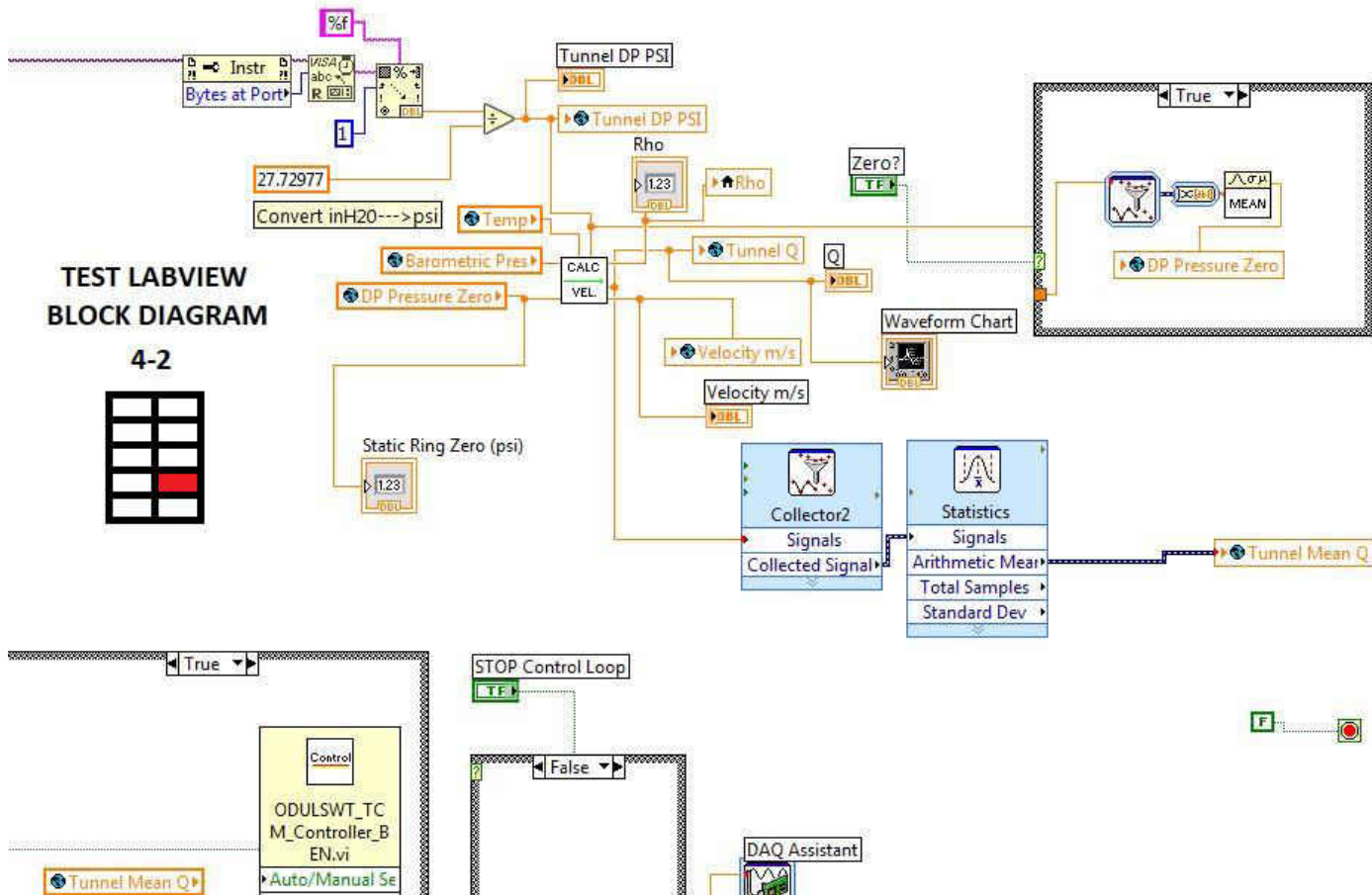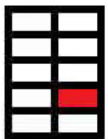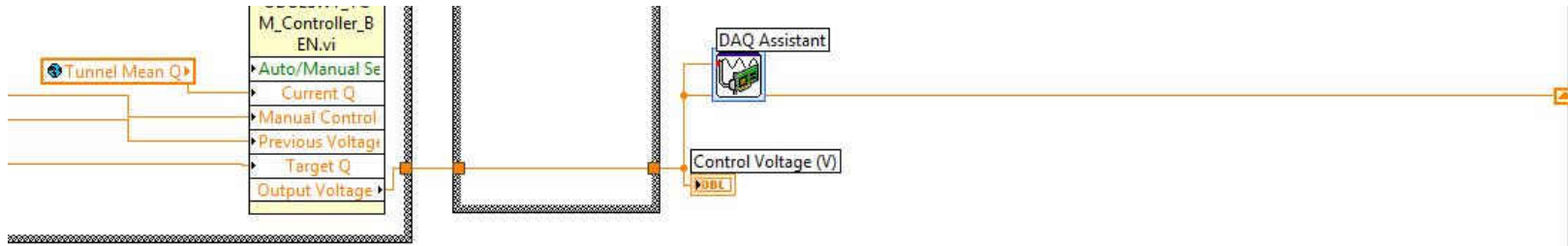
TEST LABVIEW
BLOCK DIAGRAM
5-2

TRUE/FALSE SWITCH

TRUE/FALSE SWITCH

TRUE/FALSE SWITCH

TRUE/FALSE SWITCH

Data Header
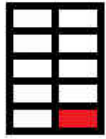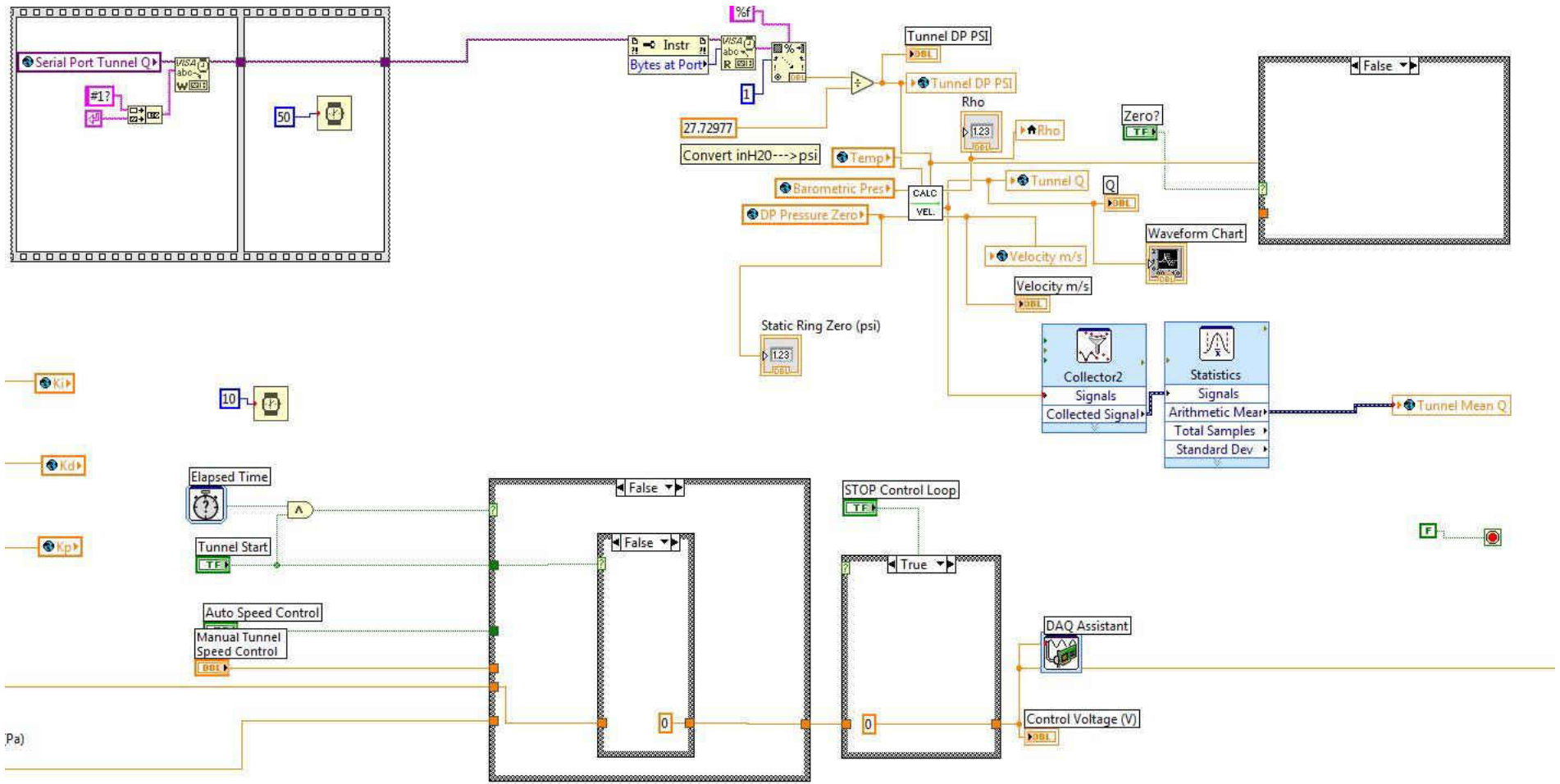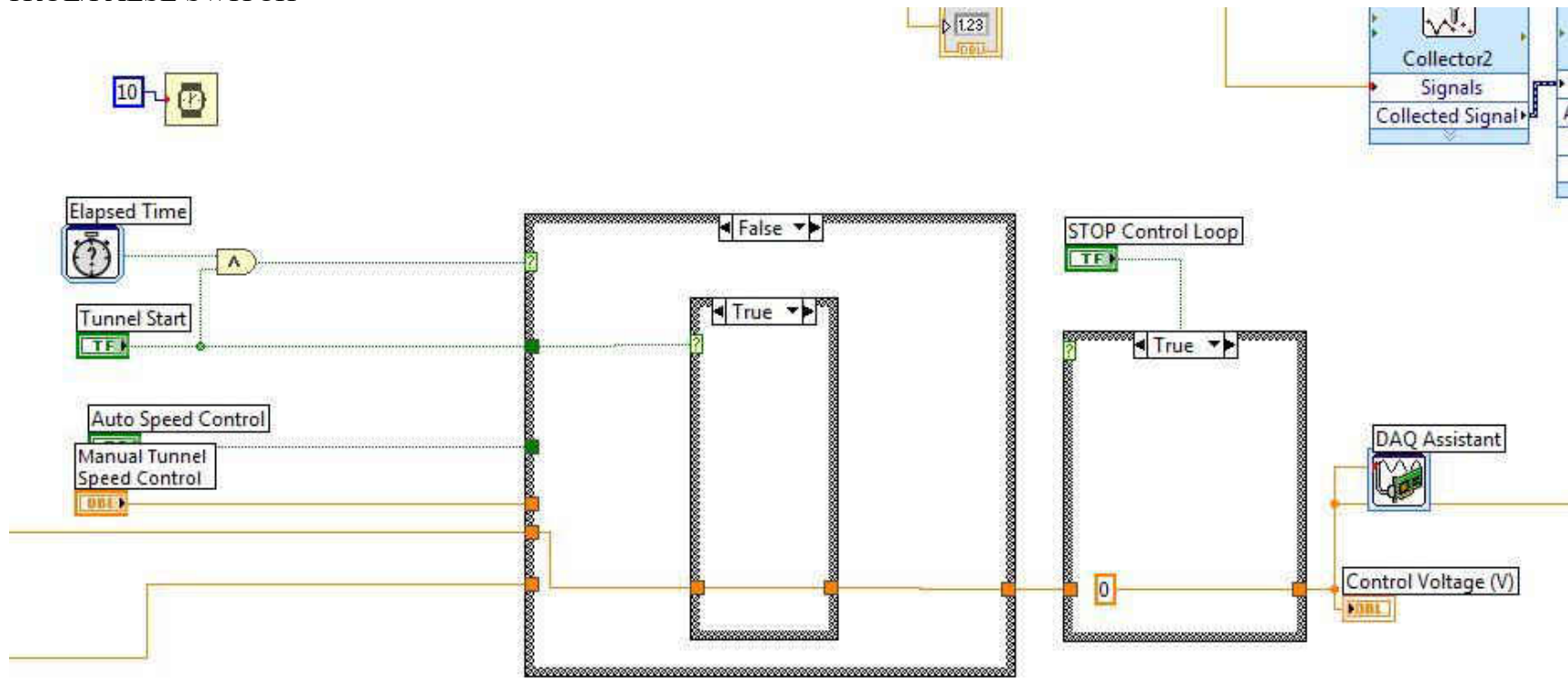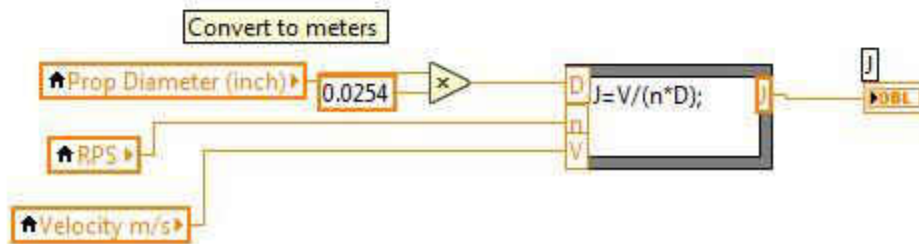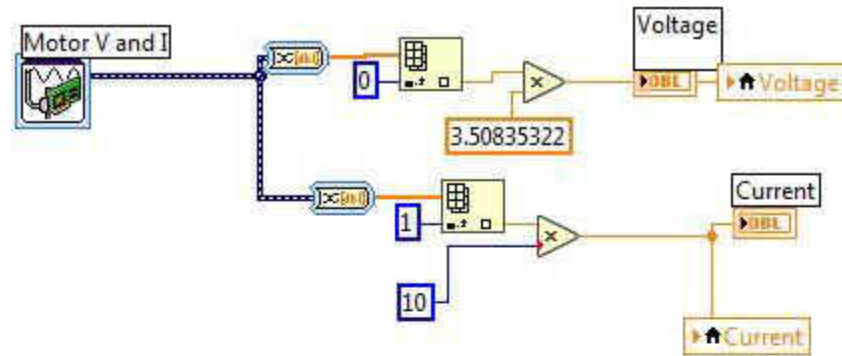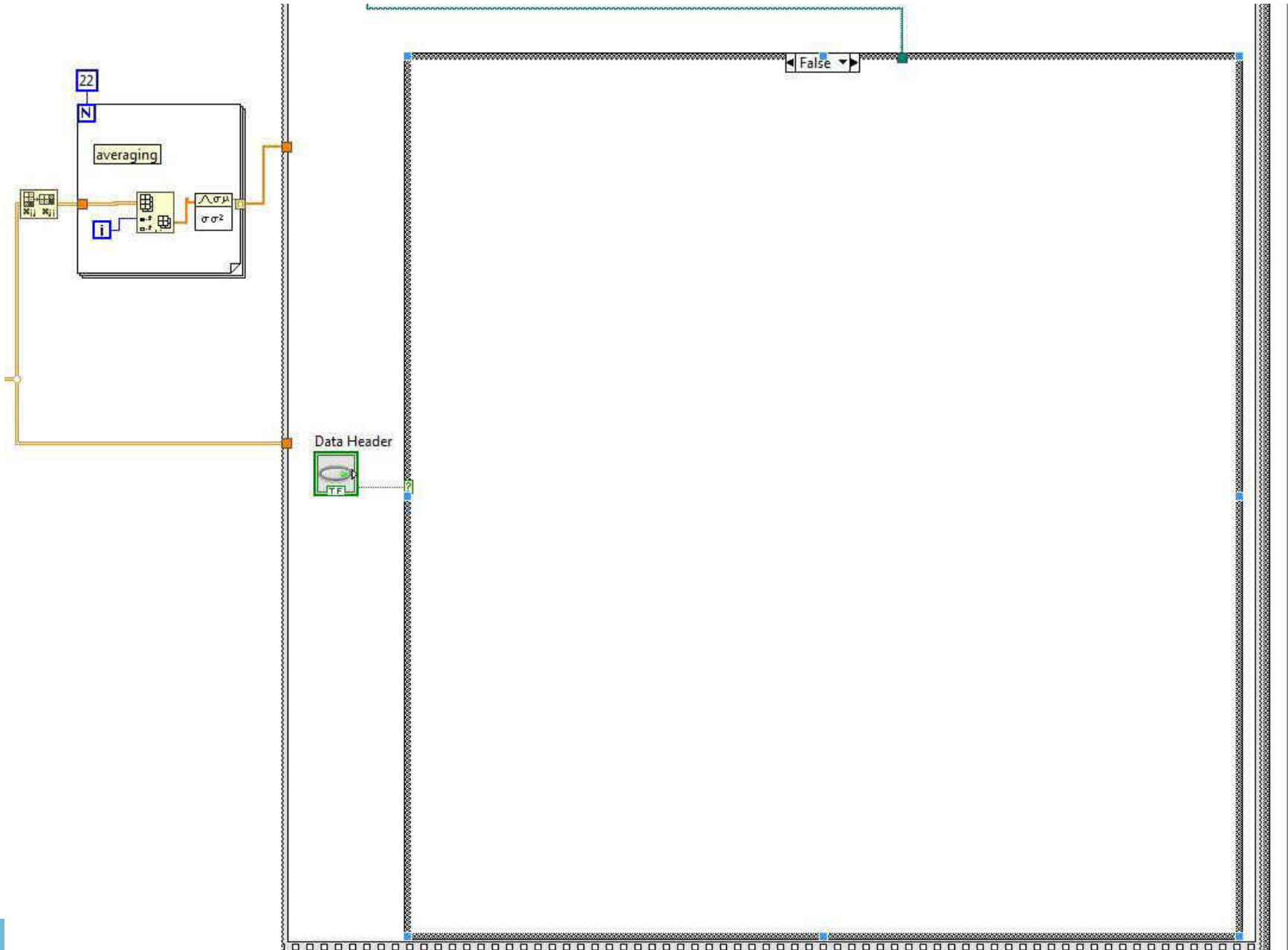
TRUE/FALSE SWITCH
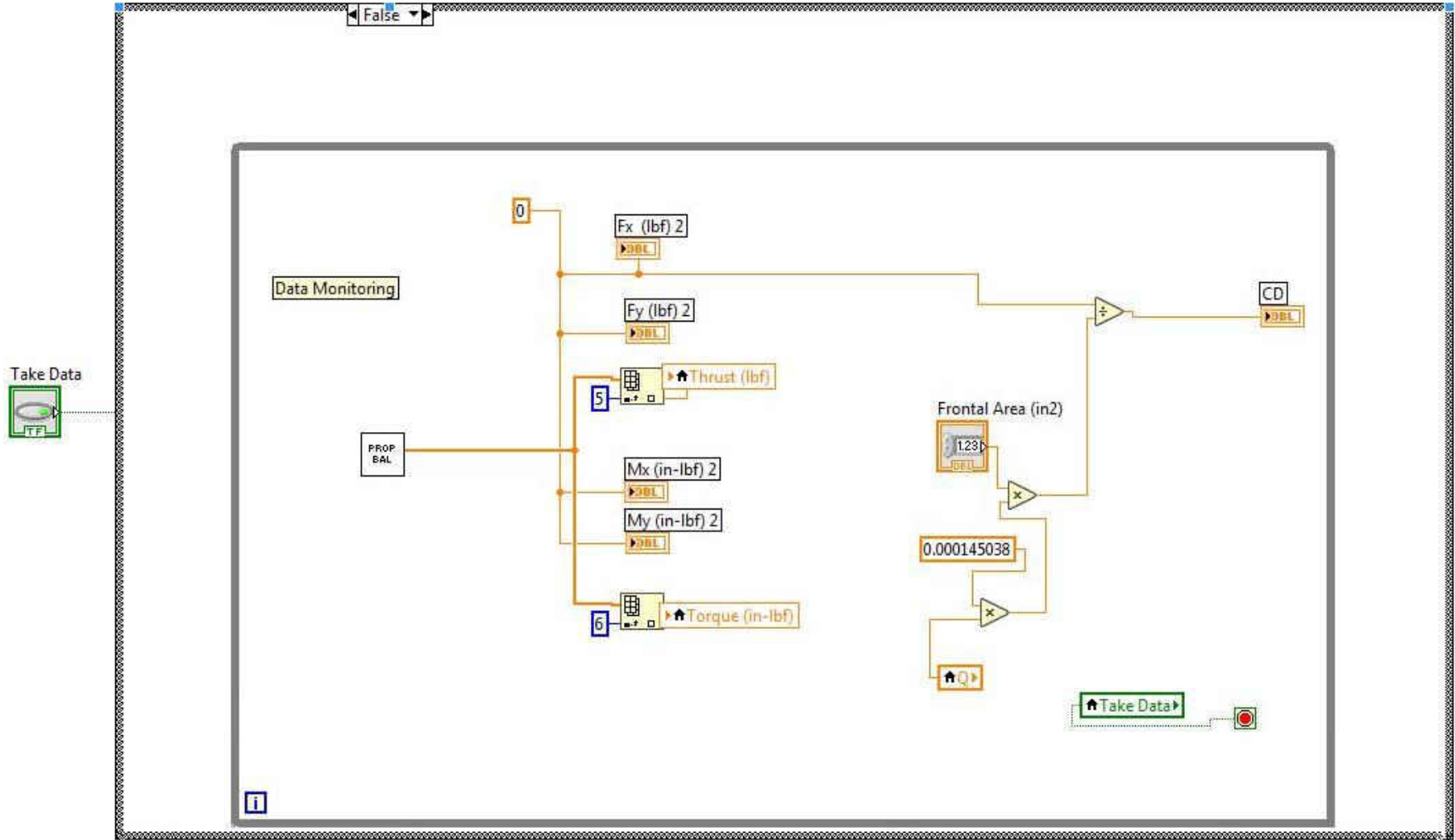
Servo Control VI
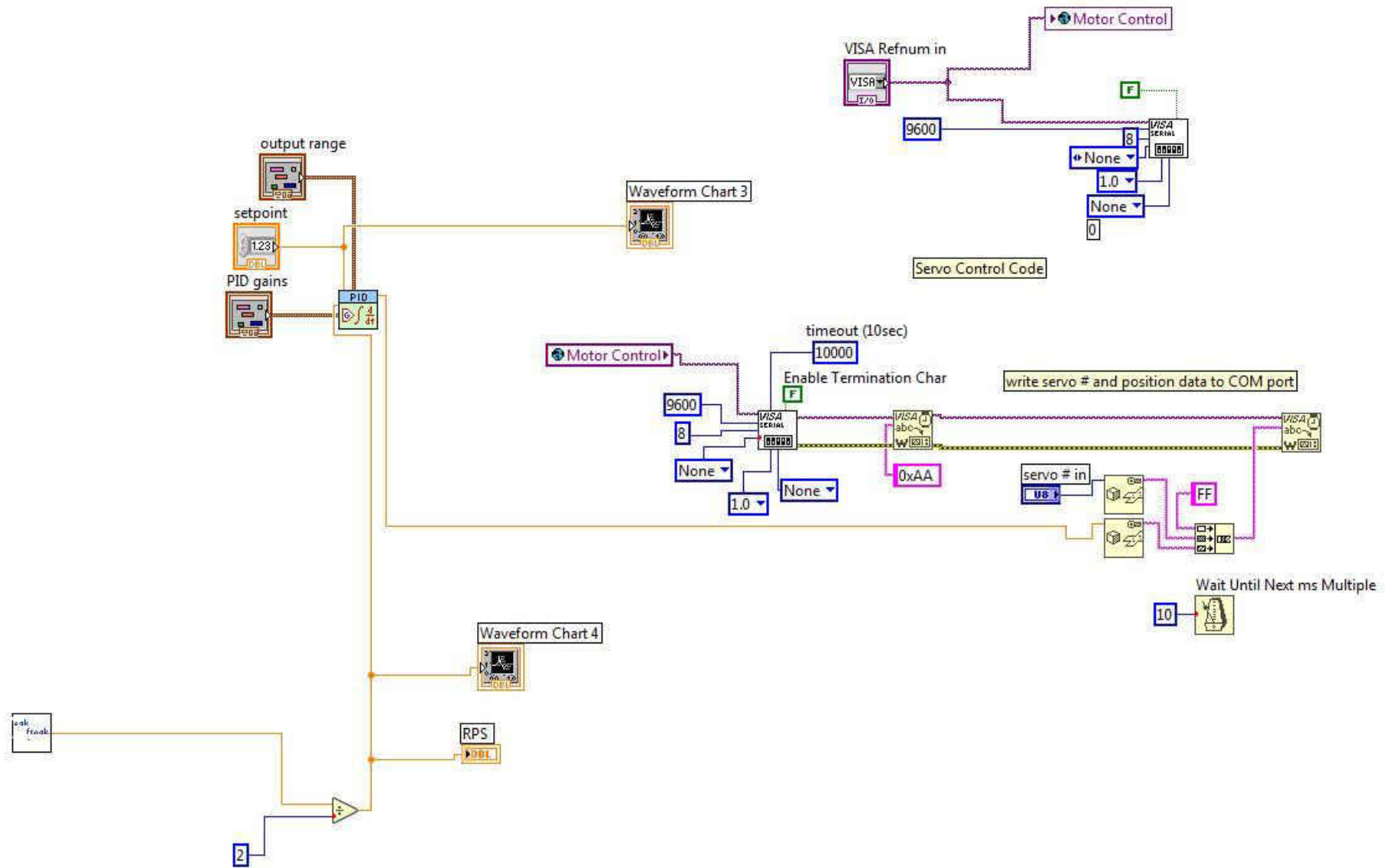
Prop Bal VI
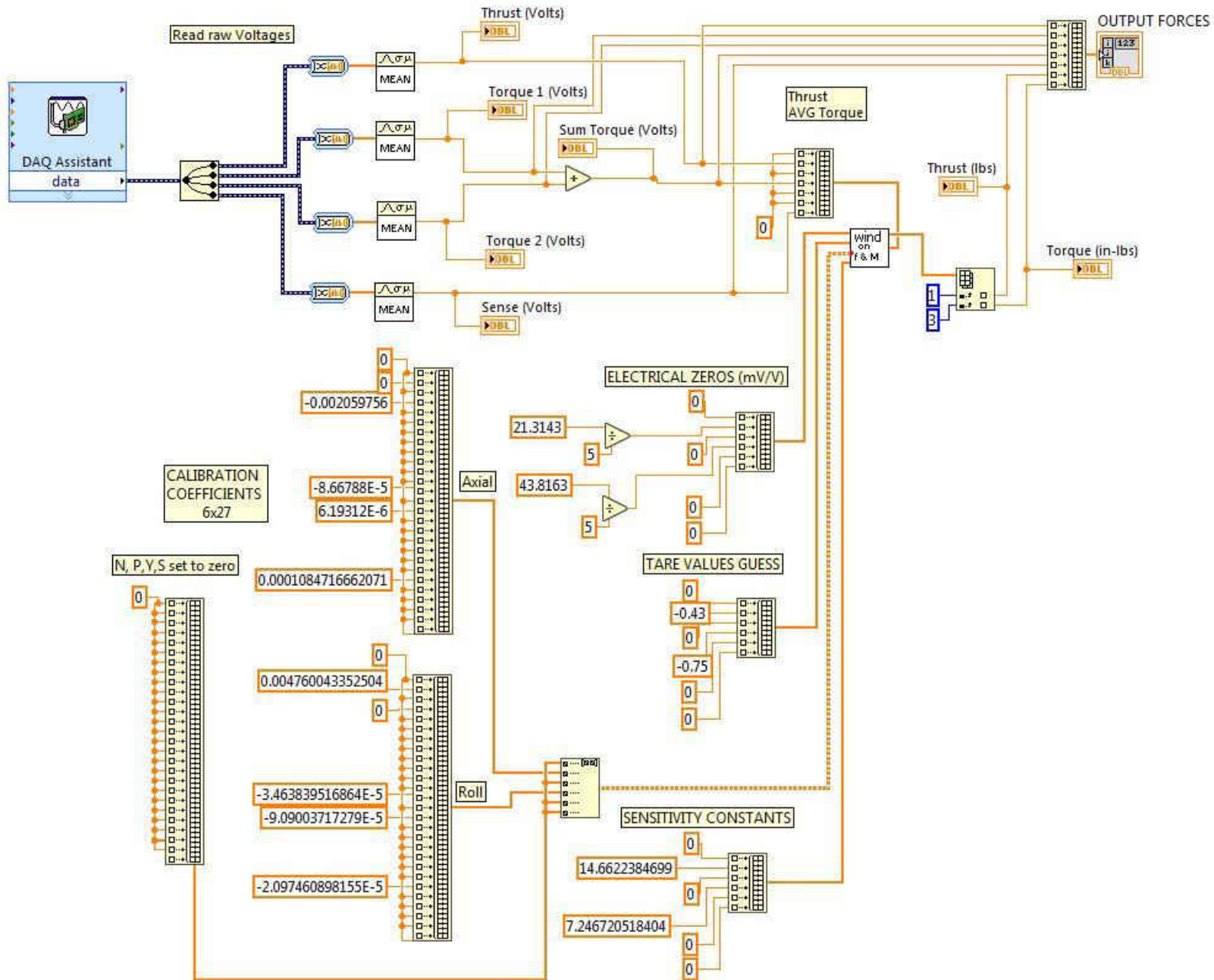
Wind on F & M VI
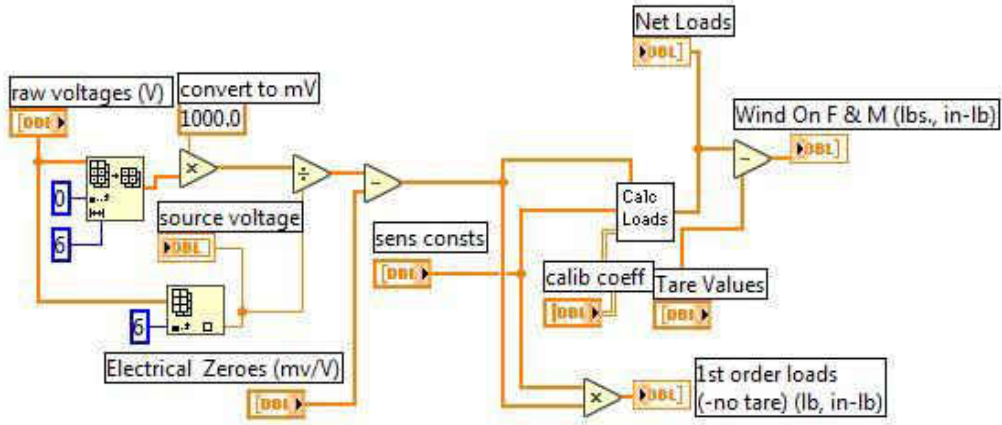
Split 6X27 VI
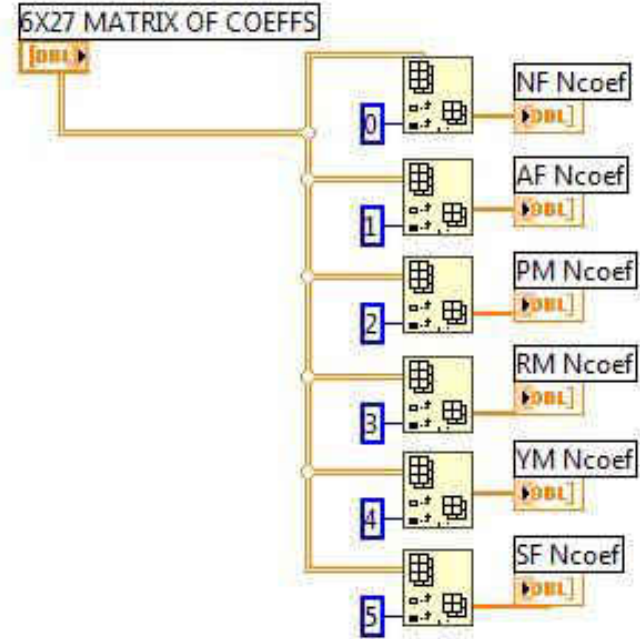
Freak VI
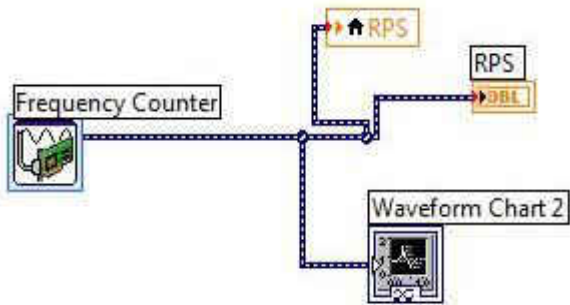
Calc Load VI
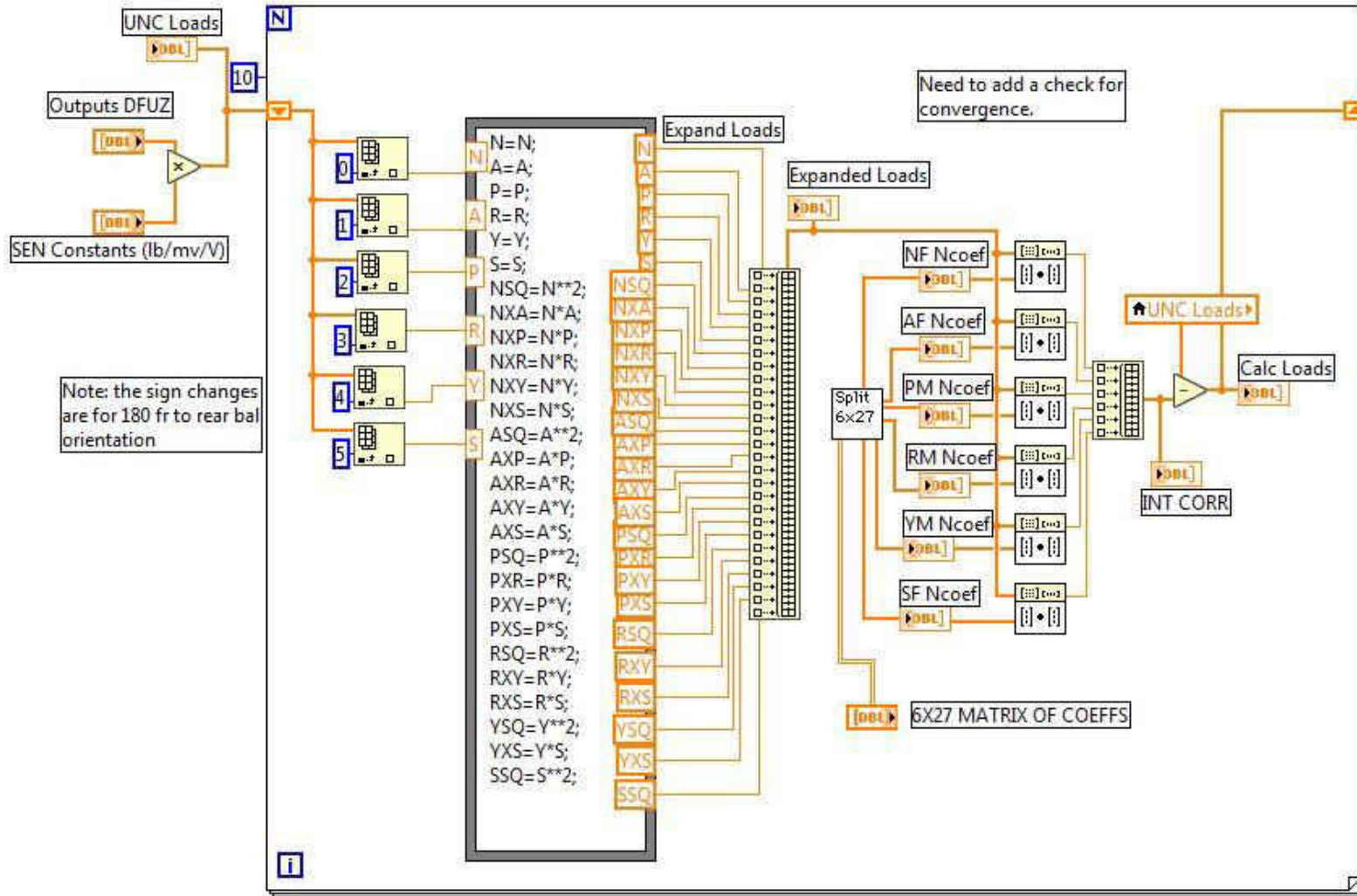
APPENDIX D. MODEL SUPPORT DRAWINGS

4 3 2 1

D D

C C

B B

A A

1-3A
ISOMETRIC

DRAWN nsado001	1/10/2017		
CHECKED			
QA		TITLE	
MFG			
APPROVED			
		SIZE C	DWG NO 15lb - 15lbin BALANCE_REV_C2	REV
		SCALE	SHEET 1 OF 8	

1/4" THRU
TYP 2 PLACES

#8-32

2-2B
ISOMETRIC

DRAWN			
nsada001	1/10/2017		
CHECKED			
QA		TITLE	
MFG			
APPROVED			
SIZE C		DWG NO 15lb – 15lbin BALANCE_REV_C2	REV
SCALE		SHEET 2 OF 8	

NOTES:

1. HOLES IN CAP AND BASE SUPPORTS TO BE DRILLED AND TAPPED POST WELDING.

2. ALL DIMENSIONS ARE IN INCHES UNLESS OTHER WISE NOTED.

3. MEASUREMENT BEAM, FLEX BEAM, AND STRAP
   DIMENSIONS ARE CRITICAL.

4. THE NUMBER OF DECIMAL PLACES DOES NOT
   REFLECT THE ACCURACY OF THE DIMENSION
   OR THE PRECISION OF MANUFACTURE.

DRAWN nsado001	1/10/2017			
CHECKED				
QA		TITLE		
MFG				
APPROVED				
		SIZE C	DWG NO 15lb - 15lbin BALANCE_REV_C2	REV
		SCALE	SHEET 3 of 8	

5.00

4-2B
RIGHT SIDE

.125
.25
2.00

1.50
1.50
53 mm B.C.
Ø16 mm
2.00
4-3A
CAP DETAIL

DRAWN
nsado001   1/10/2017
CHECKED
QA
MFG
APPROVED

TITLE

SIZE
C

DWG NO
15lb - 15lbin BALANCE_REV_C2

REV

SCALE

SHEET 4 of 8

NOTES:

1. PLATE IS TO BE MADE OF STOCK ALUMINUM. IF ALUMINUM IS NOT AVAILABLE STEEL IS ACCEPTABLE.

2. SPIGOT IS TO BE MACHINED TO FIT BALANCE.

3. DR. LANDMAN IS TO PROVIDE 3D CAD DRAWINGS AND BALANCE.

4 mm THROUGH TYPICAL

12.5 mm

4 mm THROUGH TYPICAL

3mm CHAMFER TYPICAL

15.5 mm

R.25
R.25

26.5 mm

R.50

M5x0.5 THREADED THROUGH

2.00
.625
4 mm
.13
1.500

2.00
1.00
1.500
.500

5-3B
ISOMETRIC

.50

.50

.25
TYP 2
PLACES

R.25
TYP 2 PLACES

1.50

1/4"-20UNC
DEPTH 0.5"
TYP 2 PLACES

5-3A
BASE SUPPORTS

DRAWN nsads001	1/10/2017	TITLE			
CHECKED					
QA					
MFG					
APPROVED					
		SIZE C	DWG NO 15lb - 15lbin BALANCE_REV_C2		REV
		SCALE		SHEET 5 or 8	

6-2C
TOP VIEW

6-4A
FRONT VIEW

6-3A
RIGHT SIDE VIEW

DRAWN nsado001 1/10/2017
CHECKED
QA
MFG
APPROVED
SIZE C
DWG NO 15lb - 15lbin BALANCE_REV_C2
REV
SHEET 6 of 8

.04

.04

.094

.06

.06

1.00 — STRAP

.13

R.05

FLEX
BEAMS (8)

1.45

.16

.91

1.00
.50

MEASUREMENT
BEAM

R.06

1.45

DETAIL A
SCALE 5 : 1
THRUST SECTION DETAIL
RIGHT SIDE AS SHOWN
LEFT SIDE MIRRORED

DRAWN nsad0001 1/10/2017

SIZE C DWG NO 15lb - 15lbin BALANCE_REW C2

SHEET 7 of 8

.25

.89

.19

.047

.10

R.06
(TYP 4 PLACES)

Ø 3/32
(TYP 2 PLACES)

MEASUREMENT BEAM

.05

.13

R.06
(TYP 4 PLACES)

DETAIL B
SCALE 5 : 1
TORQUE SECTION DETAIL
ALL DIMENSIONS
TYPICAL 4 SIDES

DRAWN nsadc001 1/10/2017
CHECKED
QA
MFG
APPROVED
SIZE C
DWG NO 15lb - 15lbin BALANCE_REV C2
SCALE
SHEET 8 of 8

SEE SHEET 2.

SEE SHEET 10

SEE SHEET 6

(18.00)

CALIBRATION SET UP

NOTE:

1. TUBING MCMASTER-CARR PART NUMBER 6566K25

2. PLATE MADE OF ALUMINUM.

3. THRUST STRING TO WRAP AROUND BOLT HOLDING
   THE TUBING TO THE PLATE.

DRAWN nsado001 2/6/2017
CHECKED
QA
MFG
APPROVED

SIZE C
DWG NO
REV
SCALE
SHEET 2 of 13

| 4 | 3 | 2 | 1 |

1.000

.25

2.00

NOTES:

1. MADE OF ALUMINUM.

2. QTY 1 REQUIRED.

3. MACHINE FINISH MATING FACES.

1/4"-20UNC

Ø4.00 mm
TYP 4 PLACES

.500 .500

Ø53.00 mm

1.000

2.00

0.252" - 0.250"
THRU HOLE

(15.00)

7.500

7.500

Ø.13

.50

Ø.252/.250 THRU

Ø.25 THRU

Ø.252/.250 THRU

.500

.438

.500

(.035)

(1.00)

(.50)

16.00

NOTES:

1. MATERIAL PROVIDED. POC DR. LANDMAN

2. QTY 1 REQUIRED.

DRAWN nsado001 2/6/2017

SIZE C

SHEET 4 of 13

.050
.045

.248
.245

.05

◎

1.255
1.250

DOWEL PIN
QTY 2 REQUIRED

NOTE:

PIECES ON THIS SHEET ARE NOT REQUIRED TO BE MADE.

DRAWN nsado001	2/6/2017		
CHECKED		TITLE	
QA			
HAS			
APPROVED			
		SIZE C	DWG NO	REV
		SCALE		SHEET 5 of 13

(17.063)

6-13

Ø.38 THRU
TYP 4 PLACES

Ø.50   Ø.25

1.25   2.50   .50   .50

.500   .50   .50

5.50
.30
.27   2.25   1.00

NOTES:

1. MADE OF STEEL.

2. QTY 1 REQUIRED.

3. MACHINE FINISH BOTH MATING FACES.

7 13

NOTES:

1. MADE OF STEEL SET ASIDE IN SHOP.

2. QTY 1 REQUIRED.

.75

DRILL AND TAP
0.75" DEEP 1/4"-20UNC

.50

1.00

2.50

15.804

1.00

MACHINE FINISH
BOTH SIDES

.50

DRILL AND TAP
0.75" DEEP 1/4"-20UNC

.50

1.50

8.13

124

(Ø.319)

(.759)

(.938)

NOTE:
1. PARTS ON THIS SHEET DO NOT NEED TO BE MANUFACTURED

9 .13

NOTES:

1. ALL DIMENSIONS ARE IN INCHES.

2. ALL MATERIAL IS TO BE MADE OF STEEL. STOCK
   MATERIAL HAS BEEN SET ASIDE FOR USE ON THIS
   PROJECT.

3. DEBUR ALL SURFACES.

4. ALL TOLERANCES ARE AS FOLLOWS.
   4.1. THREE DECIMAL PLACES +/- 0.005"
   4.2. TWO DECIMAL PLACES +/- 0.02"

BOLT PATTERN TYPICAL BOTH SIDES.

1.00

.38 .25

1/4"-20UN

.75

17.00

(1.50)

(.75)

APPENDIX E. EXPERIMENTAL DATA

Averaged Raw Calibration Data

Runs	Thurst (Volts)	Torque 1 (Volts)	Torque 2 (Volts)	Sense (Volts)
1	0.02167482	0.0231075	0.02066162	4.96871524
	0.02643652	0.01809224	0.01544063	4.96867638
	0.02166844	0.02310063	0.02064769	4.96643077
2	0.02166837	0.02310119	0.02064864	4.96641383
	0.02640524	0.02311539	0.02067474	4.96639175
	0.02166797	0.02310127	0.02064871	4.96640792
3	0.02166819	0.02310126	0.02064863	4.96640862
	0.02403742	0.02310795	0.02066112	4.9664345
	0.02166589	0.02310078	0.02064753	4.96645434
4	0.02166643	0.02310125	0.02064835	4.96646699
	0.02234468	0.02562917	0.02326932	4.96648868
	0.02166545	0.0230984	0.02065169	4.96649947
5	0.02166654	0.02309901	0.02065258	4.96652443
	0.02168644	0.0180633	0.01540509	4.96653578
	0.02166749	0.02310234	0.02064825	4.96656675
6	0.02166532	0.02310167	0.02064784	4.96659673
	0.02403285	0.02815055	0.02589008	4.96662394
	0.02166672	0.0230986	0.0206562	4.96663897
7	0.02166725	0.02309885	0.02065626	4.9666425
	0.02336011	0.02562807	0.02327481	4.96667404
	0.02166603	0.0230984	0.02065585	4.96670326
8	0.02166631	0.02309798	0.02065542	4.96670561
	0.0216649	0.02309758	0.02065513	4.96671742
	0.02166534	0.02309745	0.02065421	4.96672954
9	0.02166542	0.02309797	0.02065516	4.96677497
	0.02405358	0.01807901	0.01542453	4.96680117
	0.02166588	0.02310241	0.02064894	4.96678944

Runs	Thurst (Volts)	Torque 1 (Volts)	Torque 2 (Volts)	Sense (Volts)
10	0.02166623	0.02310383	0.02064993	4.96678644
	0.02640054	0.02815598	0.0259042	4.96681189
	0.02166597	0.02309906	0.02065689	4.96683618
11	0.02166548	0.02309853	0.02065615	4.96684168
	0.02639933	0.02815612	0.02590431	4.96688489
	0.02166384	0.02309948	0.02065764	4.96689778
12	0.02166447	0.02310007	0.02065769	4.96691457
	0.02639888	0.02311256	0.02068386	4.96692499
	0.0216636	0.02309913	0.02065625	4.96694851
13	0.02166349	0.02309907	0.0206567	4.96694764
	0.02303076	0.02058554	0.01804063	4.96696461
	0.02166228	0.02310125	0.02065292	4.9669923
14	0.02166359	0.02310264	0.02065382	4.96702782
	0.02405081	0.01807349	0.01542095	4.96704026
	0.02166235	0.02310271	0.02064958	4.96706463
15	0.02166264	0.0231031	0.02065065	4.96708144
	0.02168055	0.01805988	0.01540349	4.96713773
	0.02166153	0.02310166	0.0206487	4.96713642
16	0.02166316	0.02310379	0.02065097	4.96714262
	0.0257222	0.02563723	0.02328843	4.96717964
	0.02166172	0.02310018	0.02065306	4.9671859
17	0.02166221	0.02310047	0.02065334	4.9672116
	0.02403143	0.02815701	0.02589641	4.96724997
	0.02166302	0.02309889	0.02065582	4.96726172
18	0.02166238	0.02309826	0.02065595	4.96727747
	0.02166303	0.02309857	0.02065668	4.96729509
	0.0216629	0.02309809	0.02065634	4.9672953

| Runs	Thurst (Volts)	Torque 1 (Volts)	Torque 2 (Volts)	Sense (Volts)
19	0.02166376	0.02309882	0.02065634	4.96730078
	0.02403321	0.02310562	0.02066969	4.96731934
	0.02166358	0.02309913	0.02065683	4.96732968
20	0.02166305	0.02309833	0.0206557	4.96734919
	0.02641569	0.01808685	0.01543793	4.96740179
	0.02166441	0.02310448	0.02064987	4.96747235
21	0.02166542	0.02310537	0.02065161	4.96748534
	0.02166297	0.02815299	0.02588381	4.96747061
	0.0216647	0.02310037	0.02065817	4.96746633
22	0.02166647	0.02310106	0.02065927	4.96748617
	0.02166264	0.02815118	0.02588202	4.96747846
	0.02166414	0.02310022	0.02065795	4.96747368
23	0.02166448	0.02309958	0.02065737	4.96747913
	0.02403376	0.02310649	0.0206699	4.96748184
	0.021664	0.02309959	0.02065716	4.96750776
24	0.02166412	0.02309928	0.0206568	4.96751296
	0.02403397	0.02310635	0.02066974	4.96751057
	0.02166431	0.02309953	0.02065691	4.96752571
25	0.02166442	0.02309991	0.02065702	4.9675351
	0.02573358	0.02059722	0.01805818	4.96755725
	0.02166472	0.02310294	0.0206533	4.96758734
26	0.02166534	0.02310371	0.02065312	4.96758382
	0.02403523	0.02311096	0.02066712	4.96758496
	0.02166473	0.02310368	0.02065433	4.96759831

Note: Applied loads to balance are per load schedule shown in Table 1.

Averaged Raw Test Data

Runs	Fx (lbf)	Fy (lbf)	Fz (lbf)	Mx (in-lb)	My (in-lb)	Mz (in-lb)	Velocity (m/s)	Temp (C)	q (Pa)	Baro P (pa)	RPS	CT
1	0	0	5.8072323	0	0	-6.42645457	3.95808376	19.95	9.42284766	101608.4	82.9	0.11458962
	0	0	4.84072145	0	0	-5.85974131	6.42755547	20.9	24.85387445	101610.1	79.65	0.10344196
	0	0	3.33909404	0	0	-5.08300279	11.61547147	19.855	81.75698977	101610.45	79.45	0.07121259
	0	0	2.76925551	0	0	-4.73931896	13.84315712	19.95	115.2571036	101620.2	80.25	0.05830817
	0	0	1.94376414	0	0	-3.95037393	15.99020532	18.945	156.0224183	101620	79.8	0.04079509
	0	0	1.22065796	0	0	-3.19972327	18.31128692	17.935	203.0788625	101620.05	80.6	0.02530104
	0	0	0.53669127	0	0	-2.32620015	20.14475422	21.18	243.9224401	101619.1	79.5	0.01152036
	0	0	0.0386128	0	0	-1.74134831	21.83735428	20.16	288.7200979	101620	81.9	0.00077513
2	0	0	0.06078	0	0	-1.78995077	21.92997142	20.255	288.9584986	101623.1	81.45	0.00124389
	0	0	0.72854771	0	0	-2.6899935	19.9942769	19.27	243.7225688	101627	81.9	0.01454986
	0	0	1.17691334	0	0	-3.13632685	18.38642068	20.52	202.927153	101628	80	0.02498232
	0	0	1.97521987	0	0	-4.01423309	16.06434301	20.52	156.0826205	101635.65	80.1	0.04151025
	0	0	2.73584752	0	0	-4.71118863	13.81819559	19.395	115.0825172	101643.9	80	0.05784166
	0	0	3.29833923	0	0	-5.04175439	11.5559819	20.33	80.82746787	101649	78.75	0.07167617
	0	0	4.75557709	0	0	-5.79197056	6.41533273	21.4	24.72744984	101651	79	0.10342468
	0	0	5.11733772	0	0	-5.81070778	4.31321002	19.265	11.30356425	101652	78.55	0.11136334
3	0	0	5.34755807	0	0	-6.19532711	4.40065926	21.3	11.72738771	101660.1	80.5	0.11117377
	0	0	4.88916929	0	0	-6.05647256	6.4160621	20.235	24.74310241	101658	80	0.10364607
	0	0	3.36020679	0	0	-5.23275716	11.62021223	21.245	81.1766406	101657	79.9	0.07140066
	0	0	2.77543318	0	0	-4.86536124	13.8586084	20.235	115.4377101	101655.95	80.2	0.05854565
	0	0	1.98813294	0	0	-4.13313511	16.11329183	20.305	156.0103779	101655	80	0.04215933
	0	0	1.20570232	0	0	-3.28319026	18.38474408	21.4	203.0824746	101655	80.1	0.02550642
	0	0	0.67795208	0	0	-2.67765832	20.17943744	21.52	244.57744	101656	81.8	0.0137569
	0	0	0.01183455	0	0	-1.80748537	21.91033365	20.675	288.1060356	101659.95	81.1	0.00024454

Runs	CQ	CP	J	Efficiency	Motor Voltage	Motor Current	Power Output (W)	Rho	Power Input (W)	Velocity(ft/sec)
1	0.00792543	0.04979692	0.11748425	0.27035127	28.35130128	-18.28662068	31.51702292	0.00233334	-518.443799	12.98568121
	0.00782595	0.0491719	0.19857451	0.41773391	28.48096415	-16.11249413	27.6112419	0.00233417	-458.8884773	21.08752398
	0.00677503	0.0425688	0.35976439	0.60184316	28.51927103	-13.70783032	23.89113594	0.00235204	-390.8957108	38.1080388
	0.0062368	0.03918697	0.42447195	0.63159126	28.58296407	-12.74138981	22.49972443	0.00233361	-364.1545453	45.41662988
	0.00518232	0.03256147	0.49305939	0.61777228	28.34310486	-10.60684939	18.64935884	0.00236917	-300.6485865	52.46066563
	0.00414526	0.02604543	0.55902672	0.54304786	28.47561369	-8.75038174	15.25705329	0.00235084	-249.2161174	60.07567014
	0.00312124	0.01961134	0.62352811	0.36629066	28.340885	-6.82317916	10.94040124	0.00233216	-193.3906037	66.09090965
	0.00218563	0.01373269	0.65608478	0.03688535	28.49041282	-5.19481547	8.43698179	0.00235004	-148.0035989	71.64399193
2	0.00228902	0.01438232	0.66253346	0.0572681	28.39188502	-5.29556408	8.62473466	0.00233126	-150.2920082	71.94785025
	0.00335257	0.02106481	0.60072618	0.4173865	28.40309813	-7.53263761	13.03381613	0.00236704	-213.9506772	65.59722365
	0.00416092	0.02614384	0.56552723	0.54040892	28.55962707	-8.49567107	14.84323355	0.00232904	-242.6526828	60.32216896
	0.00527328	0.03313297	0.49349303	0.6183091	28.48403784	-10.78352451	19.02183496	0.00234763	-307.1254674	52.70389655
	0.00622532	0.03911485	0.42501833	0.62850624	28.46377448	-12.80368847	22.29655148	0.00233901	-364.3536531	45.33473609
	0.00684777	0.04302579	0.36109473	0.60155584	28.44425104	-13.45182173	23.48837812	0.00234937	-382.6246555	37.91286542
	0.00787277	0.04946604	0.19981975	0.41779069	28.54972303	-15.62205431	27.0689029	0.00233115	-446.0508528	21.04742364
	0.00790312	0.04965676	0.13511758	0.30302445	28.50839945	-15.72199176	27.00181657	0.00235853	-448.218314	14.15077944
3	0.00804947	0.05057028	0.13452011	0.29568739	28.5623592	-16.55036946	29.50385205	0.00235034	-472.7780234	14.43768291
	0.00802449	0.05041937	0.19734444	0.40567827	28.34686158	-16.49861613	28.66335075	0.0023321	-467.6789126	21.04981653
	0.0069494	0.04366438	0.35786624	0.58518558	28.41823872	-13.78440577	24.73406631	0.00233255	-391.7267909	38.12359228
	0.0064147	0.04030477	0.42520756	0.61765475	28.33285935	-12.791683	23.08398653	0.00233205	-362.4071338	45.46732242
	0.00547783	0.03441819	0.49561062	0.60708911	28.43628225	-10.74264101	19.56080877	0.0023314	-305.4778783	52.86448782
	0.00434098	0.02727521	0.56477466	0.52813445	28.50065833	-8.71761004	15.55769296	0.00233124	-248.4764373	60.31666837
	0.00339603	0.02133786	0.60703248	0.39136003	28.46400214	-7.22925611	12.9577067	0.00233039	-205.7743067	66.20469834
	0.00233396	0.01466468	0.66478174	0.01108732	28.43480235	-4.9558417	8.67184991	0.00232855	-140.9251653	71.88342263

...
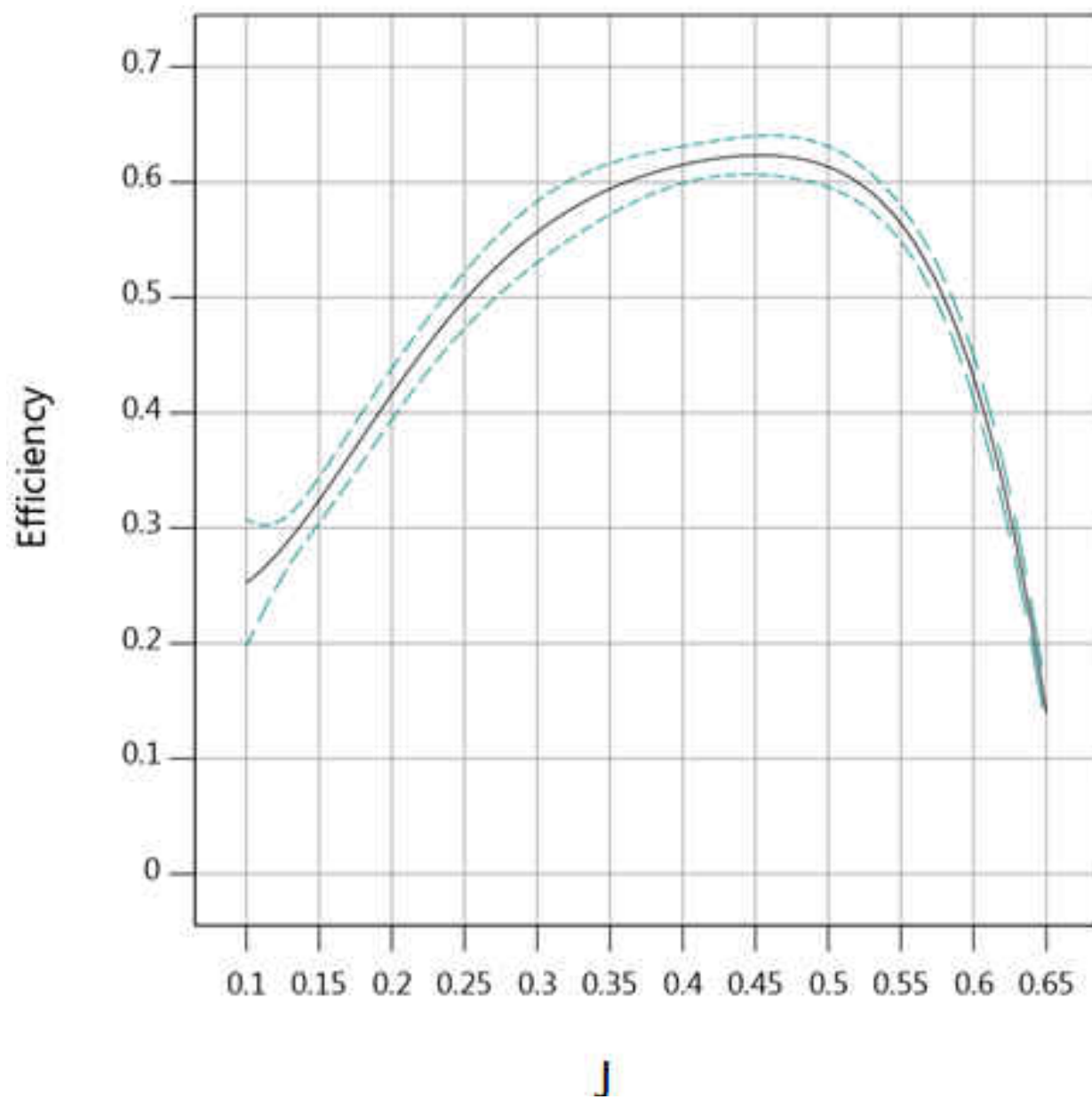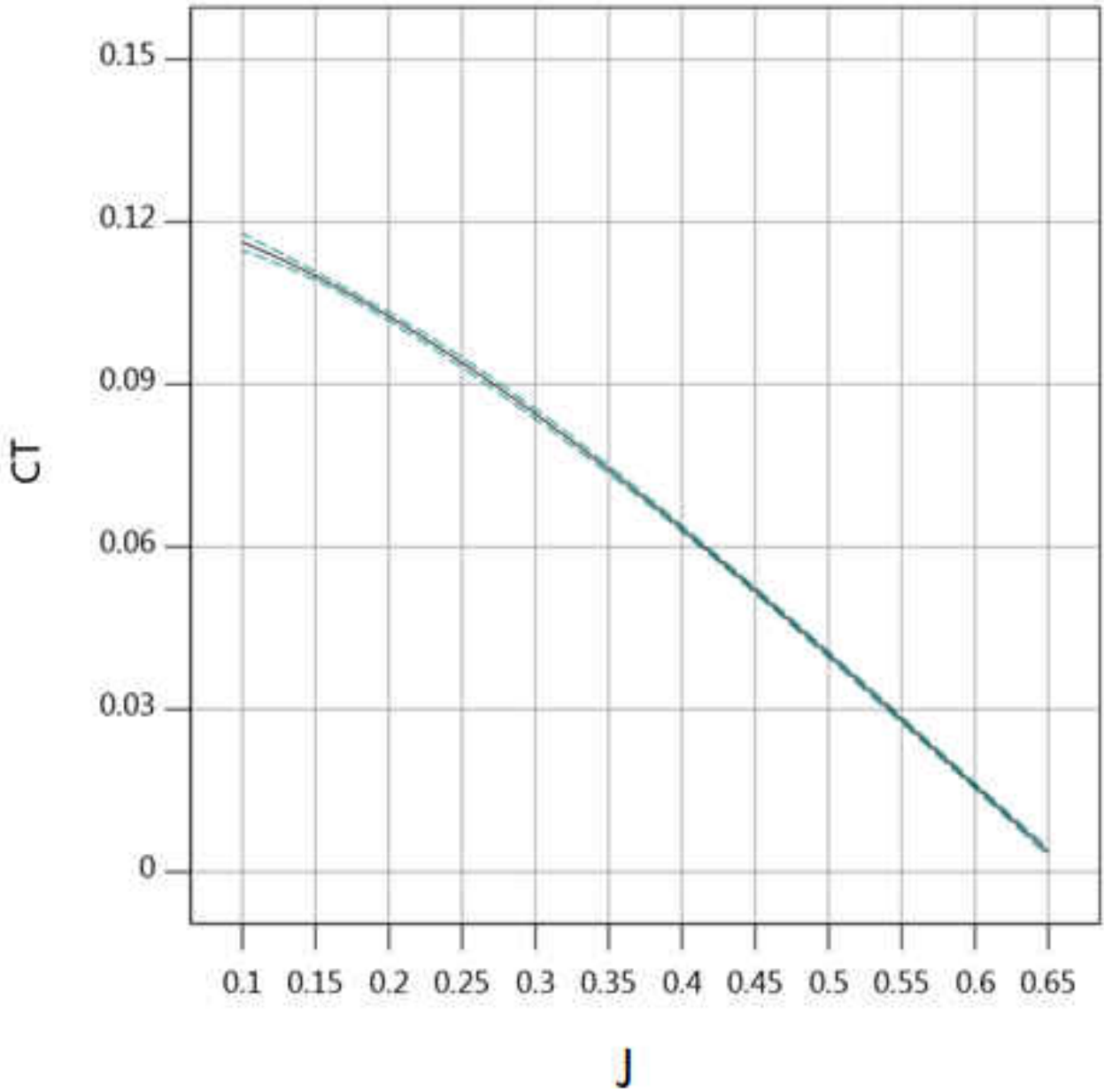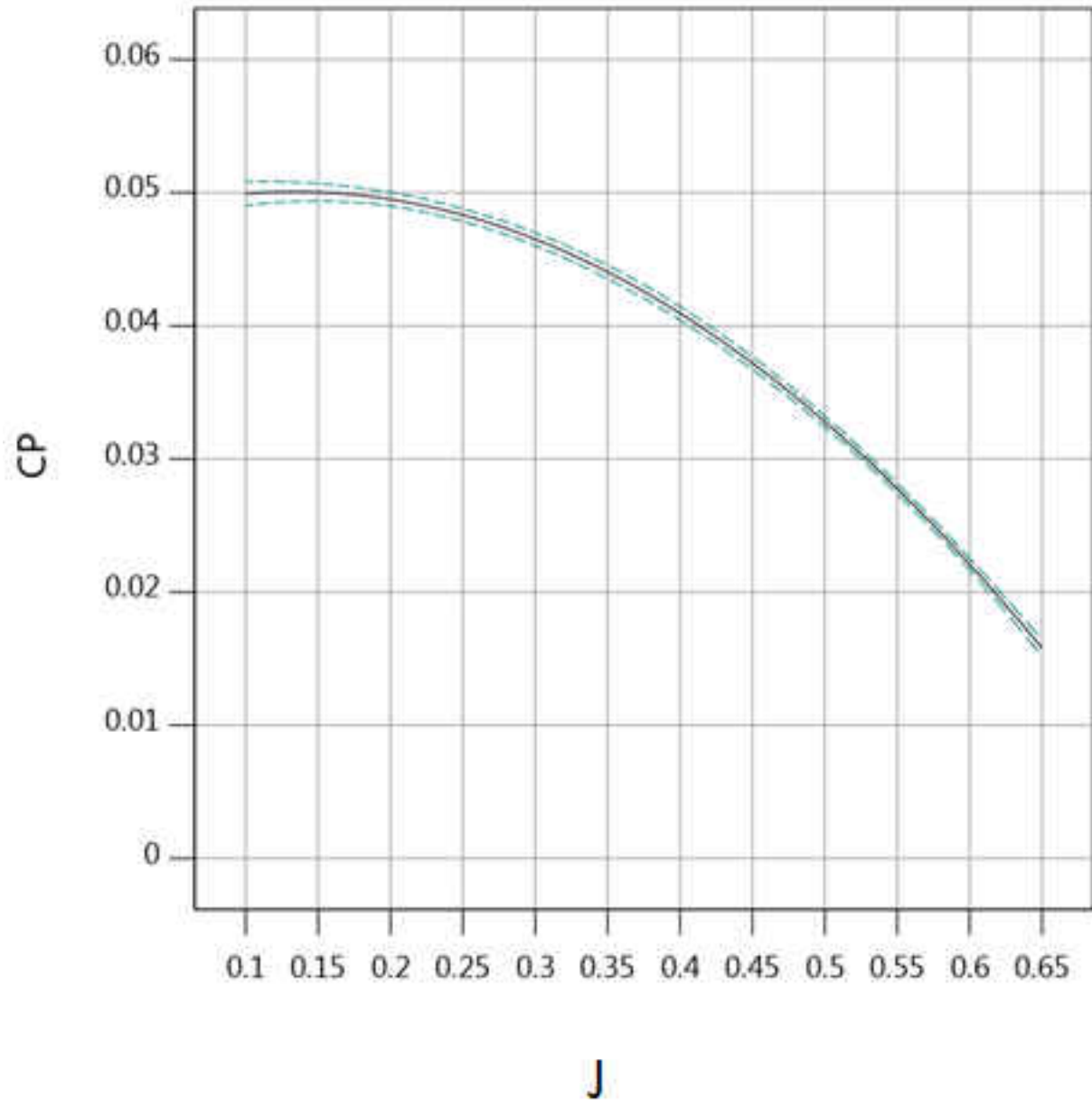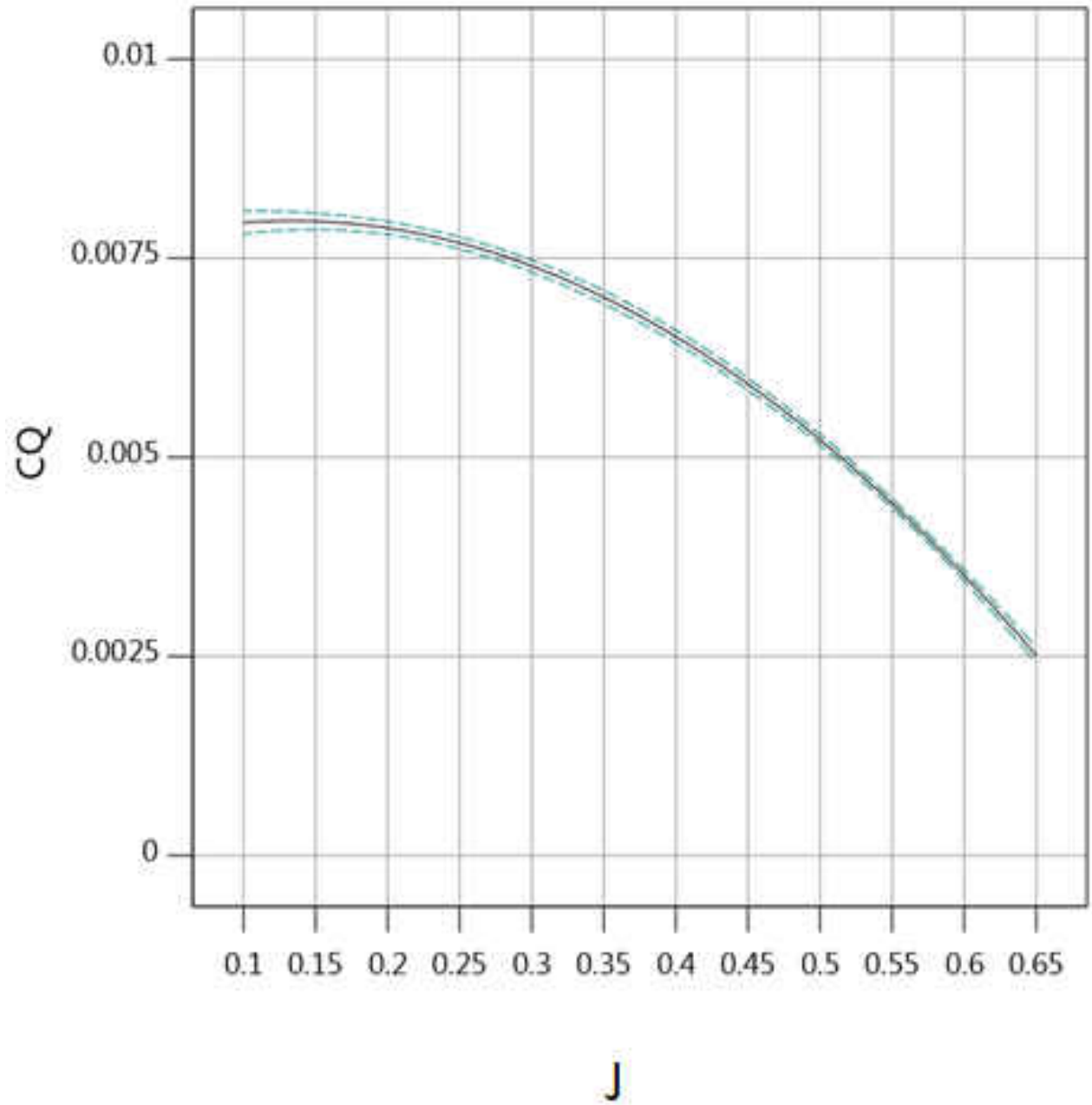
VITA

Nicholas B. Sadowski was born in Virginia Beach, Virginia, on January 30th 1991. He studied engineering at the Virginia Military Institute. There he received a Bachelor of Science in Mechanical Engineering with a minor in applied mathematics. Following his undergraduate degree he moved to Michigan to work as a contractor for Ford Motor Company as a Chassis Engineer. There he designed air suspension components from June 2013 to April 2014. He then obtained a job at his current employer Newport News Shipbuilding a division of Huntington Ingalls Industries where he works as an Aircraft Carrier Overhaul Engineer. After moving back to Virginia Beach in April of 2014 he started taking courses towards obtaining Master of Science in Mechanical Engineering, which he will obtain from Old Dominion University in May of 2018.